

THERMAL SPRAY COATING OF RED MUD ON METALS

A THESIS SUBMITTED
IN PARTIAL FULFILMENT OF THE REQUIREMENT FOR THE DEGREE OF

Doctor of Philosophy

in

Mechanical Engineering

By

Alok Satapathy



**Department of Mechanical Engineering
National Institute of Technology
Rourkela, India
November, 2005**

THERMAL SPRAY COATING OF RED MUD ON METALS

A Thesis Submitted to

National Institute of Technology, Rourkela

(Deemed University)

In partial fulfilment of the requirement for the degree of

Doctor of Philosophy

in

Mechanical Engineering

By

Alok Satapathy

under the guidance and supervision of

Dr. Subash Chandra Mishra

Department of Metallurgical & Materials Engineering



**Department of Mechanical Engineering
National Institute of Technology
Rourkela, India**

November, 2005

*Dedicated To
My Grand Father
Late Udayanath Satapathy*



NATIONAL INSTITUTE OF TECHNOLOGY
ROURKELA

CERTIFICATE

This is to certify that the thesis entitled “ **Thermal Spray Coating of Red Mud on Metals**” being submitted by **Sri Alok Satapathy** to the National Institute of Technology, Rourkela (India) , for the award of the degree of **Doctor of Philosophy** in Mechanical Engineering , is an authentic record of research work carried out by him under my supervision and guidance and the work incorporated in this thesis has not been, to the best of my knowledge, submitted to any other University or Institute for the award of a degree or diploma.

Rourkela

Dr. Subash Chandra Mishra
(Guide)

Acknowledgement

The author wishes to express his deep sense of gratitude to his guide and supervisor, **Dr. Subash Chandra Mishra**, Assistant Professor, Department of Metallurgical & Materials Engineering , National Institute of Technology, Rourkela for his invaluable guidance, motivation, untiring efforts and meticulous attention at all stages of this research work.

He appreciates the co-operation extended by the scientists at the Laser and Plasma Technology Division, Bhabha Atomic Research Center (B.A.R.C), Mumbai in carrying out the experimental work. He is extremely thankful to the scientific officers **Dr. P. V. Ananthapadmanabhan**, **Mr. K. P. Sreekumar** and **Mr. R. U. Satpute** in the thermal plasma section of this division for all the technical help and advice rendered by them throughout the course of this work.

The author is grateful to **Professor Sunil Kumar Sarangi**, Director, National Institute of Technology, Rourkela who has been a constant source of inspiration for him. He is also grateful to **Professor B.K. Nanda**, Head of the Department of Mechanical Engineering for his help and cooperation. He appreciates the encouragement from faculty members of the Mechanical Engineering Dept. and the Metallurgical & Materials Engineering Dept. of N.I.T. Rourkela.

The author gratefully appreciates the help and support of his undergraduate and postgraduate project students at N.I.T. Rourkela. He also wishes to acknowledge with gratitude the endless inspiration and sacrifice that came from his family members, friends and relatives to see the completion of this work.

N.I.T. Rourkela

(**Alok Satapathy**)

LIST OF FIGURES

- 2.1 Various forms of surface modification technologies
- 2.2 Categorization of common thermal spray processes
- 2.3 Arrangement for the wire flame spraying
- 2.4 Arrangement for the flame spraying with powders
- 2.5 Arrangement for the detonation gun coating
- 2.6 Arrangement for the HVOF spraying
- 2.7 Arrangement for the electric arc spraying
- 2.8 Arrangement for the plasma spraying
- 3.1 General arrangement of the plasma spraying equipment
- 3.2 Schematic diagram of the plasma spraying process
- 3.3 Jig used for the test
- 3.4 Specimen under tension
- 3.5 Adhesion test set up **Instron-1195**
- 4.1 Thickness of red mud coatings made at different power level
- 4.2 Adhesion strength of red mud coatings made at different power level on different substrates
- 4.3 Adhesion strength of red mud + 10% fly ash coatings made at different power level on different substrates
- 4.4 Adhesion strength of red mud + 30% fly ash coatings made at different power level on different substrates

- 4.5** Adhesion strength of red mud +50% fly ash coatings made at different power level on different substrates
- 4.6** Adhesion strength of red mud + 20% carbon coatings made at different power level on different substrates
- 4.7** Adhesion strength of red mud + 5 % aluminium coatings made at different power level on different substrates
- 4.8** Adhesion strength of coatings made of different feed materials on mild steel substrates
- 4.9 (a)** Surface morphology (S E M micrographs) of red mud coatings deposited at 6 kW operating power level
- 4.9 (b)** Surface morphology (S E M micrographs) of red mud coatings deposited at 9 kW operating power level
- 4.9 (c)** Surface morphology (S E M micrographs) of red mud coatings deposited at 12 kW operating power level
- 4.9 (d)** Surface morphology (S E M micrographs) of red mud coatings deposited at 16 kW operating power level
- 4.10 (a)** Surface morphology of red mud + 30% fly ash coatings deposited at 6 kW operating power level
- 4.10 (b)** Surface morphology of red mud + 30% fly ash coatings deposited at 9 kW operating power level
- 4.10 (c)** Surface morphology of red mud + 30% fly ash coatings deposited at 12 kW operating power level
- 4.10 (d)** Surface morphology of red mud + 30% fly ash coatings deposited at 16 kW operating power level
- 4.11 (a)** Surface morphology of red mud + fly ash coating deposited at 12 kW power level

- 4.11 (b)** Surface morphology of red mud + carbon coating deposited at 12 kW power level
- 4.11 (c)** Surface morphology of red mud + aluminium coating deposited at 12 kW
- 4.12 (a)** Interface morphology of red mud coatings deposited on aluminium substrates at 6 kW operating power level
- 4.12 (b)** Interface morphology of red mud coatings deposited on aluminium substrates at 9 kW operating power level
- 4.12 (c)** Interface morphology of red mud coatings deposited on aluminium substrates at 12 kW operating power level
- 4.12 (d)** Interface morphology of red mud coatings deposited on aluminium substrates at 16 kW operating power level
- 4.13 (a)** Interface morphology of red mud coatings deposited at 12 kW power level on copper substrate
- 4.13 (b)** Interface morphology of red mud coatings deposited at 12 kW power level on mild steel substrate
- 4.13 (c)** Interface morphology of red mud coatings deposited at 12 kW power level on stainless steel substrate
- 4.14 (a)** Coating interface morphology for red mud + 30 % fly ash deposited at 12 kW operating power level
- 4.14 (b)** Coating interface morphology for red mud + 50 % fly ash deposited at 12 kW operating power level
- 4.14 (c)** Coating interface morphology for red mud + 20 % carbon deposited at 12 kW operating power level
- 4.14 (d)** Coating interface morphology of red mud + 5% aluminium deposited at 12 kW operating power level

- 4.15** X Ray Diffractogram of red mud collected from NALCO
- 4.16** X Ray Diffractogram of red mud coating deposited at 6 kW operating power level
- 4.17** X Ray Diffractogram of red mud coating deposited at 9 kW operating power level
- 4.18** X Ray Diffractogram of red mud coating deposited at 12kW operating power level
- 4.19** X Ray Diffractogram of red mud coating deposited at 16kW operating power level
- 4.20** X Ray Diffractogram of coating (red mud + 20% carbon) deposited at 12 kW operating power level
- 4.21** X Ray Diffractogram of coating (red mud + 50% fly ash) deposited at 12 kW operating power level
- 4.22** X Ray Diffractogram of coating (red mud + aluminium) deposited at 12 kW operating power level
- 4.23** Cumulative mass loss of red mud coatings made at different operating power levels with 90^0 angle of impact
- 4.24** Variation of erosion wear rate of red mud coatings (deposited at 6,9,12,16 kW) with time of impact at 30^0 angle of impact
- 4.25** Variation of erosion wear rate of red mud coatings (made at 6, 9,12,16 kW) with time of impact at 60^0 angle of impact
- 4.26** Variation of erosion wear rate of red mud coatings (deposited at 6,9,12,16 kW) with time of impact at 90^0 angle of impact
- 4.27** Variation of erosion wear rate of red mud + fly ash coatings (deposited at 6, 9, 12, 16 kW) with time of impact at 90^0 angle of impact

- 4.28** Variation of erosion wear rate of red mud + aluminium coatings (deposited at 6,9,12,16 kW) with time at 90⁰ angle of impact
- 4.29** Variation of cumulative mass loss of different coating made at 12 kW with angle of impact
- 4.30** Deposition efficiency of red mud coatings made at different power level on different substrates
- 4.31** Deposition efficiency of red mud + 30% fly ash coatings made at different power level on different substrates
- 4.32** Deposition efficiency of red mud + 50% fly ash coatings made at different power level on different substrates
- 4.33** Deposition efficiency of red mud + 20% carbon coatings made at different power level on different substrates
- 4.34** Deposition efficiency of red mud + 5% aluminium coatings made at different power level on different substrates
- 4.35** Deposition efficiency of coatings made of different feed materials on aluminium substrates
- 4.36** Deposition efficiency of coatings made of different feed materials on copper substrates
- 4.37** Deposition efficiency of coatings made of different feed materials on mild steel substrates
- 4.38** Deposition efficiency of coatings made of different feed materials on stainless steel substrates
- 5.1** The three layer neural network

- 5.2** Comparison plot for predicted and experimental values of deposition efficiency of red mud coatings on aluminium and copper substrates
- 5.3** Predicted coating deposition efficiency for different coating materials on aluminium substrate
- 5.4** Predicted coating deposition efficiency for different coating materials on copper substrate
- 5.5** Predicted coating deposition efficiency for different coating materials on mild steel substrate
- 5.6** Predicted coating deposition efficiency for different coating materials on stainless steel substrate

LIST OF TABLES

- 2.1** Composition of red mud generated in alumina plants of different parts of the world
- 3.1** Powders used for coating deposition
- 3.2** Operating parameters during coating deposition
- 4.1** Coating adhesion strength at different spraying conditions
- 4.2** Porosity on coating surfaces for different specimens
- 4.3** Coating micro-hardness for different feed materials deposited at different operating power level
- 4.4** Coating deposition efficiency at different spraying conditions
- 5.1** Control parameters and selected test levels
- 5.2** Complete fractional factorial test grid with test outputs
- 5.3** Fractional factorial test results for deposition efficiency
- 5.4** Control factors and selected test levels
- 5.5** Experimental lay out and results with calculated S/N ratios for coating deposition efficiency
- 5.6** The S/N response table for coating deposition efficiency
- 5.7** Input parameters selected for training

ABSTRACT

Red mud emerges as the major waste material during production of alumina from bauxite by the Bayer's process. It comprises of oxides of iron, titanium, aluminium and silica along with some other minor constituents. The present investigation explores the coating potential of this industrial waste. It envisages the processing and characterization of a series of plasma sprayed coatings made with red mud and red mud pre-mixed with different proportions of fly ash and powders of aluminium and carbon. These materials do not belong to the so called "plasma sprayable" category. They have been deposited on aluminium, copper, mild steel and stainless steel substrates by atmospheric plasma spraying. The coatings are characterized to evaluate their potential as wear resistant coatings. Micro-structural characterization of the coatings has been carried out using scanning electron microscopy, x-ray diffraction and image analysis technique.

It is found that red mud is eminently coatable. The coatings possess good adhesion strength, hardness and reasonable porosity. With addition of fly ash and aluminium to red mud, the efficiency of deposition and coating properties such as adhesion, hardness are substantially improved. Premixing of carbon also favours deposition and results in better coating hardness. Due to certain phase transformations and inter-oxide formation during plasma spraying, changes in the coating characteristics are observed.

The erosion wear performance of these coatings is evaluated using a solid particle erosion test rig. Red mud coatings offer an attractive erosion wear resistance, which further improves on addition of fly ash and aluminium to the feed stock.

Statistical analysis of the experimental results using techniques like fractional factorial test and Taguchi experimental design is presented. Spraying parameters such as plasma arc current, torch input power, arc voltage, surface roughness of the substrate are identified as the significant factors affecting the efficiency of coating deposition. A prediction model using artificial neural networks is also employed to simulate property-parameter correlations and a fairly good agreement in the experimental and predicted values is obtained. This analysis makes it clear that with an appropriate choice of processing conditions a sound and adherent ceramic coating is achievable using industrial wastes like red mud and fly ash.

CONTENTS

CERTIFICATE	i
ACKNOWLEDGEMENT	ii
LIST OF FIGURES	iii
LIST OF TABLES	ix
ABSTRACT	x
CONTENTS	xii
1 INTRODUCTION	1
1.1 Background	1
1.2 Objective	6
2 LITERATURE SURVEY	7
2.1 Preamble	7
2.2 Surface Modification	7

2.3	Techniques of Surface Modification	8
2.4	Wear Resistant Coatings	28
2.5	Erosion Wear of Ceramic Coatings	38
2.6	Present Status of Red Mud Utilization	40
3	MATERIALS AND METHODS	50
3.1	Introduction	50
3.2	Processing of the Coatings	50
3.3	Characterization of the Coatings	54
3.4	Erosion Wear Behaviour of Coatings	58
4	RESULTS AND DISCUSSION	60
4.1	Introduction	60
4.2	Coating Thickness	60
4.3	Interface Bond Strength	62
4.4	Coating Morphology	73
4.5	Coating Porosity	82
4.6	Coating Hardness	85

4.7	XRD Phase Composition Analysis	86
4.8	Solid Particle Erosion Wear Behaviour	92
4.9	Coating Deposition Efficiency	102
4.10	Discussion	114
5	ANALYSIS OF EXPERIMENTAL RESULTS USING STATISTICAL TECHNIQUES	119
5.1	Introduction	119
5.2	Fractional Factorial Testing	119
5.3	Taguchi Experimental Design	123
5.4	Neural Computation	127
5.4	Remarks	137
6	CONCLUSIONS	138
	REFERENCES	141
	APPENDICES	154
	A 1. List of Publications	154
	A 2. Brief Bio Data of the Author	156

INTRODUCTION

1.1 BACKGROUND

Surface modification is a generic term now applied to a large field of diverse technologies that can be gainfully harnessed to achieve increased reliability and enhanced performance of industrial components. The incessant quest for higher efficiency and productivity across the entire spectrum of manufacturing and engineering industries has ensured that most modern-day components are subjected to increasingly harsh environments during routine operation. Critical industrial components are, therefore, prone to more rapid degradation as the parts fail to withstand the rigors of aggressive operating conditions and this has been taking a heavy toll of industry's economy. In an overwhelmingly large number of cases, the accelerated deterioration of parts and their eventual failure has been traced to material damage brought about by hostile environments and also by high relative motion between mating surfaces, corrosive media, extreme temperatures and cyclic stresses. Simultaneously, research efforts focused on the development of new materials for fabrication are beginning to yield diminishing returns and it appears unlikely that any significant advances in terms of component performance and durability can be made only through development of new alloys.

As a result of the above, the concept of incorporating engineered surfaces capable of combating the accompanying degradation phenomena like wear, corrosion and fatigue to improve component performance, reliability and

durability has gained increasing acceptance in recent years. The recognition that a vast majority of engineering components fail catastrophically in service through surface related phenomena has further fuelled this approach and led to the development of the broad interdisciplinary area of surface modifications. A protective coating deposited to act as a barrier between the surfaces of the component and the aggressive environment that it is exposed to during operation is now globally acknowledged to be an attractive means to significantly reduce/suppress damage to the actual component by acting as the first line of defense.

The increasing utility and industrial adoption of surface engineering is a consequence of the significant recent advances in the field. Very rapid strides have been made on all fronts of science, processing, control, modeling, application developments etc. and this has made it an invaluable tool that is now being increasingly considered to be an integral part of component design. Surface modification today is best defined as “the design of substrate and surface together as a system to give a cost effective performance enhancement, of which neither is capable on its own”. The development of a suitable high performance coating on a component fabricated using an appropriate high mechanical strength metal/alloy offers a promising method of meeting both the bulk and surface property requirements of virtually all imagined applications. The newer surfacing techniques, along with the traditional ones, are eminently suited to modify a wide range of engineering properties. The properties that can be modified by adopting the surface engineering approach include tribological, mechanical, thermo-mechanical, electrochemical, optical, electrical, electronic, magnetic/acoustic and biocompatible properties.

The development of surface engineering has been dynamic largely on account of the fact that it is a discipline of science and technology that is being increasingly relied upon to meet all the key modern day technological requirements: material savings, enhanced efficiencies, environmental

friendliness etc. The overall utility of the surface engineering approach is further augmented by the fact that modifications to the component surface can be metallurgical, mechanical, chemical or physical. At the same time, the engineered surface can span at least five orders of magnitude in thickness and three orders of magnitude in hardness.

Driven by technological need and fuelled by exciting possibilities, novel methods for applying coatings, improvements in existing methods and new applications have proliferated in recent years. Surface modification technologies have grown rapidly, both in terms of finding better solutions and in the number of technology variants available, to offer a wide range of quality and cost. The significant increase in the availability of coating process of wide ranging complexity that are capable of depositing a plethora of coatings and handling components of diverse geometry today, ensures that components of all imaginable shape and size can be coated economically.

Existing surface treatment processes fall under three broad categories:

(a) Overlay Coatings: This category incorporates a very wide variety of coating processes wherein a material different from the bulk is deposited on the substrate. The coating is distinct from the substrate in the as-coated condition and there exists a clear boundary at the substrate/coating interface. The adhesion of the coating to the substrate is a major issue.

(b) Diffusion Coatings: Chemical interaction of the coating-forming element(s) with the substrate by diffusion is involved in this category. New elements are diffused into the substrate surface, usually at elevated temperatures so that the composition and properties of outer layers are changed as compared to those of the bulk.

(c) Thermal or Mechanical Modifications of Surfaces: In this case, the existing metallurgy of the component surface is changed in the near-surface region either by thermal or mechanical means, usually to increase its hardness.

The type of coating to be provided depends on the application. There are many techniques available, e.g. electroplating, vapour depositions, thermal spraying etc. Of all these techniques, thermal spraying is popular for its wide range of applicability, adhesion of coating with the substrate and durability. It has gradually emerged as the most industrially useful method of developing a variety of coatings, to enhance the quality of new components as well as to reclaim worn/wrongly machined parts.

The type of thermal spraying depends on the type of heat source employed and consequently flame spraying (FS), high velocity oxy-fuel spraying (HVOF), plasma spraying (PS) etc. come under the umbrella of thermal spraying. Plasma spraying utilizes the exotic properties of the plasma medium to impart new functional properties to conventional and non-conventional materials and is considered as one highly versatile and technologically sophisticated thermal spraying technique. It is a very large industry with applications in corrosion, abrasion and temperature resistant coatings and the production of monolithic and near net shapes [1]. The process can be applied to coat on variety of substrates of complicated shape and size using metallic, ceramic and /or polymeric consumables. The production rate of the process is very high and the coating adhesion is also adequate. Since the process is almost material independent, it has a very wide range of applicability, e.g., as thermal barrier coating, wear resistant coating etc. Thermal barrier coatings are provided to protect the base material, e.g., internal combustion engines , gas turbines etc. at elevated temperatures. Zirconia (ZrO_2) is a conventional thermal barrier coating material. As the name suggests, wear resistant coatings are used to combat wear especially in cylinder liners, pistons, valves, spindles, textile mill rollers etc. alumina (Al_2O_3), titania (TiO_2) and zirconia (ZrO_2) are the some of the conventional wear resistant coating materials [2].

One major limitation of the process is a relatively high price of the plasma sprayable consumables. The objective of this work is to evaluate the potential

of red mud, an industrial waste as plasma consumable. Red mud does not belong to the so called plasma sprayable category and being a waste, is quite cheap. Another industrial waste fly ash, which is also considered in this work, has been pre-mixed with red mud in different proportions (10%, 30%, 50% by weight) to develop a series of plasma sprayed coatings. Mixtures of red mud with aluminium powder (5% wt) and with carbon (20% wt) are also deposited as coatings. Coatings have been produced on four selected substrates (commercially available aluminium, copper, stainless steel and mild steel) using all these non-conventional coating materials. The performance of the coatings developed using all the mixtures have been compared.

The coatings have been characterized for their hardness, porosity, adhesion strength and microstructure. The significant phase changes associated with the plasma processing during the coating deposition have been studied. In addition, the coating deposition efficiencies at various operating conditions have also been evaluated.

One less studied area in case of ceramic coatings is their resistance to solid particle erosion. This aspect is studied in the present work by subjecting the coatings to solid particle impingement at different impact angles. The capabilities of the coatings to sustain the erosive attack have been assessed.

A qualitative analysis of the experimental results with regard to coating deposition efficiency using statistical techniques is presented. The analysis is aimed at identifying the operating variables/factors significantly influencing the deposition of red mud on metals. Factors are identified in accordance to their influence on the coating deposition. A prediction model based on artificial neural network is also presented considering the significant factors. Neural computation is used since plasma spraying is a complex process that has many variables and multilateral interactions. This technique involves construction of

a database, training, validation and then provides a set of predicted results related to the coating deposition efficiency at various operating parameters.

1.2 OBJECTIVE

The objective of the present investigation can be stated as following:

- a. To explore the coating potential of red mud (the waste generated during production of alumina from bauxite) on metal substrates by plasma spraying.
- b. To develop a series of plasma sprayed coatings from red mud, red mud pre-mixed with fly ash in different proportions, with aluminium powder and with carbon. All these materials do not belong to the so-called “plasma sprayable” category.
- c. Micro-structural characterization to evaluate the soundness of the coatings.
- d. Mechanical characterization to evaluate the micro-hardness and interface bond strength of the coatings.
- e. To assess the capabilities of the coatings to combat wear with a special reference solid particle erosion wear.
- f. To analyze the experimental results using statistical techniques so as to identify significant factors/interactions influencing the coating deposition.
- g. Complementing the experimental results, in regard to coating deposition efficiency, by predicted results obtained from an artificial neural network analysis.

LITERATURE SURVEY

2.1 PREAMBLE

This chapter deals with the literature survey of the broad topic of interest namely the development of surface modification technology for tribological applications. This treatise embraces various coating techniques with a special reference to plasma spraying, the coating materials and their characteristics. The performances of wear resistant coatings under various conditions have been reviewed critically along with the corresponding failure mechanisms. It also presents a review of the efforts that have been directed worldwide towards management issues of utilization, storage and disposal of red mud, which is the material of interest in this work.

At the end of the chapter a summary of the literature survey and the knowledge gap in the earlier investigations are presented.

2.2 SURFACE MODIFICATION

Surface modification is a relatively new term that has come up in the last two decades or so to describe interdisciplinary activities aimed at tailoring the surface properties of engineering materials. The object of surface engineering is to upgrade their functional capabilities keeping the economic factors in mind [3]. 'Surface Engineering' is the name of the discipline - surface modification is the philosophy behind it. To elucidate the matter an example can be taken.

Tungsten carbide cobalt composite is a very popular cutting tool material, and is well known for its high hardness and wear resistance. If a thin coating of TiN is applied on to the WC-Co insert, its capabilities increase considerably [4]. Actually a cutting tool, in action, is subjected to a high degree of abrasion, and TiN is more capable of combating abrasion. On the other hand, TiN is extremely brittle, but the relatively tough core of WC-Co composite protects it from fracture. Thus through a surface modification process we assemble two (or more) materials by the appropriate method and exploit the qualities of both [5,6]. It is a very versatile tool for technological development provided it is applied judiciously keeping the following restrictions in mind:

- (i) The technological value addition should justify the cost, and
- (ii) The choice of technique must be technologically appropriate.

2.3 TECHNIQUES OF SURFACE MODIFICATION

Today a large number of commercially available technologies are present in the industrial scenario and figure 2.1 exhibits some of them [5]. An overview of such technologies is presented below.

2.3.1 Plating

Amongst plating processes, electroplating is quite popular. The substrate (necessarily conducting) forms an electrode (cathode) and is submerged in an appropriate electrolyte [7]. As current passes through the electrolytic cell, ions of plating material emerge from the electrolyte and deposit on to the cathode (the substrate). In electroless plating, deposition occurs by catalytic reduction of the solute present in the plating bath. Electrochemical conversion coating appears on the surface of the substrate (which acts as an electrode) as a result of a chemical reaction between the electrolyte and the surface. For example in presence of H_2SO_4 (electrolyte) the top layer of aluminium (electrode) is oxidized to form aluminium oxide [8]. Electroforming is the process of electro-

SURFACE MODIFICATION TECHNOLOGIES

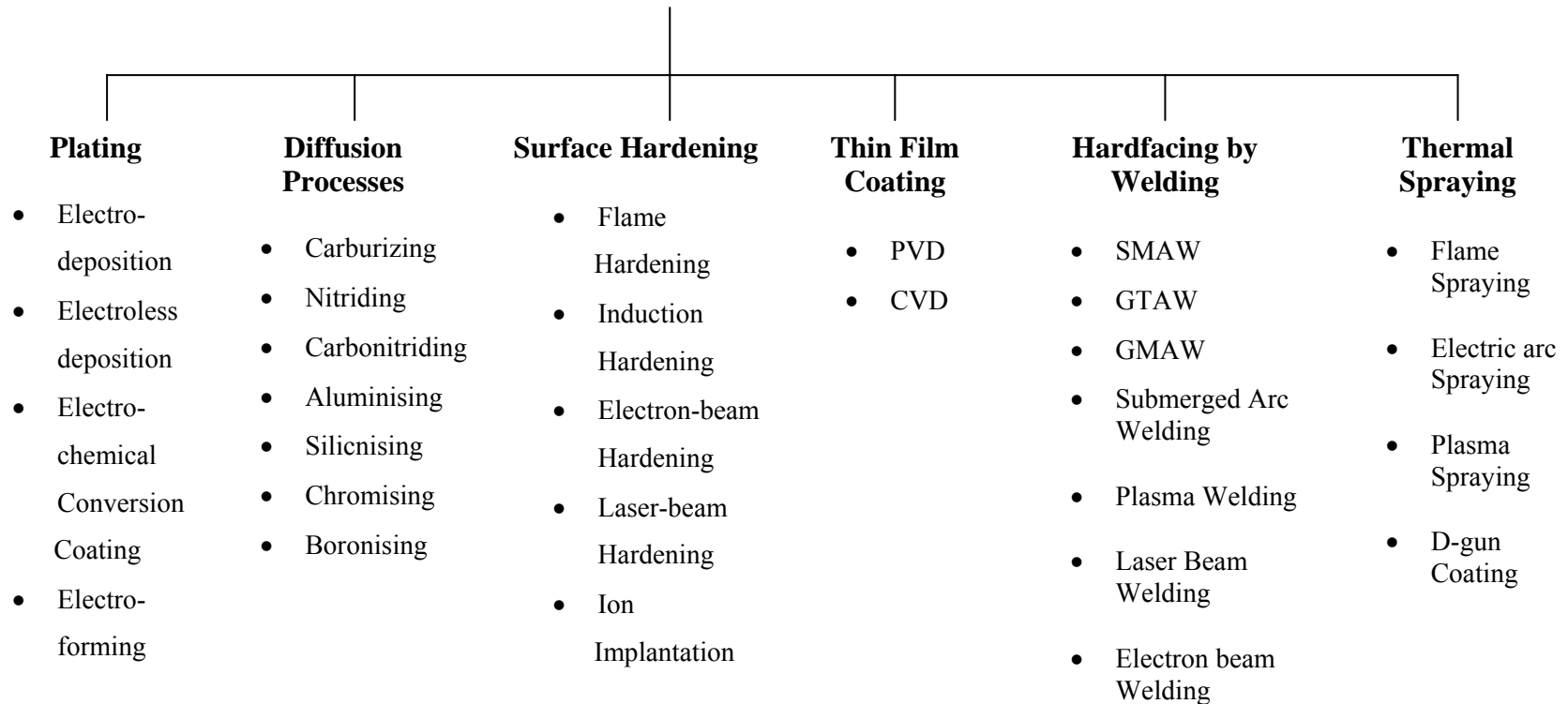


Fig. 2.1 Various forms of surface modification technologies

depositing a material on a removable mandrel to make a part. Plating can be used for modification of physical, mechanical or corrosion properties [9].

Plating techniques cater to a large number of materials. Composite coatings with non-conducting materials like diamond, PTFE is also possible by plating. It caters to wear, corrosion, rebuilding and electrical applications. Some of the processes are capable of providing uniform coating throughout the surface even in deep holes and re-entrant corners (electroless plating). Selective areas of a surface can be plated too [8,10,11].

But electroplating is prone to metallurgical embrittlement and provides only moderate adhesion where as electroless plating is quite slow [7,12].

2.3.2 Diffusion Processes

As the name suggests, the process involves the diffusion of an element into the substrate matrix [13]. The process is normally conducted at an elevated temperature to promote diffusion. The diffusing species create a layer on the substrate and the properties of that layer are modified. The elements used as diffusing species are carbon, nitrogen, aluminium, chromium, silicon, boron, etc. The choice of the diffusing species depends on applications, but carbon and nitrogen are the two most widely used elements and the processes are known as carburising and nitriding respectively [14]. Both processes are normally carried out on steel substrates. The substrate is kept in an environment rich in carbon or nitrogen. At a high temperature, the elements slowly diffuse into the substrates owing to the concentration gradient. Carburising enriches the carbon content of the substrate case and upon quenching the case layer hardens owing to the martensitic transformation. Nitriding also creates a very hard layer on the substrate surface. Here hardening occurs owing to a solid solution strengthening . These two processes are mainly used for wear applications and

so are boronising and carbonitriding. Chromising, siliconising, and aluminising on the other hand are for corrosion /oxidation resistance applications [15, 16] .

But diffusion processes have certain limitations as well. They cannot cater to applications like rebuilding. Some processes often create distortion (case carburising). Some of the processes are very slow and the case depth obtained is limited (gas carburising). Some of the processes are carried out in aggressive environment (salt nitriding) with potential environmental hazard. Applications are limited to metals only.

2.3.3 Surface Hardening

The process involves heating a component surface (or part of it) beyond a critical temperature and quickly cooling it by quenching to induce martensitic transformation. The process is restricted to cast iron and steels. Here a heat source for raising the temperature of the work piece is needed. The process is named after the heat source used and typical examples are flame hardening (oxy-acetylene flame), induction hardening (induction heating), laser hardening (laser beam), electron beam hardening (electron beam) etc. [17] . The carbon content of the work piece must be at least 0.6%, otherwise martensitic transformation may not occur. Except for the ion implantation process, these processes do not involve any material addition. In the ion implantation process, suitable materials are taken in ion form and they are directed at the surface to be implanted on. These processes are utilized to develop a hard case of low thickness, while retaining the softness of the core [18] .

A small part of a big component can be hardened (flame hardening) and no material addition is required. Adhesion does not impose any restriction, since the hardened layer is an integral part of the original component. But the process is restricted to ferrous materials. Sometime the process is prone to distortion.

Some of the processes require highly skilled manpower (e.g., flame hardening). Except for flame hardening, the set-up cost is high for all other processes.

2.3.4 Thin Film Coating

In this process a thin layer of a pure element or a compound can be deposited on substrate [5]. This technique can be broadly classified into two categories:

- Physical vapour deposition,
- Chemical vapour deposition

2.3.4a Physical Vapour Deposition (PVD)

This process is carried out in an evacuated chamber. The target (substrate) and the coating material are kept facing each other. The coating material is heated using a heat source like electrical heater or electron beam, in low pressure. The coating material evaporates directly from solid state and deposits on the target. This is known as thermal evaporation [19]. In another process, known as sputter coating [20], the target and coating materials are connected to two electrodes (anode and cathode, respectively) of a suitable power supply and an inert gas is released in the space between them. The gas undergoes ionization in the electric field. The positive ions rush towards the cathode (i.e., the coating material) and dislodge ions from it. These ions move toward the anode and deposit on the target. Ion plating is a combination of these two processes where the coating material is heated and at the same time a gas plasma is created to expedite the process [21].

Using this process pure elements as well as compounds can be deposited. It is quite simple, involves low cost equipment and addresses many fields of applications, e.g., electronic, electrical, wear, etc. This is a line of sight process, and therefore parts having complicated shape may not be coated. Since it is conducted in vacuum, large parts cannot be coated [5].

2.3.4b Chemical Vapour Deposition (CVD)

The material to be coated is kept in an evacuated chamber equipped with the facility of electrical heating. After the substrate is heated to the required temperature, the appropriate gases are introduced into the reactor for chemical reaction in contact with the hot substrate. One of the reaction products is a solid, which deposits on the substrate surface. The residual gases are taken out of the chamber [22].

Intricate shapes can be coated by this technique. Rate of deposition is higher than PVD. Certain items can be deposited using CVD only. But since it is carried out at a high temperature (700°C or above) , thermal damages may come into play. Set up is more complicated than PVD [23].

2.3.5 Hard facing by Welding

Welding conventionally is a process of joining two metallic parts. Shield Metal Arc Welding (SMAW) is the most common welding process. Here the base metals are kept close to each other and an electric arc is created between the base metal (near the junction) and the consumable electrode. As a result both the consumable electrode (filler material) and the edge of the base metal melt. The filler material of the electrode transfers to the molten weld pool and upon freezing of such pool a solid weld bead is formed. The strength of the weldment is supposed to be greater than that of the base material [24]. In the case of the hard facing, the filler material is deposited onto the base material to form a metallurgically bonded second layer. Now the first layer of the deposit is diluted by the diffusion of the base material constituents into it. Normally a second layer is also deposited at the top of the first one. In welding either similar or otherwise compatible filler material are normally used for the joining purpose. Alloyed electrodes, with a tailored composition to suit particular

situations of surfacing, are also used [25]. There are many techniques of welding and are shown in Figure 2.1. Each has its own application domain.

Strongest possible bonding is obtained in this process. All weldable metals and alloys can be used. It can be carried out with low cost equipment. A thick layer can be built up rapidly. The process can be entirely automated. But this technique is restricted to metallic materials. Products are vulnerable to residual stress related distortion. The hard faced layer may undergo dilution by the diffusion of base material constituents. Products may require a post-weld finishing operation in many applications [24, 26].

2.3.6 Thermal Spraying

It is the generic category of material processing technique that apply consumables in the form of a finely divided molten or semi molten droplets to produce a coating onto the substrate kept in front of the impinging jet. The melting of the consumables may be accomplished in a number of ways, and the consumable can be introduced into the heat source in wire or powder form. Thermal spray consumables can be metallic, ceramic or polymeric substances. Any material can be sprayed as long as it can be melted by the heat source employed and does not undergo degradation during heating [24 , 27]. The nature of bonding at the coating-substrate interface is not completely understood. It is normally assumed that bonding occurs by the mechanical interlocking. Under this circumstance it is generally possible to ignore the metallurgical compatibility [5]. This is an extremely significant feature of thermal spraying. Another interesting aspect of thermal spraying is that the surface temperature seldom exceeds 200⁰ C. Hard metal or ceramic coating can be applied to thermosetting plastics. Stress related distortion problems are also not so significant. The spraying action is achieved by the rapid expansion of combustion gases (which transfer the momentum to the molten droplets) or by a separate supply of compressed air.

There are two basic ways of generating heat required for melting the consumables, [27,28]

- (i) combustion of a fuel gas
- (ii) high energy electric arc

Figure 2.2 shows the common thermal spray processes fitting into the above mentioned categories.

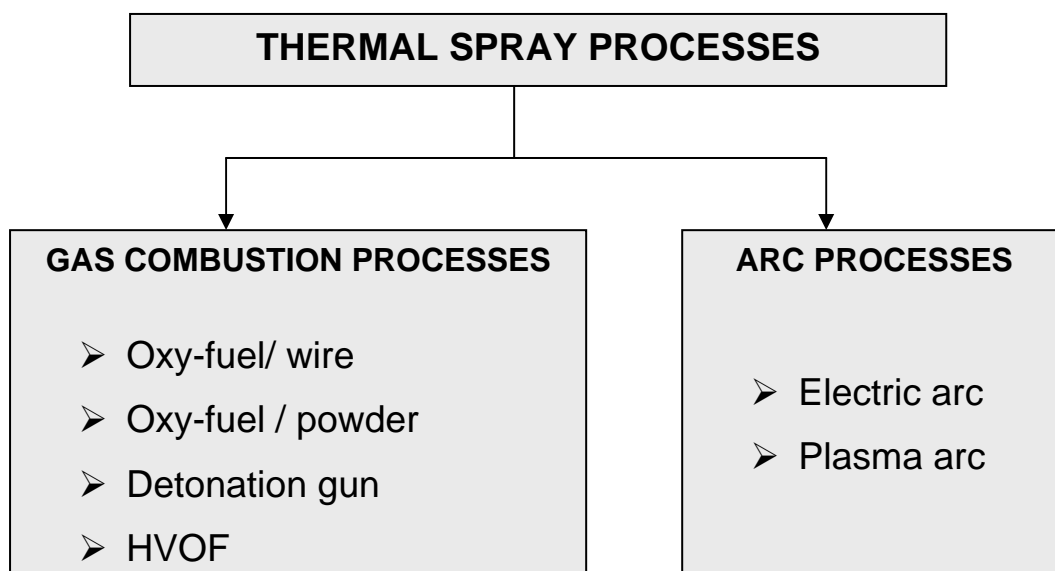


Fig. 2.2 Categorization of common thermal spray processes

The processes mentioned above are discussed briefly in the following articles but plasma spraying has been discussed separately.

2.3.6a Flame Spraying with Wire

The arrangement is shown in figure 2.3, and the set-up consists of a spraying gun, a wire feeding arrangement, oxygen and acetylene gas cylinders and an air compressor [5]. A proportionate mixture of oxygen and acetylene is taken inside a chamber located in the gun itself, and the mixture is set ablaze. The flame comes out through the muzzle of the gun. The tip of the wire is fed to the flame which melts quickly and forms a droplet. A compressed air jet dislodges the molten droplet and carries it, in atomized form, to the target surface kept in front of the gun. Meanwhile the roller of the wire feeding arrangement rotates continuously at a fixed, preset speed to advance the wire to flame [24,27,29,30].

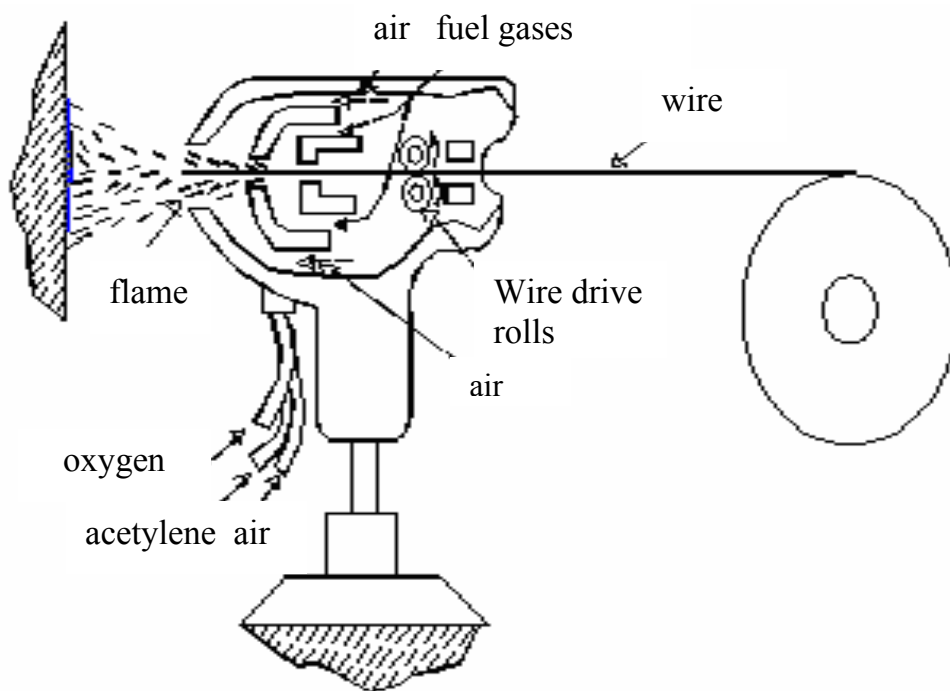


Fig. 2.3 Arrangement for the wire flame spraying

The set up cost for flame spraying is quite low. Thick metallic layer can be deposited easily and hence it is quite useful for rebuilding purpose. But it is applicable to metallic materials only [5].

2.3.6b Flame Spraying with Powder

The arrangement is shown in Figure 2.4. The process is carried out with a gun in which facility for fuel gas (oxy-acetylene) injection and powder storage are integrated. The flame is kept at a convenient distance from the substrate. The consumable-powders are kept inside the hopper integrated with the gun and can be released to the flame by the action of a trigger. The powder is gravity fed to the flame; it melts and deposits on to the substrate to form a coating. In some cases the flame is taken close to the coating immediately after deposition for further melting. In this case the bond strength achieved is higher, but the temperature of the substrate increases considerably [5,27, 28].

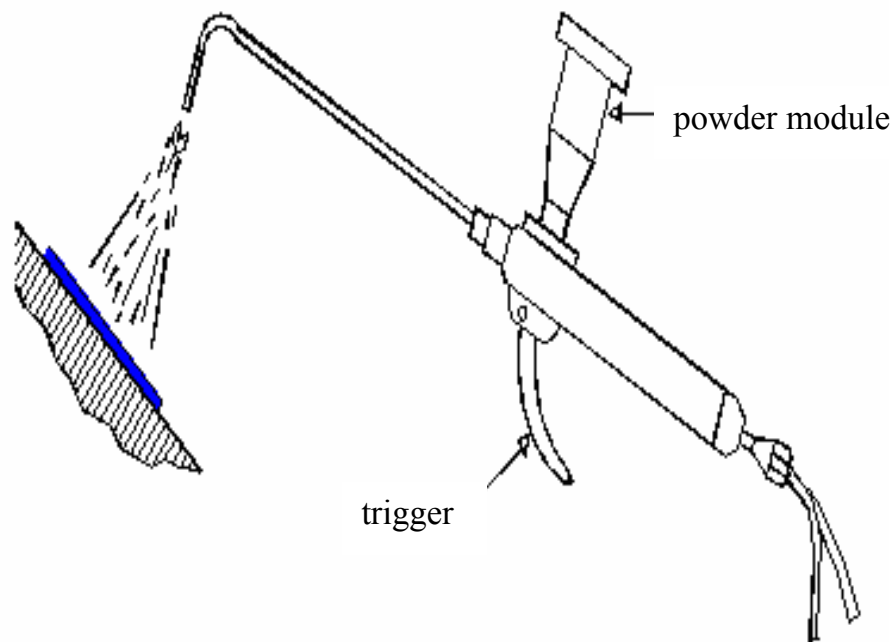


Fig. 2.4 Arrangement for the flame spraying with powders

The equipment cost is low. A large number of alloys (even cermets) are available in powder form. But ceramic materials cannot be deposited by this method. The deposition rate is very slow.

2.3.6c Detonation Gun Coating

This is a proprietary coating process. The basic set up is shown in Figure 2.5.

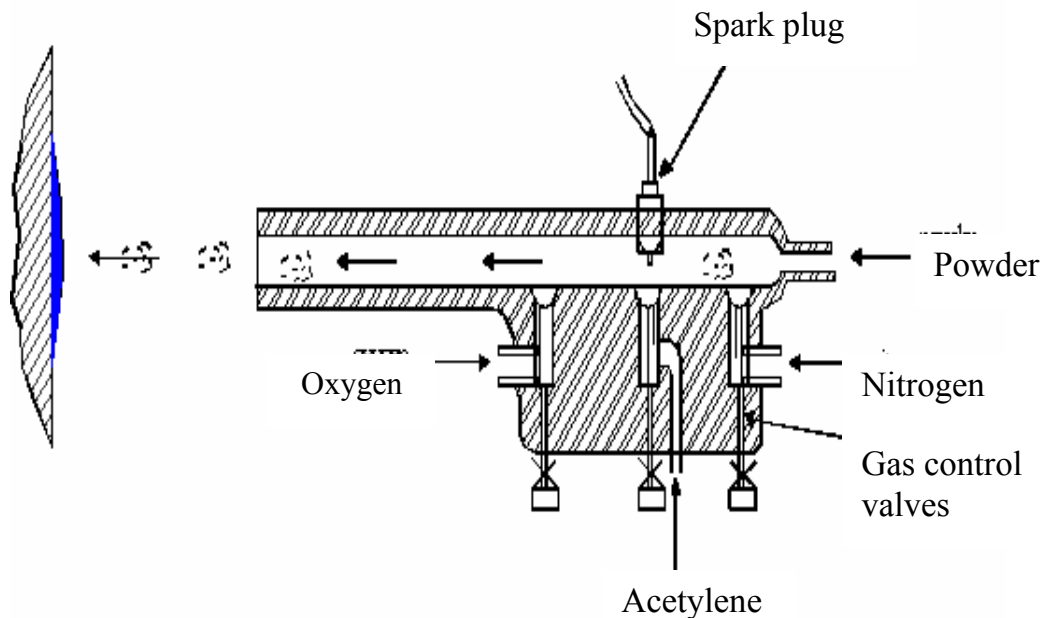


Fig. 2.5 Arrangement for the D-gun coating

Consumable powder is fed into the gun under a small gas pressure. Valves are opened to allow oxygen and acetylene to enter the combustion chamber of the gun. The mixture is then detonated by the sparks from spark plugs and an explosion occurs immediately. The temperature of the detonation fuel is about 3800°C , and it is a sufficiently high temperature to melt most of the materials. Immediately after the detonation, hot particles (undergoing melting) rush toward the target at a very high velocity. This factor is very important for having a well-bonded, dense coating. Detonation cycles are repeated four to eight times per second and nitrogen gas is used to flush out the combustion products after each cycle. This process produces very loud noise, and therefore the spraying is conducted inside a sound proof room. It also requires an elaborate arrangement for fuel and purge gas control, powder feeding, gun cooling and spark plug operation [5, 27, 28]. Using this technique metals,

alloys and ceramics can be melted .Well bonded and dense coating can be produced. But the process is expensive and involves very elaborate arrangement. The process also produces loud noise.

2.3.6d High Velocity Oxy-Fuel Spraying (HVOF)

The arrangement is shown in Figure 2.6. Oxygen and fuel gas (propylene or hydrogen) mixture is introduced in the combustion chamber of the gun. It lights into a flame when ignited and the burnt gas acquires a very high temperature and escapes from the confinement of the small chamber at a high velocity in the process of expansion. The flame is at right angle to the muzzle of the gun. From one end of the gun, powder is fed in the center of the flame by a carrier gas. The particles melt and are immediately carried to the target by the gas, escaping at a very high velocity through the nozzle of the gun [31, 32, 33] .

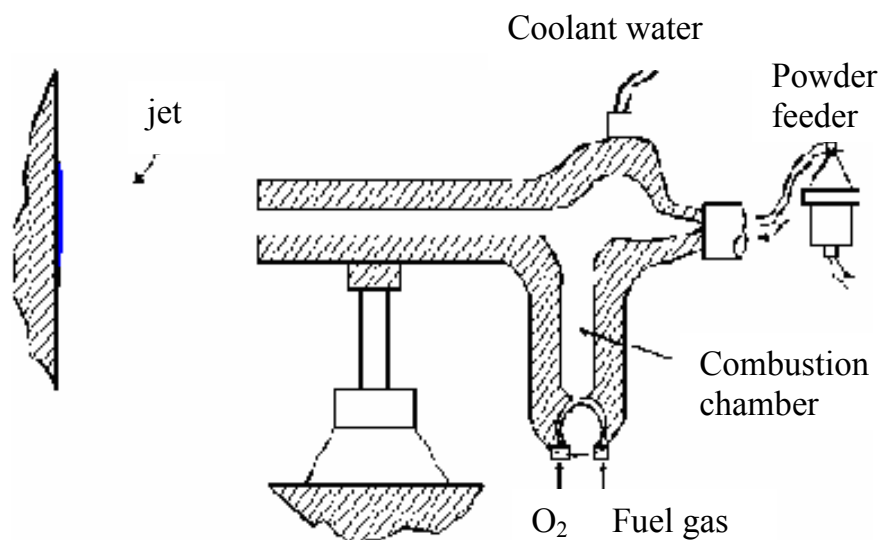


Fig. 2.6 Arrangement for the HVOF spraying

Advantages of this spraying technique include good substrate-coating adhesion, high coating density. It is applicable to both metals and ceramics. It involves less set up cost as compared to plasma or detonation gun.

2.3.6e Electric Arc Spraying

The arrangement is shown in Figure 2.7.

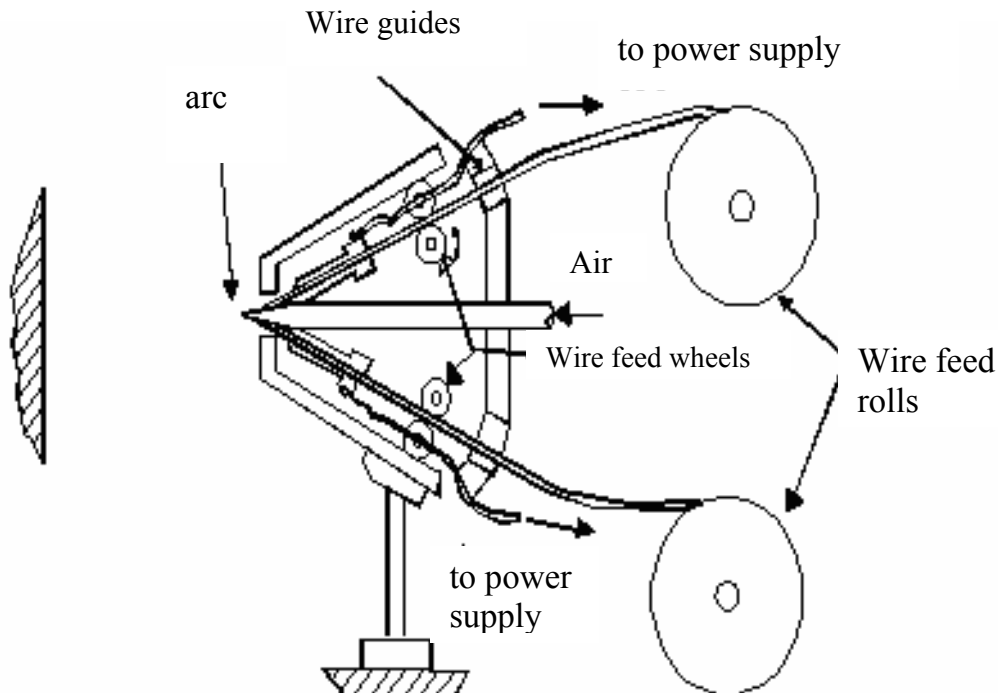


Fig. 2.7 Arrangement for the electric arc spraying

An electric arc is created between the tips of two conducting wires. The heat produced melts the tips and these molten tips are dislodged and directed to a target by a compressed air jet. The wires are fed by the independent wire feed mechanisms. Electric power is supplied by a rugged welding power supply. The process is capable of spraying at a very high deposition rate [5, 34]. The set up for electric arc spraying is simple and cheap. But only conducting materials can be sprayed. The substrate-coating adhesion and density is not comparable to plasma spraying or detonation gun.

2.3.6f Plasma Spraying

Plasma spraying is the most versatile thermal spraying process and the general arrangement is shown in Figure 2.8. An arc is created between tungsten tipped copper cathode and an annular copper anode (both water cooled). Plasma generating gas is forced to pass through the annular space between the electrodes. While passing through the arc, the gas undergoes ionization in the high temperature environment resulting plasma. The ionization is achieved by collisions of electrons of the arc with the neutral molecules of the gas. The plasma protrudes out of the electrode encasement in the form of a flame. The consumable material, in the powdered form, is poured into the flame in metered quantity. The powders melt immediately and absorb the momentum of the expanding gas and rush towards the target to form a thin deposited layer. The next layer deposits onto the first immediately after, and thus the coating builds up layer by layer [3, 5, 24, 30]. The temperature in the plasma arc can be as high as 10,000⁰C and it is capable of melting anything. Elaborate cooling arrangement is required to protect the plasmatron (i.e., the plasma generator) from excessive heating. The equipment consists of the following modules [35].

- The plasmatron : It is the device which houses the electrodes and in which the plasma reaction takes place. It has the shape of a gun and it is connected to the water cooled power supply cables, powder supply hose and gas supply hose.
- The power supply unit : Normally plasma arc works in a low voltage (40-70 volts) and high current (300-1000 Amperes), DC ambient. The available power (AC, 3 phase, 440 V) must be transformed and rectified to suit the reactor. This is taken care of by the power supply unit.

- The powder feeder : The powder is kept inside a hopper. A separate gas line directs the carrier gas which fluidizes the powder and carries it to the plasma arc. The flow rate of the powder can be controlled precisely.
- The coolant water supply unit : It circulates water into the plasmatron, the power supply unit, and the power cables. Units capable of supplying refrigerated water are also available.
- The control unit : Important functions (current control, gas flow rate control etc.) are performed by the control unit. It also consists of the relays and solenoid valves and other interlocking arrangements essential for safe running of the equipment. For example the arc can only be started if the coolant supply is on and water pressure and flow rate is adequate.

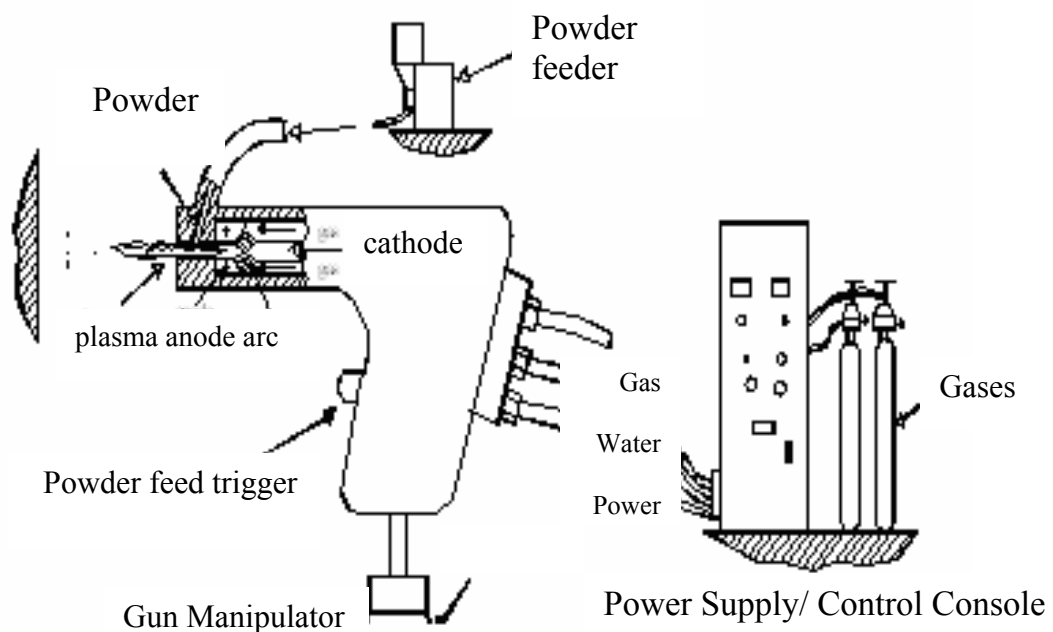


Fig. 2.8 Arrangement for the plasma spraying

The Requirements for Plasma Spraying

Roughness of the substrate surface : A rough surface provides a good coating adhesion. A rough surface provides enough room for anchorage of the splats facilitating bonding through mechanical interlocking. A rough surface is generally created by shot blasting technique. The shots are kept inside a hopper, and compressed air is supplied at the bottom of the hopper. The shots are taken afloat by the compressed air stream into a hose and ultimately directed to an object kept in front of the exit nozzle of the hose. The shots used for this purpose are irregular in shape, highly angular in nature, and made up of hard material like alumina, silicon carbide, etc. Upon impact they create small craters on the surface by localized plastic deformation, and finally yield a very rough and highly worked surface. The roughness obtained is determined by shot blasting parameters, i.e., shot size, shape and material, air pressure, standoff distance between nozzle and the job, angle of impact, substrate material etc. [36] . The effect of shot blasting parameters on the adhesion of plasma sprayed alumina has been studied [33, 37]. Mild steel serves as the substrate material. The adhesion increases proportionally with surface roughness and the parameters listed above are of importance. A significant time lapse between shot blasting and plasma spraying causes a marked decrease in bond strength [38].

Cleanliness of the substrates: The substrate to be sprayed on must be free from any dirt or grease or any other material that might prevent intimate contact of the splat and the substrate. For this purpose the substrate must be thoroughly cleaned (ultrasonically, if possible) with a solvent before spraying. Spraying must be conducted immediately after shot blasting and cleaning. Otherwise on the nascent surfaces, oxide layers tend to grow quickly and moisture may also affect the surface. These factors deteriorate the coating quality drastically [38].

Bond coat : Materials like ceramic cannot be sprayed directly onto metals, owing to a large difference between their thermal expansion coefficients. Ceramics have a much lower value of α and hence undergo much less shrinkage as compared to the metallic base to form a surface in compression. If the compressive stress exceeds a certain limit, the coating gets peeled off. To alleviate this problem a suitable material, usually metallic of intermediate value is plasma sprayed on to the substrate followed by the plasma spraying of ceramics. Bond coat may render itself useful for metallic top coats as well. Molybdenum is a classic example of bond coat for metallic top coats. Molybdenum adheres very well to the steel substrate and develops a somewhat rough top surface ideal for the top coat spraying. The choice of bond coats depends upon the application. For example, in wear application, an alumina and Ni-Al top and bond coats combination can be used [39]. In thermal barrier application, CoCrAlY or Ni-Al bond coat [40] and zirconia top coat are popular. Ceramic coatings when subjected to hertzian loading deform elastically and the metallic substrate deforms plastically. During unloading, elastic recovery of the coating takes place, whereas for the metallic substrate a permanent set has already taken place. Owing to this elastoplastic mismatch the coating tends to spall off at the interface. A bond coat can reduce this mismatch as well [41].

Cooling water : For cooling purpose distilled water should be used, whenever possible. Normally a small volume of distilled water is recirculated into the gun and. it is cooled by an external water supply from a large tank. Sometime water from a large external tank is pumped directly into the gun [35] .

Process parameters in plasma spraying

In plasma spraying one has to deal with a lot of process parameters, which determine the degree of particle melting, adhesion strength and deposition efficiency of the powder [42]. Deposition efficiency is the ratio of amount of

powder deposited to the amount fed to the gun. An elaborate listing of these parameters and their effects are reported in the literature [43 - 46].

Some important parameters and their roles are listed below:

Arc power : It is the electrical power drawn by the arc. The power is injected in to the plasma gas, which in turn heats the plasma stream. Part of the power is dissipated as radiation and also by the gun cooling water. Arc power determines the mass flow rate of a given powder that can be effectively melted by the arc.. Deposition efficiency improves to a certain extent with an increase in arc power, since it is associated with an enhanced particle melting [38,43,47]. However, increasing power beyond a certain limit may not cause a significant improvement. On the contrary, once a complete particle melting is achieved, a higher gas temperature may prove to be harmful. In the case of steel, at some point vaporization may take place lowering the deposition efficiency.

Plasma gas: Normally nitrogen or argon doped with about 10% hydrogen or helium is used as a plasma gas. The major constituent of the gas mixture is known as primary gas and the minor is known as the secondary gas. The neutral molecules are subjected to the electron bombardment resulting in their ionization. Both temperature and enthalpy of the gas increase as it absorbs energy. Since nitrogen and hydrogen are diatomic gases, they first undergo dissociation followed by ionization. Thus they need higher energy input to enter the plasma state. This extra energy increases the enthalpy of the plasma. On the other hand, the mono-atomic plasma gases, i.e. argon or helium, approach a much higher temperature in the normal enthalpy range. Good heating ability is expected from them for such high temperature [48]. In addition, hydrogen followed by helium has a very high specific heat, and therefore is capable of acquiring very high enthalpy. When argon is doped with helium the spray cone becomes quite narrow which is especially useful for spraying on small targets.

Carrier gas: Normally the primary gas itself is used as a carrier gas. The flow rate of the carrier gas is an important factor. A very low flow rate cannot convey the powder effectively to the plasma jet, and if the flow rate is very high then the powders might escape the hottest region of the jet. There is an optimum flow rate for each powder at which the fraction of unmelted powder is minimum and hence the deposition efficiency is maximum [43].

Mass flow rate of powder : Ideal mass flow rate for each powder has to be determined. Spraying with a lower mass flow rate keeping all other conditions constant results in under utilization and slow coating buildup. On the other hand, a very high mass flow rate may give rise to an incomplete melting resulting in a high amount of porosity in the coating. The unmelted powders may bounce off from the substrate surface as well keeping the deposition efficiency low [42, 43].

Torch to base distance : It is the distance between the tip of the gun and the substrate surface. A long distance may result in freezing of the melted particles before they reach the target, whereas a short standoff distance may not provide sufficient time for the particles in flight to melt [38, 43]. The relationship between the coating properties and spray parameters in spraying alpha alumina has been studied in details [49]. It is found that the porosity increases and the thickness of the coating (hence deposition efficiency) decreases with an increase in standoff distance. The usual alpha-phase to gamma-phase transformation during plasma spraying of alumina has also been restricted by increasing this distance. A larger fraction of the unmelted particles go in the coating owing to an increase in torch to base distance.

Spraying angle: This parameter is varied to accommodate the shape of the substrate. In coating alumina on mild steel substrate, the coating porosity is found to increase as the spraying angle is increased from 30° to 60°. Beyond 60° the porosity level remains unaffected by a further increase in spraying

angle [50]. The spraying angle also affects the adhesive strength of the coating [51, 52]. The influence of spraying angle on the cohesive strength of chromia, zirconia 8-wt% yttria and molybdenum has been investigated, and it has been found that the spraying angle does not have much influence on the cohesive strength of the coatings [53].

Substrate cooling: During a continuous spraying, the substrate might get heated up and may develop thermal-stress related distortion accompanied by a coating peel-off. This is especially true in situations where thick deposits are to be applied. To harness the substrate temperature, it is kept cool by an auxiliary air supply system. In addition, the cooling air jet removes the unmelted particles from the coated surface and helps to reduce the porosity [38].

Powder related variables: These variables are powder shape, size and size distribution, processing history, phase composition etc. They constitute a set of extremely important parameters. For example, in a given situation if the powder size is too small it might get vaporized. On the other hand a very large particle may not melt substantially and therefore will not deposit. The shape of the powder is also quite important. A spherical powder will not have the same characteristics as the angular ones, and hence both could not be sprayed' using the same set of parameters [30, 54, 55].

Preheating of the substrate: The nascent shot blasted surface of the substrate absorbs water and oxygen immediately after shot blasting. Before spraying, the substrate should be preheated to remove moisture from the surface and also for a sputter cleaning effect of the surface by the ions of the plasma [38].

Angle of powder injection: Powders can be injected into the plasma jet perpendicularly, coaxially, or obliquely. The residence time of the powders in the plasma jet will vary with the angle of injection for a given carrier gas flow rate. The residence time in turn will influence the degree of melting of a given

powder. For example, to melt high melting point materials a long residence time and hence oblique injection may prove to be useful. The angle of injection is found to influence the cohesive and adhesive strength of the coatings as well [3,35].

2.4 WEAR RESISTANT COATINGS

Today a variety of materials, e.g., carbides, oxides, metallic, etc., belonging to the above category are available commercially. The wear resistant coatings can be classified into the following categories: [3]

- (i) Carbides: WC, TiC, SiC, ZrC, Cr₂C₃ etc.
- (ii) Oxides: Al₂O₃, Cr₂O₃, TiO₂, ZrO₂ etc.
- (iii) Metallic: NiCrAlY, Triballoy etc.
- (iv) Diamond

The choice of a material depends on the application. However, the ceramic coatings are very hard and hence on an average offer more abrasion resistance than their metallic counterparts.

2.4.1 Carbide Coatings

Amongst carbides, WC is very popular for wear and corrosion applications [56]. The WC powders are clad with a cobalt layer. During spraying the cobalt layer undergoes melting and upon solidification form a metallic matrix in which the hard WC particles remain embedded. Spraying of WC-Co involves a close control of the process parameters such that only the cobalt phase melts without degrading the WC particles. Such degradation may occur in two ways:

- Oxidation of WC leading to the formation of CoWO₄ and WC₂ [57].
- Dissolution of WC in the cobalt matrix leading to a formation of brittle phases like CoW₃C which embrittles the coating [58].

An increase in the spraying distance and associated increase of time in flight lead to a loss of carbon and a pickup of oxygen. As a result the hardness of the coating decreases [59]. An increase in plasma gas flow rate reduces the dwell time and hence can control the oxidation to some extent. However, it increases the possibility of cobalt dissolution in the matrix [60]. The other option to improve the quality of such coating is to conduct the spraying procedure in vacuum [58].

Often carbides like TiC, TaC and NbC are provided along with WC in the cermet to improve upon the oxidation resistance, hardness, and hot strength. Similarly the binder phase is also modified by adding chromium and nickel with cobalt [3]. The wear mechanism of plasma sprayed WC-Co coatings depends on a number of factors, e.g., mechanical properties, cobalt content, experimental conditions, mating surfaces, etc. The wear mode can be abrasive, [61, 62, 63] adhesive or surface fatigue [64, 65]. The coefficient of friction of WC-Co (in self mated condition) increases with increasing cobalt content [64]. A WC-Co coating when tested at a temperature of 450°C exhibits signs of melting [66]. The wear resistance of these coatings also depends on porosity [62]. Pores can also act as source from where the cracks may grow. Thermal diffusivity of the coatings is another important factor. In narrow contact regions, an excessive heat generation may occur owing to rubbing. If the thermal diffusivity of the coating is low the heat cannot escape from a narrow region easily resulting a rise in temperature and thus failure occurs owing to thermal stress [62, 66]. The wear mechanism of WC-Co nanocomposite coating on mild steel substrates has been studied in details [67]. The wear rates of such coatings are found to be much greater than that of commercial WC-Co composite coating, presumably owing to an enhanced decomposition of nanoparticles during spraying. Wear has been found to occur by subsurface cracking along the preferred crack paths provided by the binder phase or failure at the inter-splat boundary.

Coatings of TiC or TiC+ TaC with a nickel cladding are alternative solutions for wear and corrosion problems. High temperature stability, low coefficient of thermal expansion, high hardness and low specific gravity of these coatings may outperform other materials, especially in steam environment [3]. Instead of nickel, nickel chromium alloy can serve as the matrix material [68, 69]. The mode of wear can be adhesive, abrasive, surface fatigue or micro-fracture depending on operating conditions [65, 69].

A coating of Cr_3C_2 (with Ni-Cr alloy cladding) is known for its excellent sliding wear resistance and superior oxidation and erosion resistance, though its hardness is lower than that of WC [3]. After spraying in air, Cr_3C_2 loses carbon and transforms to Cr_7C_3 . Such transformation generally improves hardness and erosion resistance of the coating [70]. The sliding wear behaviour of the Cr_3C_2 -Ni -Cr composite has been studied by several authors against various metals and ceramics [62, 65, 71]. It is felt that at lower loads the wear is owing to the detachment of splats from the surface. As the load increases, melting, plastic deformation and shear failure come into play.

2.4.2 Oxide Coatings

Metallic coatings and metal containing carbide coatings sometime are not suitable in high temperature environments in both wear and corrosion applications. Often they fail owing to oxidation or decarburization. In such case the material of choice can be an oxide ceramic coating, e.g., Al_2O_3 . Cr_2O_3 , TiO_2 , ZrO_2 or their combinations. However, a high wear resistance, and chemical and thermal stability of these materials are counterbalanced by the disadvantages of low values of thermal expansion coefficient, thermal conductivity, mechanical strength, fracture toughness and somewhat weaker adhesion to substrate material. The thickness of these coatings is also limited by the residual stress that grows with thickness. Therefore, to obtain a good quality coating it is

essential to exercise proper choice of bond coat, spray parameters and reinforcing additives [3].

2.4.2a Chromia (Cr_2O_3) Coatings

These coatings are applied when corrosion resistance is required in addition to abrasion resistance. It adheres well to the substrate and shows an exceptionally high hardness 2300 HV_{0.5 kg} [3]. Chromia coatings are also useful in ship and other diesel engines, water pumps, and printing rolls [3]. A Cr_2O_3 - 40 wt% TiO_2 coating provides a very high coefficient of friction (0.8), and hence can be used as a brake liner [3]. The wear mode of chromia coatings has been investigated under various conditions. Depending on experimental conditions, the wear mode can be abrasive [64], plastic deformation [65, 66, 72], microfracture [73] or a conglomerate of all of these [74]. This material has also been tested under lubricated conditions, using inorganic salt solutions (NaCl , NaNO_3 , Na_3PO_4) as lubricants and also at a high temperature. The wear rate of self-mated chromia is found to increase considerably at 450°C, and plastic deformation and surface fatigue are the predominant wear mechanisms [75]. Under lubricated condition, the coatings exhibit tribochemical wear [76]. It has also been tested for erosion resistance [77].

2.4.2b Zirconia (ZrO_2) Coatings

Zirconia is widely used as a thermal barrier coating. However, it is endowed with the essential qualities of a wear resistant material, i.e., hardness, chemical inertness, etc. and shows reasonably good wear behaviour. In the case of a hot pressed zirconia mated with high chromium containing iron (martensitic, austenitic, or pearlitic), it has been found that in course of rubbing the iron transfers on to the ceramic surface and the austenitic material adheres well to the ceramic as compared to their martensitic or pearlitic counterparts [78]. The thick film improves the heat transfer from the contact area keeping the contact

temperature reasonably low; thus the transformation of ZrO_2 is prevented. On the other hand with the pearlitic or martensitic iron the material transfer is limited. The contact temperature is high enough to bring about a phase transformation and related volume change in ZrO_2 causing a stress induced spalling. In a similar experiment the wear behaviour of sintered, partially stabilized zirconia (PSZ) with 8 wt% yttria against PSZ and steels has been tested at 200°C. When metals are used as the mating surface, a transferred layer soon forms on the ceramic surface (coated or sintered) [79]. In ceramic-ceramic system the contact wear is abrasive in nature. However, similar worn particles remain entrapped between the contact surfaces and induce a polishing wear too. In the load range of 10 to 40 N, no transformation of ZrO_2 occurs [79, 80]. However, similar tests conducted at 800°C show a phase transformation from monoclinic ZrO_2 to tetragonal ZrO_2 [81]. The wear debris of ZrO_2 sometimes get compacted in repeated loading and gets attached to the worn surface forming a protective layer [82]. During rubbing, pre-existing or newly formed cracks may grow rapidly and eventually interconnect with each other, leading to a spallation of the coating [83]. The worn particles get entrapped between the mating surfaces and abrade the coating. The wear performance of ZrO_2 -12 mol% CeO_2 and ZrO_2 -12 mol% CeO_2 -10 mol% Al_2O_3 coatings against a bearing steel under various loads has been studied [84]. Introduction of alumina as a dopant, has been found to improve the wear performance of the ceramic significantly. Here plastic deformation is the main wear mode. The wear performance of zirconia at 400°C and 600°C has been reported in the literature [85]. At these temperatures the adhesive mode of wear plays the major role.

2.4.2c Titania (TiO_2) Coating

Titania coating is known for its high hardness, density, and adhesion strength [62, 65]. It has been used to combat abrasive, erosive and fretting wear either in essentially pure form or in association with other compounds [86, 87]. The

mechanism of wear of TiO₂ at 450°C under both lubricated and dry contact conditions has been studied [65, 66]. It has been found to undergo a plastic smearing under lubricated contact, where as it fails owing to the surface fatigue in dry condition. TiO₂-stainless steel couples in various speed load conditions have also been investigated in details [88]. At a relatively low load, the failure is owing to the surface fatigue and adhesive wear, whereas at a high load the failure is attributed to the abrasion and delamination associated with a back and forth movement [89]. At low speed the transferred layer of steel oxidizes to form Fe₂O₃ and the wear progresses by the adhesion and surface fatigue. At a high speed, Fe₃O₄ forms instead of Fe₂O₃ [90]. The TiO₂ top layer also softens and melts owing to a steep rise in temperature, which helps in reducing the temperature subsequently [91]. The performance of the plasma sprayed pure TiO₂ has been compared with those of Al₂O₃ – 40 wt% TiO₂ and pure Al₂O₃ under both dry and lubricated contact conditions [92]. TiO₂ shows the best results. TiO₂ owing to its relatively high porosity can provide good anchorage to the transferred film and also can hold the lubricants effectively [93].

2.4.2d Alumina (Al₂O₃) Coatings

Alumina is obtained from a mineral called bauxite, which exists in nature as a number of hydrated phases, e.g., boehmite (γ -Al₂O₃, H₂O), hydrargillate , diaspore (α -Al₂O₃. 3H₂O). It also exists in several other metastable forms like β , δ , θ , η , κ and X [94]. α -Al₂O₃ is known to be a stable phase and it is available in nature in the form of corundum. In addition, α -Al₂O₃ can be extracted from the raw materials by fusing them.

The phase transformation during freezing of the plasma sprayed alumina droplets has been studied in details [95, 96]. From the molten particles, γ -Al₂O₃ tends to nucleate, since liquid to γ transformation involves a low interfacial energy. The phase finally formed upon cooling depends on the particle diameter. For particle diameter less than 10 μ m, the metastable form is retained

(γ , δ , β or θ). Plasma spraying of alumina particles having a mean diameter of 9 μm results in the development of the gamma phase in the coating after cooling [97]. The α form is found in the large diameter particle. In fact larger is the diameter; greater is the fraction of $\alpha\text{-Al}_2\text{O}_3$ in the cooled solid. This form is desirable for its superior wear properties. Other than the cooling rate, one way to achieve the phase finally formed is to vary the temperature of the substrate. If the substrate temperature is kept at 900°C , the δ phase forms. The $\alpha\text{-Al}_2\text{O}_3$ can be formed by raising the temperature of the substrate to 1100°C resulting a slow cooling. During freezing the latent heat of solidification is absorbed in the still molten pool. If this heat generation is balanced by the heat transfer to the substrate, columnar crystals grow. On the other hand, if the aforesaid heat transfer is faster than the heat injection rate from the growing solidification front, equi-axed crystals are supposed to form. In reality columnar crystals are generally found.

There are several advantages of alumina as a structural material, e.g., availability, hardness, high melting point, resistance to wear and tear etc. It bonds well with the metallic substrates when applied as a coating on them. Some of the applications of alumina are in bearings, valves, pump seals, plungers, engine components, rocket nozzles, shields for guided missiles, vacuum tube envelops, integrated circuits, etc. Plasma sprayed alumina-coated railroad components are presently being used in Japan [98].

Properties of alumina can be further complemented by the particulate (TiO_2 , TiC) or whisker (SiC) reinforcement [99]. TiC reinforcement limits the grain growth, improves strength and hardness, and also retards crack propagation through the alumina matrix [100]. The sliding wear behaviour of both monolithic and SiC whisker reinforced alumina has been studied [101]. The whisker reinforced composite has been found to have good wear resistance. The monolithic alumina has a brittle response to sliding wear, whereas the

worn surface of the composite reveals signs of plastic deformation along with fracture. The whiskers also undergo pullout or fracture.

TiO₂ is a commonly used additive in plasma sprayable alumina powder [102, 103]. TiO₂, has a relatively low melting point and it effectively binds the alumina grains. However, a success of an Al₂O₃ - TiO₂ coating depends upon a judicious selection of the arc current, which can melt the powders effectively. This results in a good coating adhesion along with high wear resistance [47]. The wear performance of Al₂O₃ and Al₂O₃ -50 wt% TiO₂ has been reported in the literature [92]. In dry sand abrasion testing, alumina outperformed others presumably owing to its high hardness [104]. In dry sliding at low velocity range, the tribocouple (ceramic and hardened stainless steel) exhibits stick-slip [105]. At relatively high speed range, the coefficient of friction drops owing to the thermal softening of the interface [91]. The wear of alumina is found to increase appreciably beyond a critical speed and a critical load. Alumina has been found to fail by plastic deformation, shear and grain pullout. In dry and lubricated sliding as well, the mixed ceramic has been found to perform better than pure alumina. A coating of Al₂O₃ -50 wt% TiO₂ is quite porous and hence is quite capable of holding the transferred metallic layer which protects the surface [93]. Wear performance of such coatings can further be improved by a sealing of the pores by polymeric substances [39]. A low thermal diffusivity of the alumina coatings results in a high localized thermal stress on the surface. The mode of wear of alumina is mainly abrasive. The pore size and pore size distribution also play a vital role in determining the wear properties. The Al₂O₃ - TiO₂ coating has a high thermal diffusivity and hence it is less prone to wear.

The sliding wear behaviour of plasma sprayed alumina against AISI-D2 steel under different speed load conditions has been reported [106]. Within the load range used (45N-133N), the wear vs load plot shows a maxima. In the initial phase, the wear volume increases with the load for a given number of sliding cycles. Beyond a certain load, owing to both load and frictional heating, a

major plastic flow occurs on the coating surface. The plastic flow leads to an increase in real area of contact and a corresponding reduction of normal stress, though the normal load increases [107]. As a result, wear decreases with an increase in load beyond a critical normal load. On the other hand, the wear vs. sliding speed plot also displays a maxima within the speed range used (0.31 to 8 m/s). At a low speed range, the asperities move against each other and deform each other in the process. As the speed is increased, the asperities are subjected to heavy impacts and tend to get fractured from the root producing a higher volume of debris. At a very high velocity the friction related temperature rise becomes high enough to soften the asperities and thereby to protect them from fracture. The wear rate keeps low under such circumstances. Therefore, the plastic deformation and brittle fracture form the failure mechanisms.

2.4.3 Metallic Coatings

Metallic coatings can be easily applied by flame spraying or welding techniques making the process very economical. Moreover plasma sprayable metallic consumables are also available in abundant quantity. Metallic wear resistant materials are classified into three categories:

- (i) cobalt based alloys
- (ii) nickel based alloys
- (iii) iron based alloys

The common alloying elements in a cobalt-based alloy are Cr, Mo, W and Si. The microstructure is constituted by dispersed carbides of M_7C_3 type in a cobalt rich FCC matrix. The carbides provide the necessary abrasion resistance and corrosion resistance. Hardness at elevated temperatures is retained by the matrix [108, 109]. Sometimes a closed packed intermetallic compound is formed in the matrix, which is known as the Laves phase. This phase is relatively soft but offers significant wear resistance [110]. The principal alloying elements in Ni-based alloys are Si, B, C and Cr. The abrasion

resistance can be attributed to the formation of extremely hard chromium borides. Besides carbides, Laves phase is also present in the matrix [108].

Iron based alloys are classified into pearlitic steels, austenitic steels, martensitic steels and high alloy irons. The principal alloying elements used are Mo, Ni, Cr and C. The softer materials, e.g., ferritic, are for rebuilding purpose. The harder materials, e.g., martensitic, on the other hand provide wear resistance. Such alloys do not possess much corrosion, oxidation or creep resistance [108, 111, 112]. Nickel aluminide is another example of coating material for wear purpose. The prealloyed Ni-Al powders, when sprayed, react exothermically to form nickel aluminide. This reaction improves the coating substrate adhesion. In addition to wear application, it is also used as bond coat for ceramic materials [40].

NiCoCrAlY is an example of plasma sprayable superalloy. It shows an excellent high temperature corrosion resistance and hence finds application in gas turbine blades. The compositional flexibility of such coatings permits tailoring of such coating composition for both property improvement and coating substrate compatibility. In addition, it serves as a bond coat for zirconia based thermal barrier coatings [3, 113].

2.4.4 Diamond Coatings

Thin diamond films for industrial applications are commonly produced by CVD, plasma assisted CVD, ion beam deposition, and laser ablation technique [114, 115]. Such coatings are used in electronic devices and ultra wear resistant overlays. The limitation of the aforesaid methods is their slow deposition rates. The DIA-JET process involving a DC Ar/H₂ plasma with methane gas supplied at the plasma jet is capable of depositing diamond films at a high rate [116]. However, the process is extremely sensitive to the process parameters. Deposition of diamond film is also possible using a oxy-acetylene torch [117].

One significant limitation of a diamond coating is that it cannot be rubbed against ferrous materials, owing to a phase transformation leading to the formation of other carbon allotropes [118]. Diamond films are tested for the sliding wear against abrasive papers, where wear progresses by micro fracturing of protruding diamond grits. The process continues till the surface becomes flat and thereafter wear progresses by an interfacial spalling. Therefore, the life of the coating is limited by its thickness [119].

2.5 EROSION WEAR OF CERAMIC COATINGS

Solid Particle Erosion (SPE) is a wear process where particles strike against surfaces and promote material loss. During flight a particle carries momentum and kinetic energy, which can be dissipated during impact, due to its interaction with a target surface. Different models have been proposed that allow estimations of the stresses that a moving particle will impose on a target [120]. It has been experimentally observed by many investigators that during the impact the target can be locally scratched , extruded , melted and/or cracked in different ways [121, 122, 123] . The imposed surface damage will vary with the target material, erodent particle, impact angle, erosion time, particle velocity, temperature and atmosphere [121, 124] .

Plasma sprayed coatings are used today as erosion or abrasion resistant coatings in a wide variety of applications [125] . Extensive research shows that the deposition parameters like energy input in the plasma and powder properties affect the porosity, splat size, phase composition, hardness etc. of plasma sprayed coatings [126 - 130] . These in turn, have an influence on the erosion wear resistance of the coatings. Quantitative studies of the combined erosive effect of repeated impacts are very useful in predicting component lifetimes, in comparing the performance of materials and also in understanding the underlying damage mechanisms involved.

Resistance of engineering components encountering the attack of erosive environments during operation can be improved by applying ceramic coatings on their surfaces. Alonso et. al. [131] experimented with the production of plasma sprayed erosion-resistant coatings on carbon-fiber-epoxy composites and the studied of their erosion behaviour. The heat sensitivity of the composite substrate requires a specific spraying procedure in order to avoid its degradation. In addition, several bonding layers were tried to allow spraying of the protective coatings. Two different functional coatings; a cermet (WC-12 Co) and a ceramic oxide (Al_2O_3) were sprayed onto an aluminium-glass bonding layer. The microstructure and properties of these coatings were studied and their erosion behaviour determined experimentally in an erosion-testing device. Tabakoff and Shanov [132] designed a high temperature erosion test facility to provide erosion data in the range of operating temperatures experienced in compressors and turbines. In addition to the high temperatures, the facility properly simulates all the erosion parameters important from the aerodynamics point of view. These include particle velocity, angle of impact, particle size, particle concentration and sample size. They reported the erosion behavior of titanium carbide coating exposed to fly ash and chromite particles. Chemical vapor deposition technique (CVD) was used to apply a ceramic coating on nickel and cobalt based super-alloys (M246 and X40). The test specimens were exposed to particle-laden flow at velocities of 305 and 366 ms^{-1} and temperatures of 550°C and 815°C.

A good number of reports are available on erosion behaviour of alumina coatings. The resistance to erosion of such coatings depends upon intersplat cohesion, shape, size, and hardness of erodent particles, particle velocity, angle of impact and the presence of cracks and pores [133 -137]. The slurry (SiC and SiO_2) and airborne particle (Al_2O_3 and SiO_2) erosions of flame sprayed alumina coatings have also been reported in the literature [91]. SiC and Al_2O_3 are found to cause significant amount of erosion in slurry and airborne erosion testing respectively. High particle velocity enhances the erosion rate and the erosion

rate is maximum for an impact angle of 90^0 . The failure is by the progressive removal of splats and can be attributed to the presence of defects and pores in the inter-splat regions. Similar observation has been made for the plasma sprayed alumina coatings subjected to an erosive wear caused by the SiO_2 particles [138].

Branco *et. al.* [139] examined room temperature solid particle erosion of zirconia and alumina-based ceramic coatings, with different levels of porosity and varying microstructure and mechanical properties. The erosion tests were carried out by a stream of alumina particles with an average size of $50\ \mu\text{m}$ at 70m/s , carried by an air jet with impingement angle of 90^0 . The results indicate that there is a strong relationship between the erosion rate and the coating porosity.

2.6 PRESENT STATUS OF RED MUD UTILIZATION

Aluminium metal is commercially produced from bauxite ore through two main process steps. In the first step alumina is obtained by the Bayer's process [140] and in the second step the alumina is electrolysed in a Hall-Heroult cell [141] to yield aluminum metal. Production of alumina from bauxite by the Bayer's process is associated with the generation of red mud as the major waste material. Depending upon the quality of bauxite, the quantity of red mud generated varies from 55-65% of the bauxite processed. The enormous quantity of red mud discharged by industries producing alumina poses an environmental and economical problem. The treatment and disposal of this residue is a major operation in an alumina plant.

Red mud, as the name suggests, is brick red in colour and slimy having average particle size of about $80\ \mu\text{m}$. It comprises of the iron, titanium and the silica part of the parent ore along with other minor constituents. It is alkaline, thixotropic and possesses high surface area in the range of $13\text{-}16\ \text{m}^2/\text{g}$ with a

true density of 3.30g/cc. The leaching chemistry of bauxite suggests that the physical and chemical properties of red mud depend on the bauxite used and the manner in which the bauxite is processed. Residues from different bauxite have a wide range of composition: Fe₂O₃ 20-60%, Al₂O₃ 10-30%, SiO₂ 2-20%, Na₂O 2-10%, CaO 2-8%, TiO₂ traces – 28%. Detailed characterization of red mud generated from NALCO aluminum refinery at Damanjodi, India is reported by Mohapatra *et al.* [142] and of some other sources by various authors [143, 144, 145]. The important parameters which have significance in its further handling, disposal and use are: (i) moisture content, (ii) rheology, (iii) surface area, (iv) particle size, (v) mineralogy, (vi) contents of valuable metals, (vii) presence of rare earth metals, (viii) presence of toxic substances etc.

Country		Major constituents, wt %				
		Fe ₂ O ₃	Al ₂ O ₃	TiO ₂	SiO ₂	Na ₂ O
India	Al. Corpn.	20.26	19.60	28.00	6.74	8.09
	MALCO	45.17	27.00	5.12	5.70	3.64
	HINDALCO	35.04	23.00	17.20	5.00	4.85
	BALCO	33.80	15.58	22.50	6.84	5.20
	NALCO	52.39	14.73	3.30	8.44	4.00--
Hungary		38.45	15.20	4.60	10.15	8.12
Jamaica		50.9	14.20	6.87	3.40	3.18
Surinam		24.81	19.00	12.15	11.90	9.29
USA	ALCOA Mobile	30.40	16.20	10.11	11.14	2
	Arkansas	55.6	12.15	4.5	4.50	1.5-
	Sherwon	50.54	11.13	Traces	2.56	9.00
FRG Baudart		38.75	20.00	5.5	13.00	8.16
Taiwan		41.30	20.21	2.90	17.93	3.8
Australia		40.50	27.70	3.50	19.90	1-2

Table 2.1 Composition of red mud generated in alumina plants of different parts of the world

Composition of red mud samples from some randomly selected locations is given in table 2.1 [146]

Till today, almost all over the world, red mud is disposed off the plant site in two main ways depending on the facilities available and the surroundings. In countries such as France, England, Germany or Japan where availability of land for dumping is less and sea is nearby; the practice is to discharge the mud into the sea. Where free land is available nearby, the mud is pumped into pools and ponds constructed for this purpose.

Probably the easiest use for the mud is some sort of useful landfill instead of just dumping. Some such attempts in this direction are: filling material for mined or quarrying areas, land fill cover, road bed and levee material, alternative to natural marsh sediment, agricultural land soil neutralization, composting domestic waste etc. For use in many of these areas some sort of neutralization or red mud amendment becomes necessary. A brief description of these uses is presented below.

Bauxite mines or other quarries are being filled up by red mud. For this purpose the slurry should be neutralized and high solids pipeline transportation is necessary. Considerable progress has been made on the latter aspect. For neutralization lime, gypsum, sea water or other materials having similar neutralization properties is mixed with the red mud. In Australia and Hungary neutralization is done by adding gypsum after which the red mud is called red mud amended with gypsum [147]. Recently, Galarraga *et al.* [148] successfully pilot tested neutralization of red mud pulp from 12.20 to 7.60 pH by using carbon dioxide. Mine filling is a good use though the values (metal) in red mud are left to be recovered in future. Good progress has been reported by Kirkpatrick and Brown [149] and Kirkpatrick [150] in this regard. After caustic neutralization, red mud and local clay mixtures have been successfully used as land covers.

Brown and Kirkpatrick [149] have again reported use of red mud as roadbed and levee material. Using its compactibility to good effect, disced red mud was stacked and then compressed by heavy equipment to form hard road surfaces on the mud lake, which are used extensively to support the large trucks carrying the landfill cover and to move equipments around the lake. A study at Tulane University by Goldstein and Reimers [151] has shown that over 25 square miles of Louisiana wetlands are lost per year due to sediment starvation, coastal erosion and subsidence. Quite often the dredged sediments are found polluted and unsuitable for placement in the wetlands. Red mud, in this case, has been proposed to be a suitable alternative.

A lot of efforts are being made globally to find out suitable uses of red mud so that alumina industry may end up with no residue at all. For complete utilization of red mud, Kovalenko [152] proposed the following avenues :

- Building material production as an additive to cement;
- Production of colouring agent for paint works for ground floors of industrial and other buildings;
- Production of toned paper in the wood-pulp and paper industry;
- Production of iron ore sinter and pellets in the ferrous metallurgy;
- In agriculture for the purpose of improvement of the soil structure and as a micro fertilizer and a neutralizer of pesticides;

Attempts have been made over the years to find a use and studies have been made for usage of red mud as a partial substitute of clay in ceramic products like bricks, tiles etc. [153], as an additive for mortar and concrete [154]. Use of red mud in agricultural applications, such as, in acidic soils or as a treatment for iron deficient soils has also been reported [155]. Numerous other uses for red mud have been reported in the literature, well documented in the book by Thakur and Das [146]. The uses range from making various building materials,

adsorbents, colouring agents to even preparation of exotic ceramic glass materials.

Smirnov *et al.* [156] have proposed a technology of sulfuric acid processing of the deactivated red mud with coagulation and granulation of Fe-Al coagulants followed by burdening, forming and heat treatment to produce the building materials. Red mud can be used as an adsorbent and colouring agent. Martinet-Catalot *et al.* [157] reported its suitability for use as arsenic fixation on co-disposal projects and coloring of various materials . Liu [158] made a study to use red mud to remove toxic materials from wastewater. It indicated that only 0.5 mg/liter of red mud was sufficient for near complete removal of all the metals except selenium at an initial water pH of 8.0 and at retention time as low as one minute. Other authors [159, 160] have reported the use of red mud to adsorb nickel.

Red mud finds some applications in ceramic industries as well. Yalcin and Sevinc [161] experimented with the red mud from Seydischir Aluminium Plant, Turkey and attempted to use it in the making of ceramic glazes such as porcelain, vitreous (sanitary ware glazes), tile and electro porcelain glazes in the ceramic industry. It was found that the addition of up to 37 weight percent of the red mud waste was possible in the production of these glazes. Recently Balasubramanian *et al* [162] used specific mixtures of red mud, fly ash and spent pot liner to prepare glass-ceramic products, which showed excellent properties and aesthetic appearance for possible applications as decorative tiles in the building industry.

A recent experimental study by Mahata *et al.* [163] confirmed formation of Aluminium Titanate-Mullite composite from red mud rich in titanium. This was achieved by preferentially removing Fe_2O_3 from red mud through dilute HCl acid leaching leaving a residue rich in Al_2O_3 , TiO_2 and SiO_2 . Then pure Al_2O_3 powder was added to obtain the required molar ratios. Thus a composite

material consisting of aluminium titanate (Al_2TiO_5) – iron titanate (Fe_2TiO_5) solid solution and mullite ($3\text{Al}_2\text{O}_3 \cdot 2\text{SiO}_2$) phases after final reaction synthesis was obtained. This material has potential uses as liquid metal flow regulators, risers, thermocouple sleeves, burner nozzles, ceramic filters etc.

There can be many such uses for red mud. However, they can take care of only a small fraction of the waste material. For bulk use either the metal extraction processes and/or land fill etc. may be considered.

The analysis presented in table 2.1 shows that iron is the major constituent of red mud followed by Al_2O_3 , Na_2O , SiO_2 and TiO_2 . Of these constituents, recovery of silica is not significant. Titania has the most potential value and if successfully recovered, iron can be obtained as a value added product whereas alumina and alkali can be recycled in the Bayer's process stream. Depending on their amount in red mud, economic extraction of other metals can also be significant. Iron being the major constituent of red mud, much attention has been directed towards its recovery. Studies were initiated as early as in the nineteen fifties. A large number of processes are reported on iron recovery from red mud; either exclusively or in combination with other metals and many of these processes have been patented.

Chlorination of red mud was reported by Laszlo and Lozsef [164] on a sample containing ~ 66% of Fe_2O_3 13.30% Al_2O_3 and 6.1% TiO_2 . At 800°C most of the Fe_2O_3 could be separated as vapour but the residual Fe_2O_3 contaminated the TiO_2 , hampering its whiteness. Chlorination at 900°C converts Al_2O_3 , Fe_2O_3 , TiO_2 and SiO_2 into chlorides. From the mixture of chlorides SiO_2 is separated by addition of Al_2O_3 with the formation of equivalent amount of AlCl_3 . On treatment with TiO_2 , Al_2O_3 was precipitated along with the formation of TiCl_4 . The remaining gaseous mixture of TiCl_4 and FeCl_3 was further treated with Fe_2O_3 to get TiO_2 and FeCl_3 . The FeCl_3 was finally converted to Fe_2O_3 .

Heck [165] suggested a method of preparing Fe powder from red mud by charging red mud from the top of a vertical kiln and reducing gas (H_2 , NH_3 , fuel gas) from the bottom. The iron powder collected from the bottom was less than 10 micron in size. A method reported by Marvin [166] for recovery of Fe, TiO_2 and Al_2O_3 from red mud, used an electric arc furnace with a charge of coke and red mud for reduction of the Fe_2O_3 . The reaction at $1600^{\circ}C - 1700^{\circ}C$ resulted in recovery of 90 % Fe, the Al_2O_3 , TiO_2 and the residual Fe remaining in the slag. A scheme for recovery of iron, alumina, titania and alkali was worked out by Ni [167]. The scheme consisted of electro smelting to produce pig iron of low titania content. Treatment of the slag with concentrated NaOH in the presence of lime under pressure recovered more than 90% Al_2O_3 . Remaining mud was leached with dilute alkali followed by water and after filtration; the titania from the residue was recovered by chlorination.

Watanabe and Yuki [168] patented a method to obtain a pure Fe powder from red mud. The Fe portion of red mud was reduced by hydrogen or carbon monoxide or town gas at $300^{\circ}C - 400^{\circ}C$. Powder iron was separated by magnetic separation. Braithwait [169] has suggested for separation of iron from red mud in slurry form, through application of high intensity magnetic separation. The resulting magnetic product may be an ingredient for iron making or for pigment in pottery industry. But the recovery of iron is low. Another investigation [170] reports the reduction of iron with chlorocarbons before magnetic separation and use of the resulting magnetic portion as feed for iron making.

A study by Mozhareenko and Noskov [171] suggested the possibility of considering red mud for use in the blast furnace practice and steel making after compaction of 3-10 mm fraction with preparation of granules and lumping into briquettes. From experiments carried out on charge materials sintered with addition of granulated red mud, it was found that the compacted red mud in the composition of sinter, could be implemented as the metal and flux containing

additive in the blast furnace practice, steel making and electro-metallurgy. Red mud is a promising binder for different metallurgical wastes.

Some of the more recent studies reported on iron recovery are those by Xiang *et al.* [172], employing low temperature ($< 350^{\circ}\text{C}$) reduction of red mud and by Mishra *et al.* [173], employing a relatively high temperature (650°C - 1050°C) reduction, both followed by magnetic separation . Liu *et al.* [174] used high gradient magnetic separation to remove the hematite from the dried and milled red mud. Since in the bauxite itself the hematite particles are assumed to be reasonably well-liberated, the magnetic separation seems to be feasible in theory. But experimental results have shown the reverse. Even then this technology offers the advantage of low energy and enrichment of the titania content of the mud.

Studies related to the recovery of aluminum and titanium from red mud are mostly part of a scheme for recovery of iron and these two metals. After removing iron, the residue is subjected to various treatments for aluminum and titanium recovery. Accordingly most of the studies reported in literature provide schemes for recovery of these three metals. Dubos *et al.* [175] added 8% CaO to red mud and sintered the product with addition of coke. More than 90% of iron from the sinter was separated by magnetic separation and the non-magnetic slag was further treated with lime and soda and leached to recover 85-90% Na₂O and 75-80% Al₂O₃. Tathavadkar *et al.* [176] have claimed to have developed a novel route for extracting alumina from red mud / bauxite. The process involves roasting of red mud / bauxite with an alkali carbonate in air at temperatures above 1050 K, digestion of the reaction product in water and filtration. From the filtrate containing water-soluble alkali aluminate, Al(OH)₃ is precipitated by adjustment of the solution pH and calcined to yield pure alumina with more than 98% extraction efficiency. Alkali carbonates can be recovered by evaporating the filtrate obtained after removing Al(OH)₃

precipitate. Based on the alkali-roasting technique a zero-waste technology for alumina extraction can be devised.

Kasliwal and Sai [177] have described a process for the enrichment of titanium dioxide in red mud. The method consists of leaching the red mud with hydrochloric acid followed by roasting the leached residue with sodium carbonate. In this process TiO_2 increased from 18% to 36% in the first step and further to 76% after the second step. Sayan and Bayramoglu [178] studied sulphuric acid leaching for treating red mud for TiO_2 recovery.

Recovery of metals other than iron, aluminum and titanium from red mud is not significant in the sense that no constituent is present in appreciable concentration justifying its recovery. However, depending on the bauxite composition, certain constituents may be present in red mud in larger amounts and can be considered for recovery.

Reports have indicated a general strategy to utilize red mud. Rayzman and Filipovich [179] have suggested an integrated method where coal combustion and red mud sintering are combined in the alumina refinery. After soda and alumina recovery the residue can be utilized by metallurgical or chemical technology. Mishra *et al.* [180] also suggested a similar approach with removal of aluminium and soda through sintering and alkali washing stages followed by pyrometallurgy of the residue to get pig iron and a slag rich in titanium. The slag can further be leached with sulphuric acid to recover titanium.

With increased environmental threat it has become necessary to find out alternative uses of such industrial wastes and to develop value added products. Though substantial development has taken place in the area of disposal and utilization of red mud, no report on its use as a potential coating material has been published. As far as the field of ceramic coating is concerned, during last

decade, although a large number of investigations have been carried-out on processing of variety of plasma spray ceramic coatings, not much effort has been made to use low-grade materials for this purpose . In the year 2000, Mishra and Ananthapadmanabhan [181] made the first successful attempt to develop coatings of fly ash and fly ash pre-mixed with aluminium on some metal substrates by plasma spraying . Ramakrishna et. al. [182] reported the coatibility of fly ash on steel substrates by detonation spraying. Still, research/study on development of thermal spray coatings using low grade mineral and/or industrial waste is meager. Industrial wastes like red mud and fly ash, being rich in metal oxides, have tremendous potential to be used as coating materials and this aspect needs to be explored. More so because many of the conventional coating materials are relatively expensive, to the extent that cost of spray grade powders alone can account for even 50-60% of the cost of operating a plasma spray unit. On the contrary, industrial wastes like red mud or fly ash are not only free of cost but also are abundantly available.

Against this background, the present research work has been undertaken, with an objective to explore the coating potential of red mud. It does not belong to the so called plasma sprayable category and being a waste, is cheap. Attempts have been made in this work to deposit red mud coatings on metal substrates at various operating conditions of plasma and to establish their suitability for some typical tribological applications.

The future possesses challenges to the scientists, technologists and engineers towards sound management of industrial wastes like red mud and fly ash through disposal and deposition technologies. It will continue to be an important area of concern in coming years. The present investigation is a step in this direction.

MATERIALS AND METHODS

3.1 INTRODUCTION

This chapter deals with the details of the experimental procedures followed in this study. The coating procedure itself requires some basic preparation, i.e., shot blasting and cleaning. After plasma spraying, the coated materials have been subjected to a series of tests, e.g., microstructural characterization of the surfaces and cross sections, microhardness measurement, X - ray diffraction studies, adhesion test, erosion wear test etc. The details of each process are described here.

3.2 PROCESSING OF THE COATINGS

3.2.1 Powders for Coating

In this study, red mud, fly ash, carbon and aluminium powders are used as raw materials for coating deposition on various substrates. The different combinations of these materials chosen for spraying are listed in Table 3.1 along with the respective particle size ranges.

Red mud emerges, as a by-product from the caustic leaching of bauxites to produce alumina and its major constituents are Fe_2O_3 , Al_2O_3 , SiO_2 , TiO_2 , Na_2O and CaO . It is taken as the primary raw material in this work and is collected

in powder form the alumina plant of National Aluminium Co. (NALCO) located at Damanjodi in the state of Orissa. The as-received powder is sieved to obtain particles in the desired size range i.e. 80 - 100 micron. Raw fly ash is collected from the captive power plant of Rourkela Steel Plant and is similarly sieved in the same particle size range. This serves as the other major raw material for this work.

Carbon (activated charcoal) used in this work is prepared by activating (heating) common wood charcoal at approximately 1000⁰C in the absence of oxygen. This treatment removes residual non-carbon elements and produces a porous internal microstructure having an extremely high surface area. Activated charcoal or activated carbon is an amorphous form of carbon. Common charcoal contains other organic residues, is much less porous and has a lower surface area.

Red mud and fly ash are thoroughly mixed in three different ratios by weight (table 3.1) . Mixtures of red mud and aluminium powder (in 20:1 weight ratio) and red mud and carbon (in 5:1 weight ratio) are also prepared and are used as feed stock in the present work.

Sl. No.	Coating Materials	Mixture Composition
1	Red Mud	Red Mud 100 wt%
2	Red Mud + Fly Ash	Red Mud 90 wt%, Fly Ash 10 wt%
3	Red Mud + Fly Ash	Red Mud 70 wt%, Fly Ash 30 wt%
4	Red Mud + Fly Ash	Red Mud 50 wt%, Fly Ash 50 wt%
5	Red Mud + Carbon	Red Mud 80 wt%, Carbon 20 wt%
6	Red Mud +Aluminium	Red Mud 95 wt%, Aluminium 5 wt%

Table 3.1 Powders used for coating deposition

3.2.2 Preparation of Substrates

Commercially available aluminium, copper, mild steel and stainless steel have been chosen as different substrate materials. The specimens are rectangular having a dimension 50 mm x 25 mm x 2 mm. The specimens are grit blasted at a pressure of 3 kg/cm² using alumina grits having a grit size of 60. The standoff distance in shot blasting is kept between 120-150 mm. The average roughness of the substrates is 6.8 µm. The grit blasted specimens are cleaned in an ultrasonic cleaning unit. Spraying is carried out immediately after cleaning.

3.2.3 Plasma Spraying

The spraying is done at the Laser and Plasma Technology Division, Bhabha Atomic Research Center, Mumbai. A conventional atmospheric plasma spraying (APS) set up is used. The plasma input power is varied from 6 to 16 kW by controlling the gas flow rate, voltage and the arc current. The powder feed rate is kept constant at 10 gm/min, using a turntable type volumetric powder feeder.

The general arrangement of the plasma spraying equipment and schematic diagram of the plasma spraying process are shown in figures 3.1 and 3.2 respectively. The equipment consists of the following units:

1. Plasma spraying gun
2. Control console
3. Powder feeder
4. Power supply
5. Torch cooling system (water)
6. Hoses, cables, gas cylinders and accessories

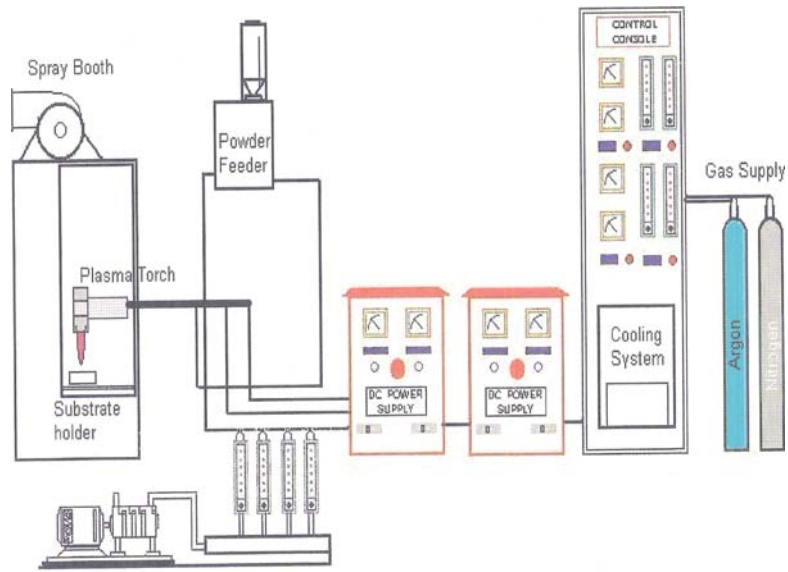


Fig. 3.1 General arrangement of the plasma spraying equipment

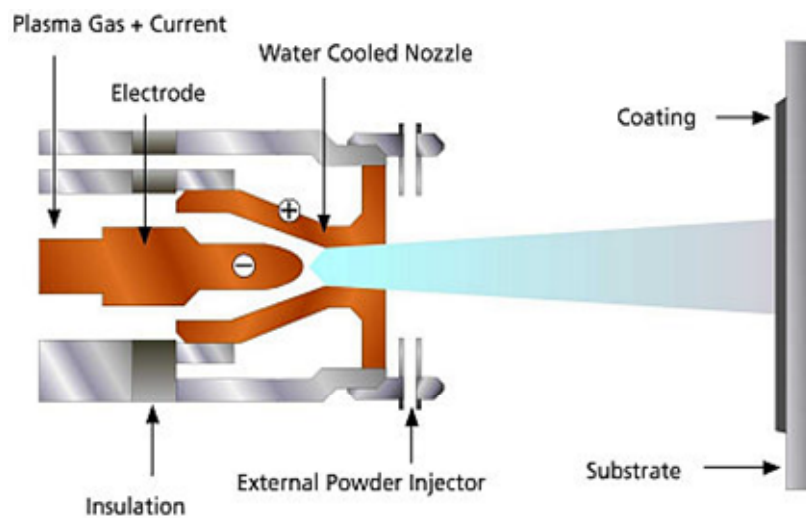


Fig. 3.2 Schematic diagram of the plasma spraying process

Argon is used as the primary plasmagen gas and nitrogen as the secondary gas. The powders are deposited at spraying angle of 90°. The powder feeding is external to the gun. The properties of the coatings are dependent on the spray process parameters. The operating parameters during coating deposition process are listed in table 3.2.

Operating Parameters	Values
Plasma Arc Current (amp)	200, 250, 300, 400
Arc Voltage (volt)	30, 36, 40
Torch Input Power (kW)	6, 9, 12, 16
Plasma Gas (Argon) Flow Rate (lpm)	20
Secondary Gas (N ₂) Flow Rate (lpm)	2
Carrier Gas (Argon) Flow Rate (lpm)	7
Powder Feed Rate (gm/min)	10
Torch to Base Distance TBD (mm)	100

Table 3.2 Operating parameters during coating deposition

3.3 CHARACTERIZATION OF COATINGS

3.3.1 Coating Thickness Measurement

Thickness of the red mud coatings on different substrates are measured on the polished cross-sections of the samples, using an optical microscope. Five readings are taken on each specimen and the average value is reported as the mean coating thickness.

3.3.2 X-Ray Diffraction Studies

The coatings are examined for the identification of the (crystalline) phases with a Philips X Ray Diffractometer. The X ray diffractograms are taken using Cu K α radiation. All coated samples have been studied.

3.3.3 Scanning Electron Microscopic Studies

Specimens of size 10 mm x 13 mm x 5 mm are sliced from the coated samples for SEM observation. Both top surface and cross section of specimens are observed in scanning electron microscope Jeol T330 mostly using the secondary electron imaging. Coating cross-sections are polished in three stages using SiC abrasive papers of reducing grit sizes and then with diamond pastes on a wheel for coating interface analysis under SEM. These specimens are also utilized for the microhardness measurement.

3.3.4 Porosity Measurement

Measurement of porosity is done using the image analysis technique. The polished top coats are kept under a microscope (Neomate) equipped with a CCD camera (JVC, TK 870E). This system is used to obtain a digitized image of the object. The digitized image is transmitted to a computer equipped with VOIS image analysis software. The total area captured by the objective of the microscope or a fraction thereof can be accurately measured by the software. Hence the total area and the area covered by the pores are separately measured and the porosity of the surface under examination is determined.

3.3.5 Microhardness Measurement

Microhardness measurement is made using Leitz Microhardness Tester equipped with a monitor and a microprocessor based controller, with a load of 0.493N and a loading time of 20 seconds. About ten or more readings are taken on each sample and the average value is reported as the data point.

3.3.6 Evaluation of Coating Deposition Efficiency

Deposition efficiency is defined as the ratio of the weight of coating deposited on the substrate to the weight of the expended feedstock. Weighing method is accepted widely to measure this. Each specimen is weighed before and after coating deposition. The difference is the weight (G_c) of coating deposited on the substrate . From the powder feed rate and time of deposition the weight of expended feed stock (G_p) is determined. The deposition efficiency (η) is then calculated using the following equation [**183**].

$$\eta = (G_c / G_p \times 100) \%$$

Weighing of samples is done using a precision electronic balance with ± 0.1 mg accuracy.

3.3.7 Evaluation of Coating Interface Bond Strength

To evaluate the coating adhesion strength, a special type jig (fig. 3.3) is fabricated. Cylindrical mild steel dummy samples (length 25 mm, top and bottom diameter 9.5 mm) are prepared. The surfaces of the dummies are roughened by punching. These dummies are then fixed on top of the coating with the help of a polymeric adhesive (epoxy 900-C) and pulled with tension after being mounted on the jig (fig. 3.4). The coating pullout test is carried out using the set up Instron 1195 at a crosshead speed of 10 m/minute.



Fig. 3.3 Jig used for the test



Fig. 3.4 Specimen under tension

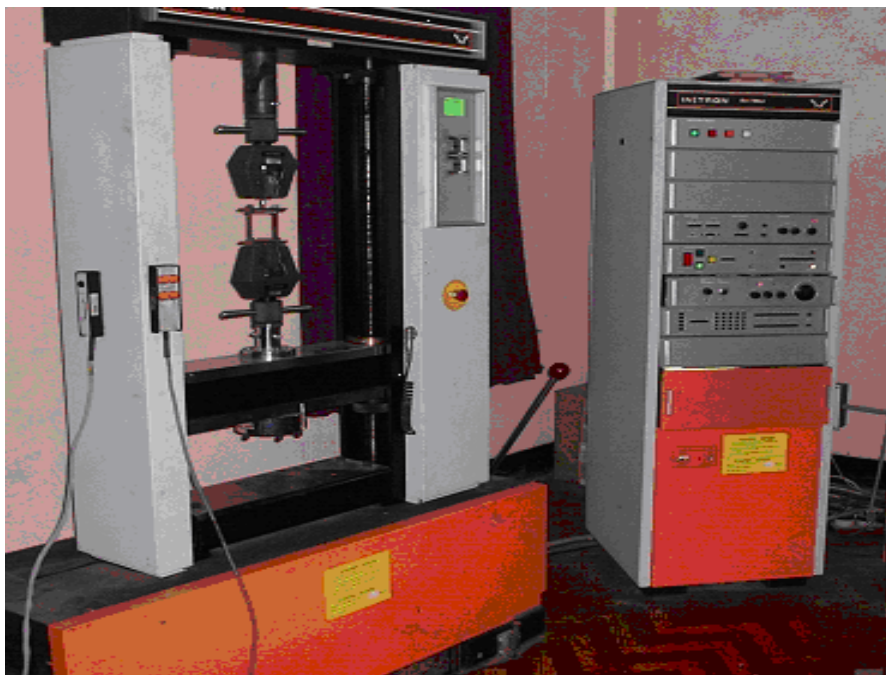


Fig. 3.5 Adhesion test set up Instron 1195

The moment coating gets torn off from the specimen, the reading (of the load), which corresponds to the adhesive strength of the coating, is recorded. A typical test set up (during testing) is shown in figure 3.5. The test is performed as per ASTM C-633.

3.4 EROSION WEAR BEHAVIOUR OF COATINGS

Solid particle erosion (SPE) is usually simulated in laboratory by one of two methods. The ‘sand blast’ method, where particles are carried in an air flow and impacted onto a stationary target and the ‘whirling arm’ method , where the target is spun through a chamber of falling particles.

In the present investigation, an erosion apparatus (self-made) of the ‘sand blast’ type is used. It is capable of creating highly reproducible erosive situations over a wide range of particle sizes, velocities, particles fluxes and incidence angles, in order to generate quantitative data on materials and to study the mechanisms of damage. The test is conducted as per ASTM G76 standards.

The jet erosion test rig used in this work employs a 300 mm long nozzle of 3 mm bore and 300 mm long. This nozzle size permits a wider range of particle types to be used in the course of testing, allowing better simulations of real erosion conditions. The mass flow rate is measured by conventional method. Particles are fed from a simple hopper under gravity into the groove. Velocity of impact is measured using double disc method [184]. Some of the features of this test set up are:

- Vertical traverse for the nozzle: provides variable nozzle to target standoff distance, which influences the size of the eroded area
- Different nozzles may be accommodated: provides ability to change the particle plume dimensions and the velocity range

- Large test chamber with sample mount (typical sample size 25 mm x 25 mm) that can be angled to the flow direction: by tilting the sample stage, the angle of impact of the particles can be changed in the range of 0° – 90° and this will influence the erosion process.

In this work, room temperature solid particle erosion test on mild steel substrates coated with different feed materials is carried out under three different impact angles 30° , 60° and 90° . Coatings of three different feed material compositions (i.e. red mud, red mud + 30 wt% fly ash and red mud + 5 wt% aluminium) are considered for this investigation. The nozzle is kept at 200 mm stand-off distance from the target. 50 μm average size dry silica sand particles are used as erodent with an average velocity of 30 m/s. 6.25 cm^2 area of each coating sample is exposed to the compressed air jet carrying erodent. Amount of wear is determined on 'mass loss' basis. It is done by measuring the mass of the samples at the beginning of the test and at regular intervals in the test duration. A precision electronic balance with ± 0.1 mg accuracy is used for weighing. Erosion rate, defined as the coating mass loss per unit erodent mass (mg/g) is calculated.

RESULTS AND DISCUSSION

4.1 INTRODUCTION

Plasma sprayed coatings of red mud , red mud + fly ash , red mud + carbon and red mud + aluminium were developed on four different metals substrates (aluminium, copper, mild steel, stainless steel) using a 40 kW atmospheric plasma spray system supplied by M/s Ion Arc Machines (India) Pvt. Ltd. at the Laser and Plasma Tech. Division, Bhabha Atomic Research Center, Mumbai. Spraying was done at different input power level to the dc plasma torch in the range from 5 kW to 20 kW. Characterization of the coatings was done with respect to their quality and tribological performance. The results of various tests are presented and discussed in this chapter.

4.2 COATING THICKNESS

To ensure the coatability of red mud on different substrates, coating thickness was measured on the polished cross-sections of the samples, using an optical microscope. The thickness values obtained for coatings deposited at different power levels for Al, Cu, MS and SS substrates are presented in Fig 4.1. Each data point on the curves is the average of at least five readings/measurements.

Maximum coating thickness of ~ 200 micron on aluminium, ~ 210 micron on copper, ~ 190 micron on mild steel and ~ 170 micron on stainless steel substrates are obtained. From the figure it is evident that there is an increase in

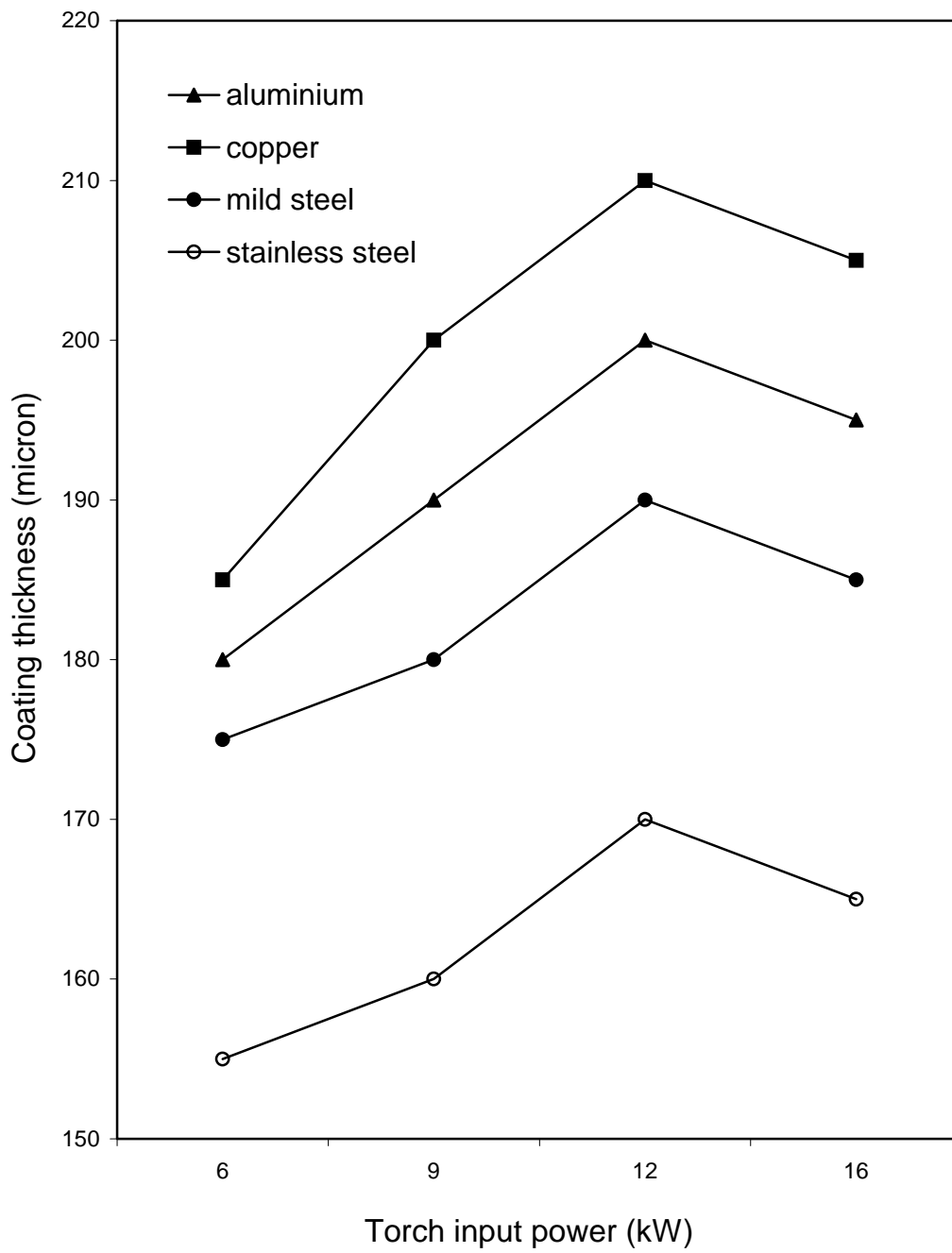


Fig. 4.1 Thickness of red mud coatings made at different power level

coating thickness with increase in input power to the plasma torch; up to about 12 kW and then for further higher input power, no improvement in coating thickness is recorded. It is also seen from the figure that there is a difference in thickness obtained for different substrates. Coating thickness is higher in case of copper than that of aluminium, mild steel or stainless steel substrates, at all power levels. This difference may be attributed to thermal conductivity of the substrate material, i.e. for materials with higher conductivity (i.e. aluminium and copper), the heat transfer from the sprayed particles (reaching on the substrate) occurs at a faster rate than in case of materials with relatively lower conductivity (i.e. MS, SS). This might be enhancing the deposition rate and hence the coating thickness.

4.3 INTERFACE BOND STRENGTH

From the microscopic point of view, adhesion is due to physico-chemical surface forces (Vander-walls, Covalent, ionic...), which can be established at the coating-substrate interface [185] and corresponds to the work of adhesion. From the mechanical point of view, adherence can be estimated by the force corresponding interfacial fracture and is macroscopic in nature. Coating adherence tests have been carried out by many investigators with various coatings. It has been stated that the fracture mode is adhesive if it takes place at the coating-substrate interface and that the measured adhesion value is the value of practical adhesion, which later is strictly an interface property, depending exclusively on the surface characteristics of the adhering phase and the substrate surface condition. [181, 186]

In this work, evaluation of coating interface bond strengths is done using coating pullout method, conforming to ASTM C-633 standard. It is found that in all the samples fracture occurred at the coating-substrate interface. The results obtained for coatings made with different feed materials (i.e. red mud,

Coating Material	Arc Current (amp)	Arc Voltage (Volt)	Torch Input Power (kW)	Adhesion Strength (MPa)			
				Al	Cu	MS	SS
RM 100%	200	30	6	6.39	5.64	4.65	4.63
RM 100%	250	36	9	6.92	6.53	6.43	5.87
RM 100%	300	40	12	5.76	6.69	7.75	6.12
RM 100%	400	40	16	3.67	3.11	7.54	3.85
RM+10%FA	200	30	6	6.75	5.85	4.79	4.88
RM+10%FA	250	36	9	7.3	6.65	6.52	6.05
RM+10%FA	300	40	12	5.98	6.83	7.83	6.29
RM+10%FA	400	40	16	3.9	3.32	8.35	3.93
RM+30%FA	200	30	6	7.122	5.022	4.29	5.06
RM+30%FA	250	36	9	8.37	6.217	6.82	5.62
RM+30%FA	300	40	12	9.31	7.618	12.78	7.2
RM+30%FA	400	40	16	5.4	3.56	10.68	4.46
RM+50%FA	200	30	6	7.29	5.22	4.49	5.66
RM+50%FA	250	36	9	8.54	6.617	6.962	5.92
RM+50%FA	300	40	12	9.63	7.918	13.78	7.674
RM+50%FA	400	40	16	5.764	3.766	10.88	4.76
RM+20%C	200	30	6	7.2	6	4.75	5
RM+20%C	250	36	9	8.35	6.82	6.78	6.3
RM+20%C	300	40	12	9.4	7.81	12.8	7.25
RM+20%C	400	40	16	5.35	3.65	10.72	4.56
RM+5%Al	200	30	6	4.360	5.100	4.900	5.034
RM+5%Al	250	36	9	4.730	8.480	5.940	7.73
RM+5%Al	300	40	12	6.060	8.600	6.134	8.825
RM+5%Al	400	40	16	3.000	6.340	4.660	8.340

Table 4.1 Coating adhesion strength at different spraying conditions

red mud + fly ash, red mud + carbon, red mud +aluminium) are tabulated in table 4.1. The variations of interface adhesion strength of these materials on different substrates (i.e. Al, Cu, MS and SS) with operating power level of the plasma torch are presented in figures 4.2 to 4.7 . Maximum adhesion strength of 13.78 MPa is recorded on mild steel substrate. Figure 4.8 presents the results obtained for mild steel substrates coated with all the feed materials at different power level.

The influence of torch input power on coating adhesion is evident from all these graphs. In case of pure red mud coating on aluminium substrate, the strength has increased from 6.39 MPa to 6.92 MPa with increase in operating power from 6 kW to 9 kW (Fig 4.3.1). Coating deposited beyond 9 kW operating power exhibited a detrimental effect on interface bond strength. Similarly, maximum coating adhesion strengths of 6.69 MPa (at 12 kW), 7.75 MPa (at 12 kW) and 6.12 MPa (at 12 kW) have been recorded on copper, mild steel and stainless steel substrates respectively. It is noted that invariably in all cases the interface bond strength increases with the input power of the torch up to a certain power level and then shows a decreasing trend in coating adhesion.

Initially, when the operating power level is increased, the melting fraction and velocity of the particles also increases. Therefore there is better splashing and mechanical inter-locking of molten particles on the substrate surface leading to increase in adhesion strength. But, at a much higher power level, the amount of fragmentation and vaporization of the particles increase. There is also a greater chance of smaller particles (during in-flight traverse through the plasma) to fly off during spraying. This results in poor adhesion strength of the coatings. In an attempt to cause reduction of oxides present in red mud , which may promote coating adhesion, coatings of red mud pre-mixed with carbon

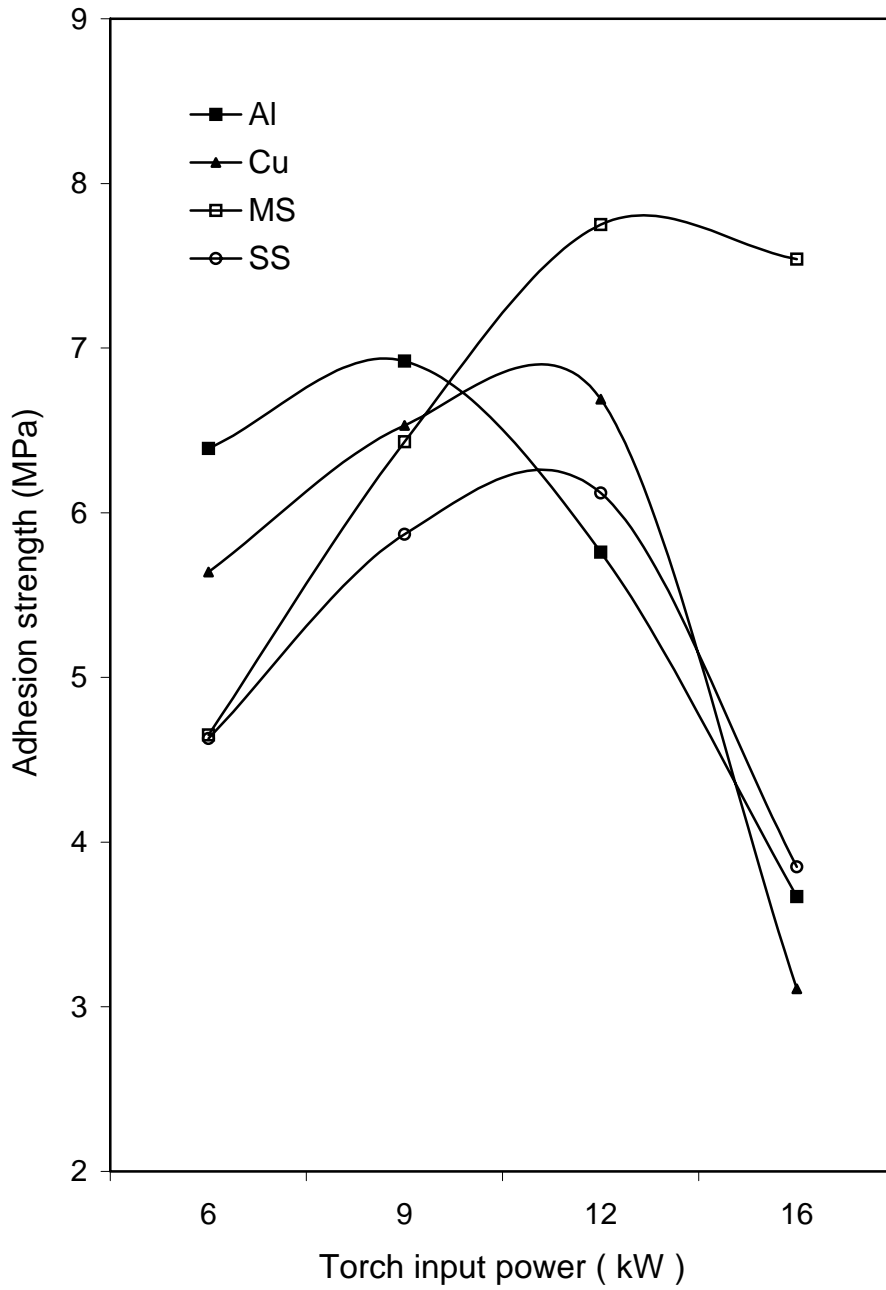


Fig. 4.2 Adhesion strength of red mud coatings made at different power level on different substrates

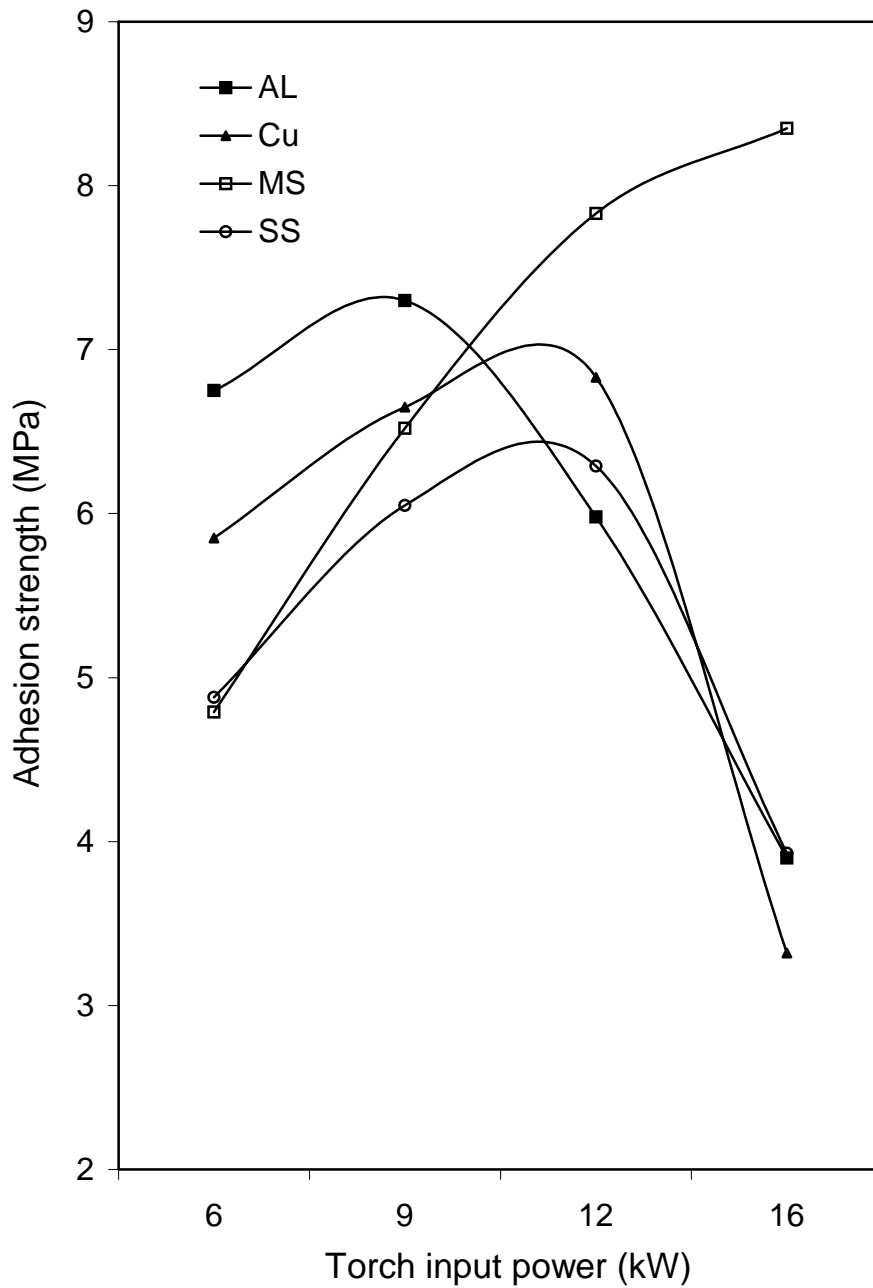


Fig. 4.3 Adhesion strength of red mud + 10% fly ash coatings made at different power level on different substrates

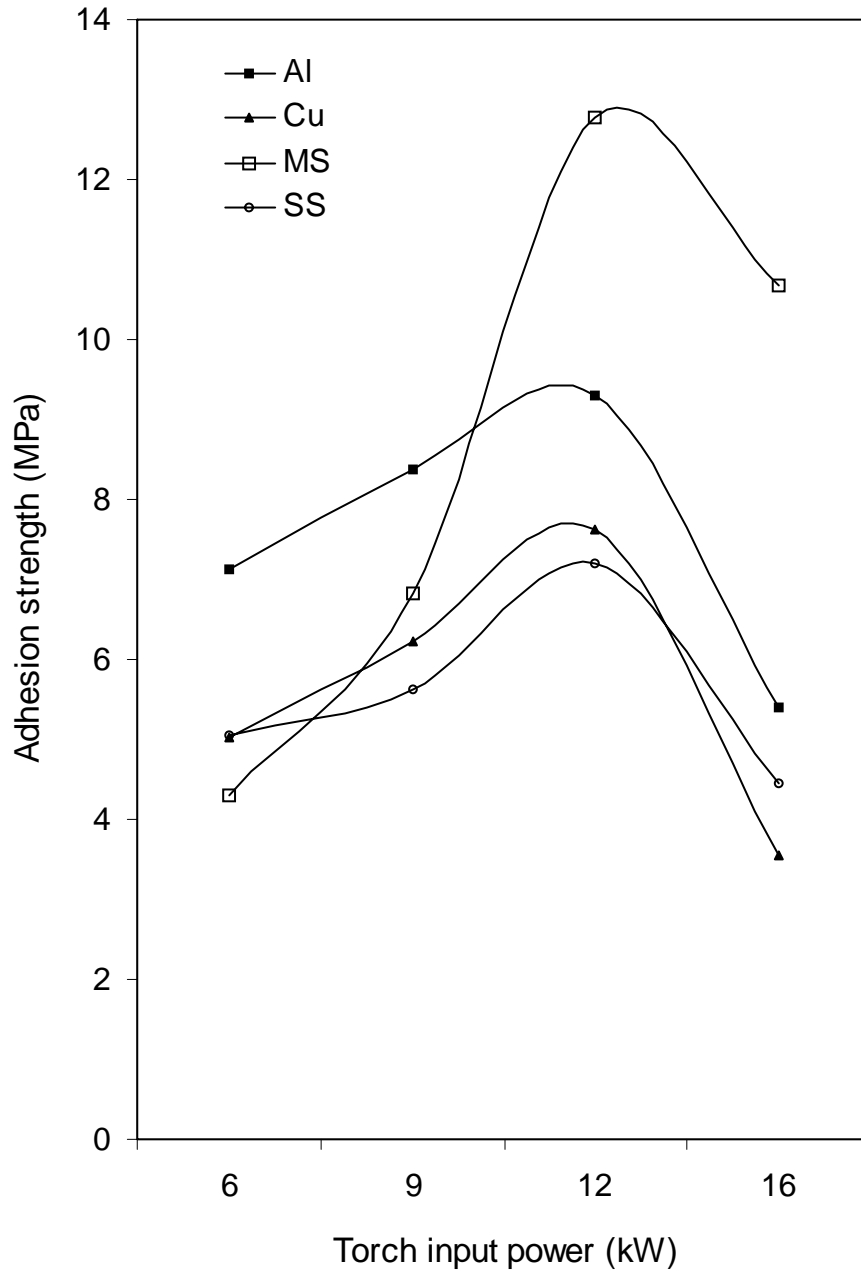


Fig. 4.4 Adhesion strength of red mud + 30% fly ash coatings made at different power level on different substrates

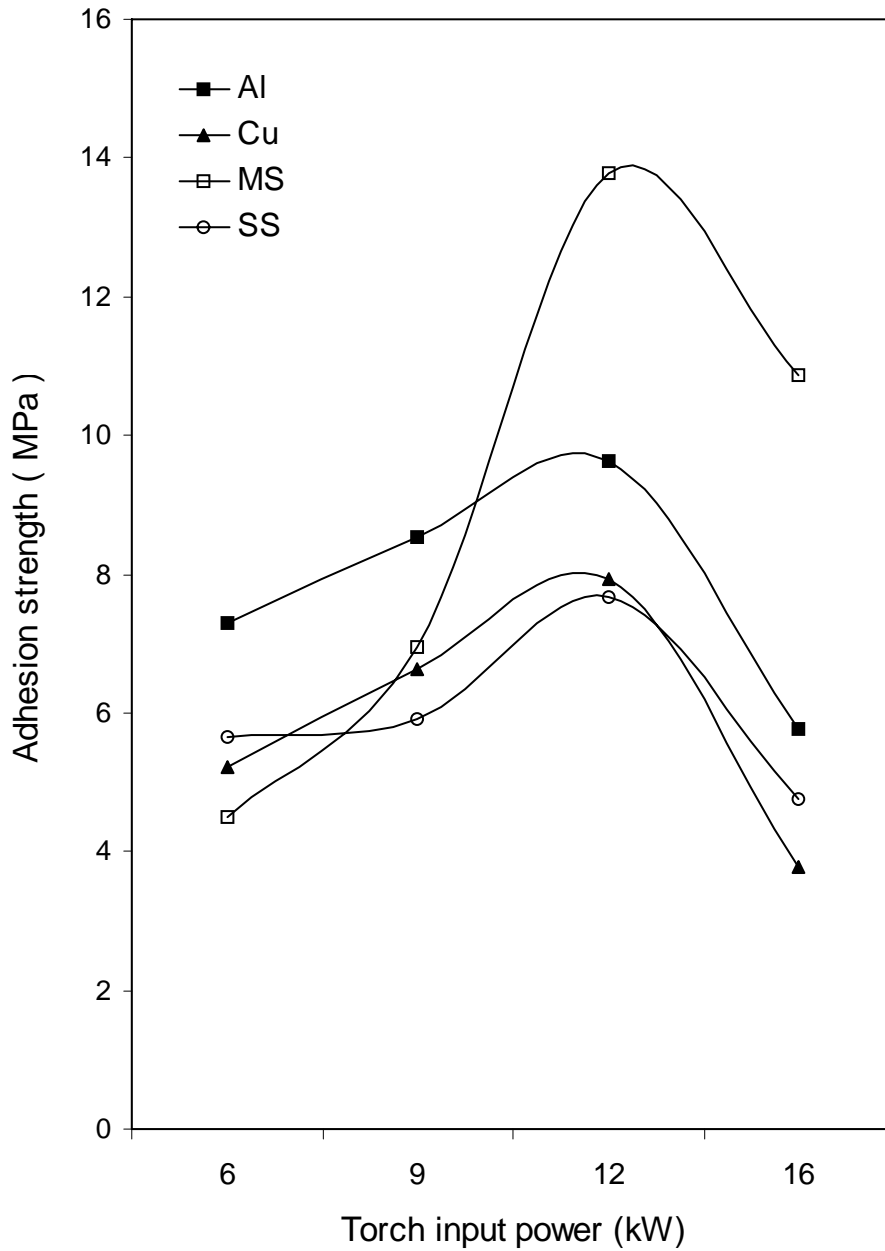


Fig. 4.5 Adhesion strength of red mud +50% fly ash coatings made at different power level on different substrates

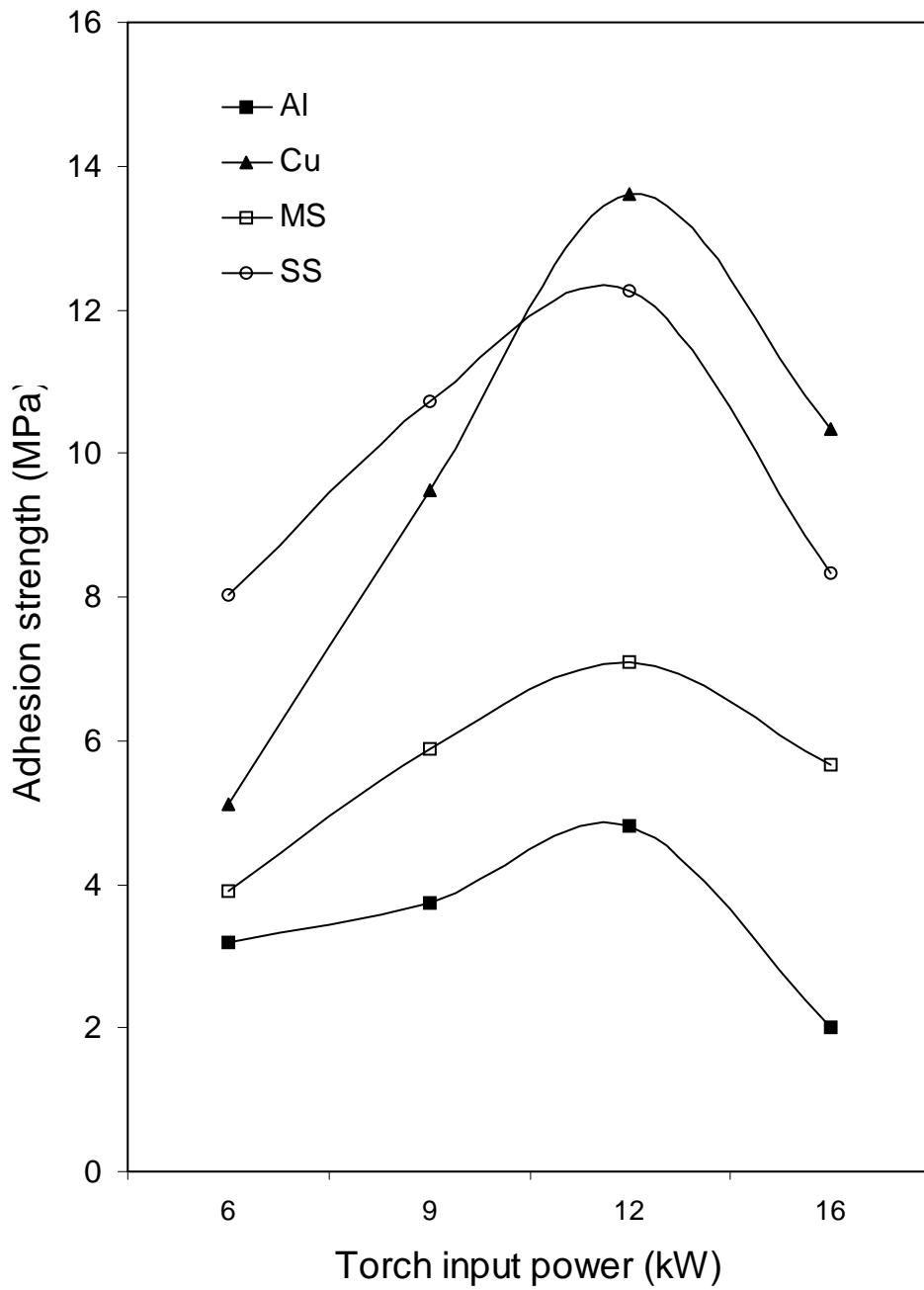


Fig. 4.6 Adhesion strength of red mud + 20% carbon coatings made at different power level on different substrates

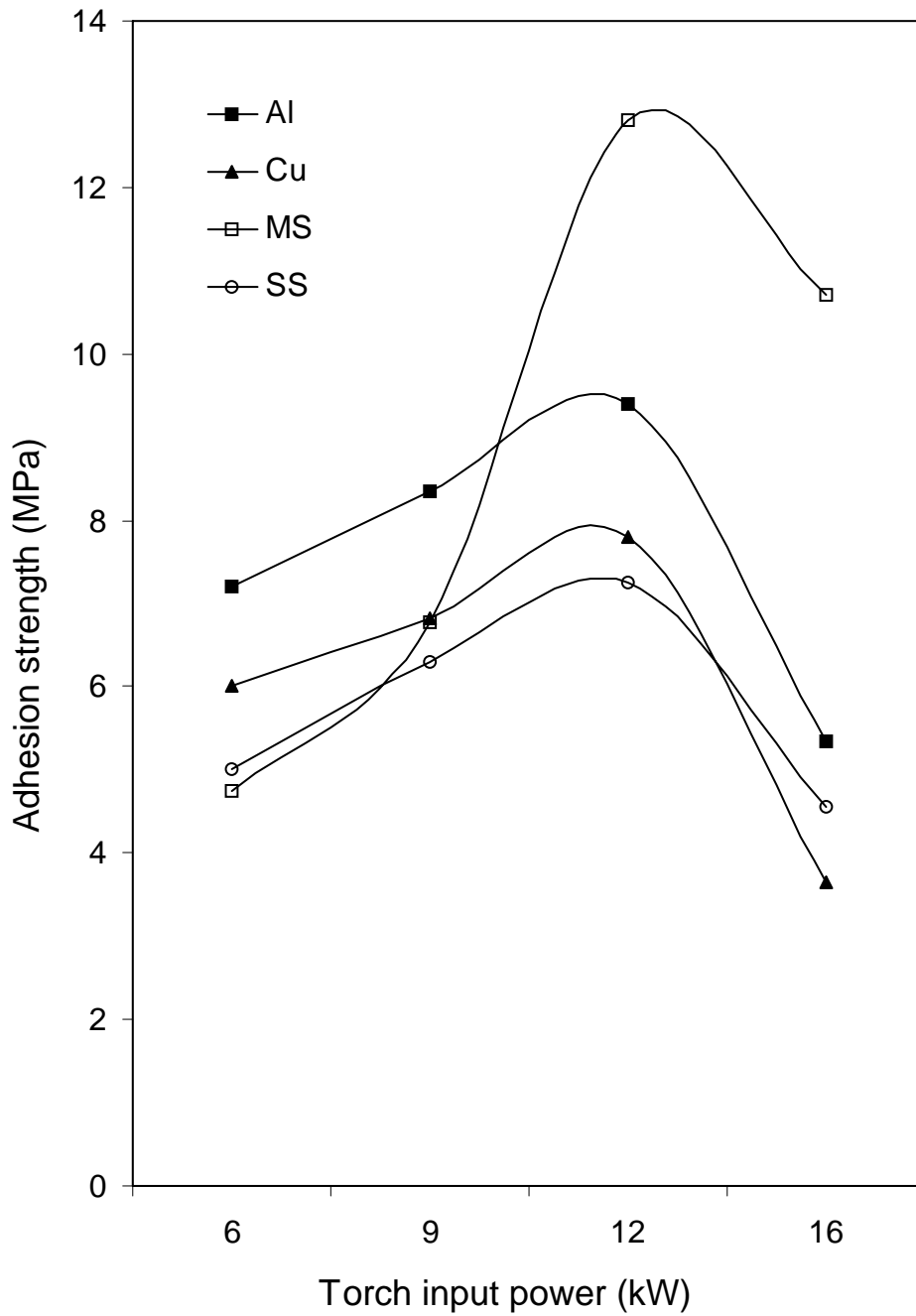


Fig. 4.7 Adhesion strength of red mud + 5% aluminium coatings made at different power level on different substrates

powder (20% by weight) are developed. But although the trend of variation of adhesion strength is found to be similar as in case of red mud coatings (fig. 4.6), not much remarkable improvement in the coating adhesion is observed with addition of carbon.

However, it is noted that the interface bond strength increases with increase in fly ash content in the red mud + fly ash composite coatings. Coatings deposited at 12 kW power level on mild steel substrate show an improvement in adhesion strength from 7.83 MPa to 13.78 MPa (table 4.2) when the weight percentage of fly ash in the feed- stock is increased from 10% to 50%. This improvement in interface adhesion with addition of fly ash may be due to increase in alumina and silica percentage in the feed material composition, which might have helped in increasing the inter-particle bonding.

It is noteworthy that, the presence of a suitable proportion of molten species i.e. aluminium has helped in inter particle bonding and also in interface bonding. The variation of adhesion strength with aluminium addition to red mud shows an improvement in interface bond strength (fig.4.7) of the red-mud coatings. Reasonably high adhesion strength of 12.8 MPa is obtained with mild steel substrate. In case of all other substrates i.e. aluminium, copper and stainless steel, the bond strength is found to be improved as compared to the coatings made with red mud only.

The investigation on interface bond strength in case of ceramic coatings deposited with premixed metal powder was carried out by Lima *e. al.* [186] and Mishra et al. [181]. They have also reported an increase in coating adhesion strength of ceramics premixed with metal powders. Thus, in the present study, the finding of greater adherence strength with the mixing of aluminium powder with red mud is not surprising.

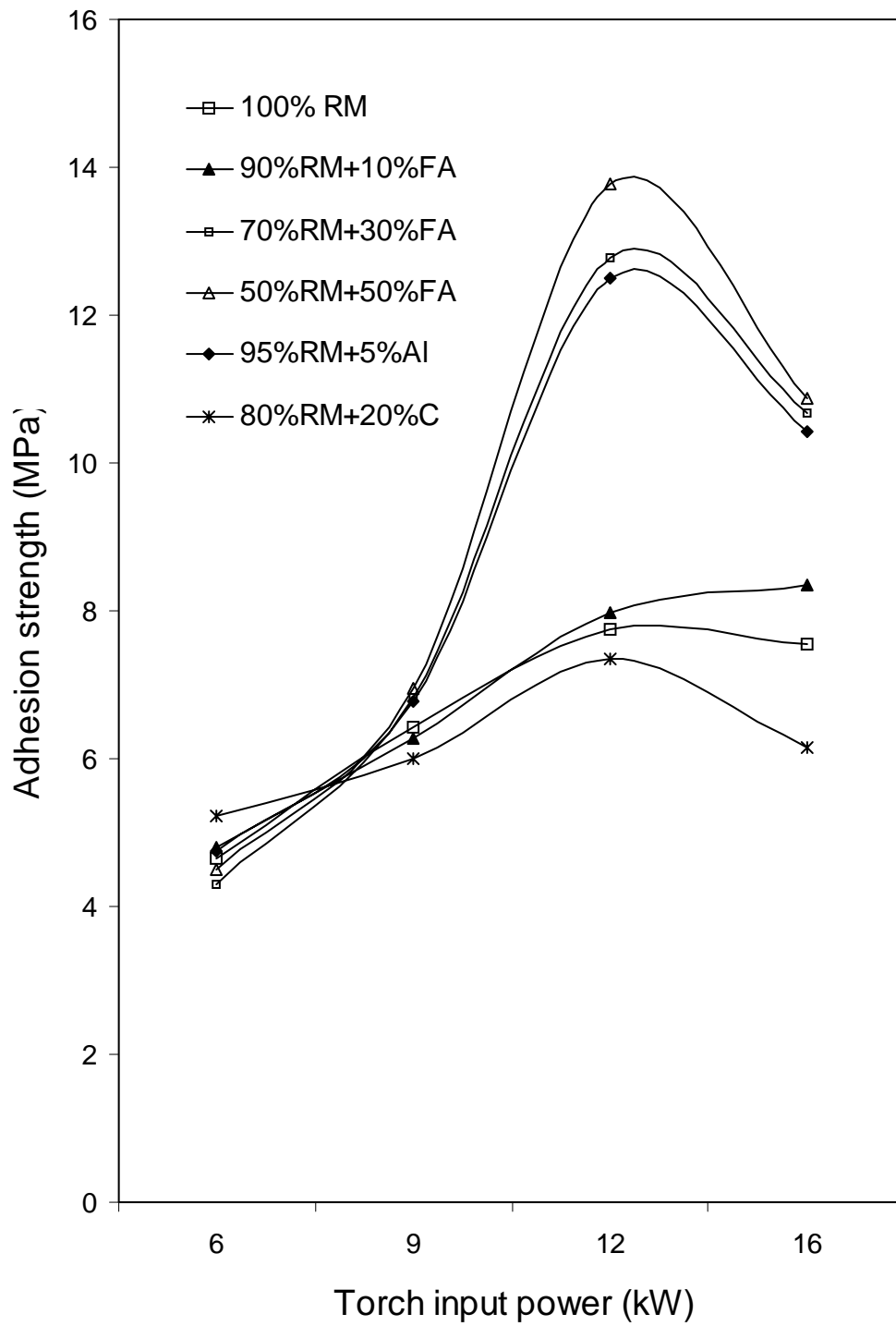


Fig. 4.8 Adhesion strength of coatings made of different feed materials on mild steel substrates

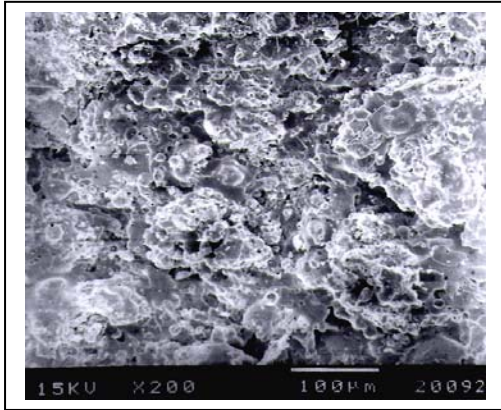
It is noted that the improvement in adhesion strength of red mud coatings with addition of 10 % of fly ash by weight to the feed stock is not significant. Hence the coatings with feed material of composition 90% red mud + 10% fly ash are not considered in further studies and experimentation.

4.4 COATING MORPHOLOGY

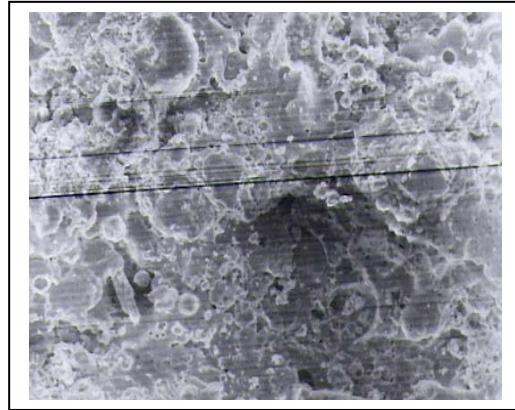
4.4.1 ANALYSIS OF COATING SURFACE

The coating-surface interface adhesion depends on the coating morphology and inter-particle bonding of the sprayed powders. In case of red mud coatings the surface morphologies of the coatings deposited at different operating power levels are shown in figures 4.9 (a), (b) (c) and (d) respectively. For the coating made at lowest power level i.e. at 6 kW, the morphology (fig. 4.9 a) shows uniform distribution of molten/semi molten particles. Little amount of cavitations is observed , other than some fine pores found on the grains, which may have originated during solidification of particles from molten state. Some amorphous and partially molten particles are also seen. The coating made at a higher power level i.e. 9 kW (fig. 4.9 b) bears a different morphology. A large number of globular particles and some flattened regions, indicative of proper melting of the particles of the sprayed powder are seen. The grains are mostly equi-axed type with little boundary mismatch between them. Amount of cavitation is less than that in the previous case. However, some cavity regions are seen along inter-particle / inter-grain boundaries.

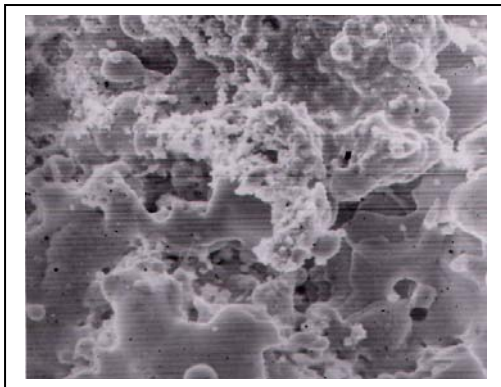
Coating deposited at further higher power level i.e. at 12 kW (fig. 4.9c) bears a still different morphology. Larger portions of the coatings exhibit flattened regions, which might have been formed during solidification of molten particles that have fused together, in lumps. Inter-granular porosity is also noticed at triple grain boundary regions. No cavitation is observed at inter grain boundary.



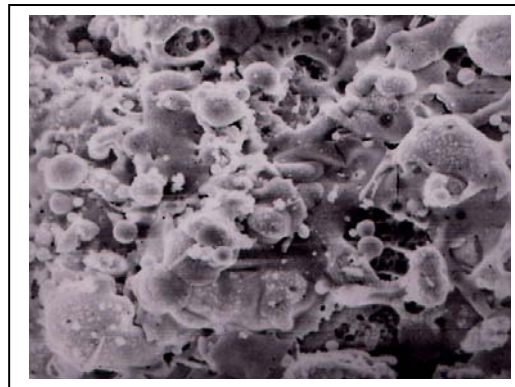
(a)



(b)

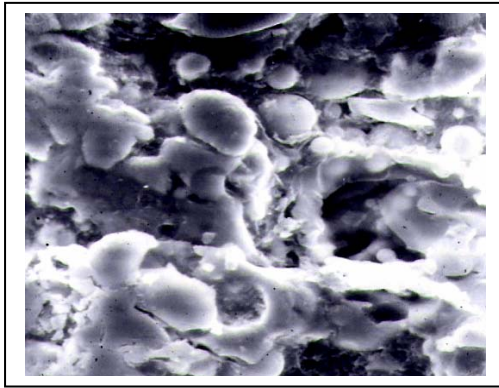


(c)

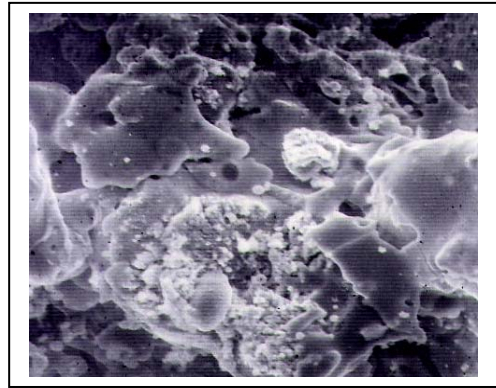


(d)

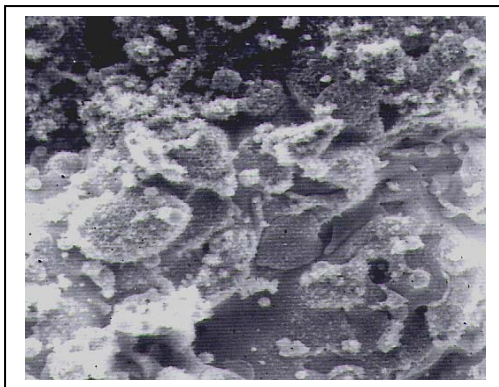
Fig. 4.9 Surface morphology (SEM micrographs) of red mud coatings deposited at (a) 6 kW (b) 9 kW (c) 12 kW and (d) 16 kW operating power level



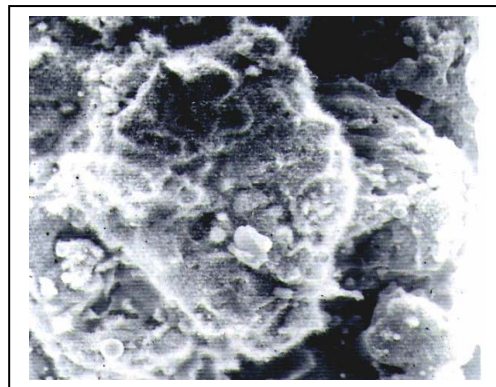
(a)



(b)



(c)

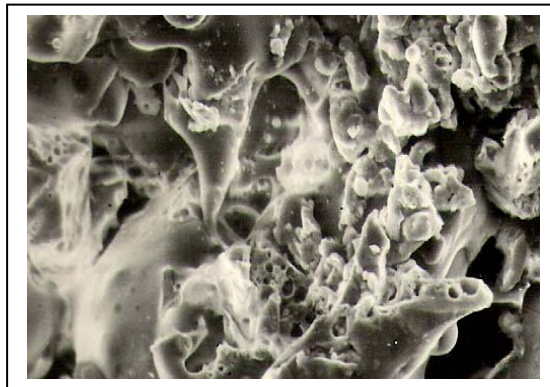


(d)

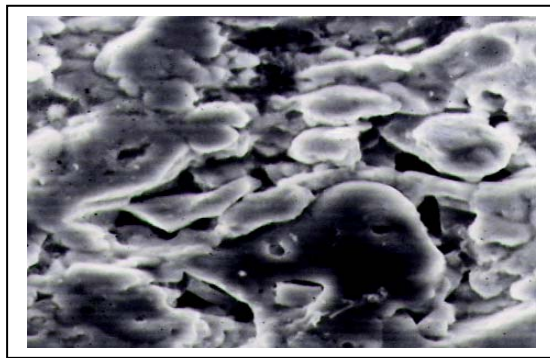
Fig. 4.10 Surface morphology of red mud + 30% fly ash coatings deposited at (a) 6 kW (b) 9 kW (c) 12 kW and (d) 16 kW operating power level

For the coatings deposited at further higher power level i.e. at 16 kW (the highest power level under this investigation), the surface morphology (fig. 4.9 d) is completely different. A large number of spheroidal particles of different diameters are seen, which might have been formed due to breaking / fragmentation of bigger particles and have melted during in flight traverse through the plasma jet. Amount of cavitation is more than those seen in all the previous conditions. This might be the cause for the improper particle-to-particle bonding and poor stacking to the substrate, which have resulted in lower interface bond strength.

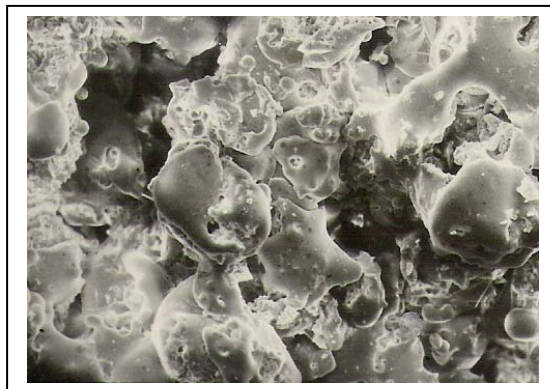
The surface morphology of the red mud + fly ash coatings (with 30% fly ash) is shown in figures 4. 10 (a,) (b) (c) and (d). Coating made at lowest power level, i.e. at 6 kW (fig. 4.10 a) shows spheroidal and elongated particle/grains with good inter particle bonding. At some region grains have fused together to form a splat / flattened area. Some cavities that are clearly visible might have been originated at inter particle boundary regions. With further increase in power level of coating deposition i.e. at 9 kW and 12 kW (fig. 4.10 b and 4.10 c) ; there is a drastic reduction in cavity regions which might be due to solidification of molten/semi molten particles forming flattened regions and reducing inter-particle mismatch/porosity. For the coating deposited at highest power level i.e. at 16 kW (fig. 4.10 d), the amount of porosity appears to have increased again. Particles are fused together to form larger chunks with cavities at the inter-boundary regions. Some smaller particles are also noticed, which might have resulted due to fragmentation of bigger ones during spraying.



(a)



(b)



(c)

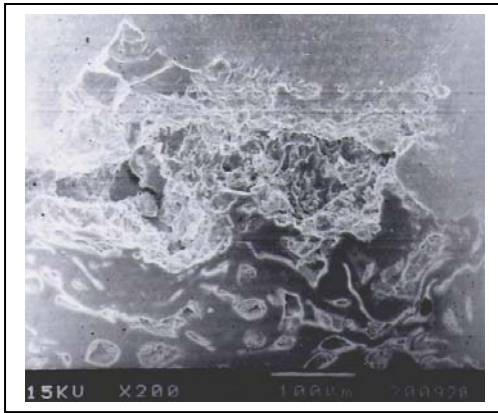
Fig. 4.11 Surface morphology of coatings (a) red mud + fly ash (b) red mud + carbon and (c) red mud + aluminium deposited at 12 kW power level

The results obtained from the measurement of interface bond strength of various coatings reveal that, with addition of fly ash, there is an improvement in adhesion strength of red mud coatings; with the maximum bond strength of ~13.78 MPa obtained for coatings deposited at 12 kW. Hence the surface morphology of the coatings deposited at 12 kW for different feed materials (i.e. red mud + 50% fly ash, red mud + carbon, red mud +5% aluminium) are compared in figures 4.11 (a), (b) and (c) respectively. For the coatings made with 50% fly ash addition shows flattened regions (of particles/ grains) and with some cavities at inter particle boundary space, which might have been caused due to improper selection of powder feed rate. There can also be possibilities (for such cavity regions) for the molten particles to coagulate/agglomerate together before solidification and reducing the surface area due to surface tension force and have flattened while impacting the substrate, resulting formation of inter particle/inter boundary cavitation. When carbon is mixed with red mud for coating deposition (fig. 4.11 b), it shows a different structure. Most of the particles have fused to form elongated shaped structures. Flattened areas are clearly visible, but with a good amount of cavities at inter particle/granular boundaries. When aluminium is added to red mud for coating deposition, as shown in fig 4.11(c), a great change in the coating morphology is found. Most of the particles/grains are equi-axed type and are flattened with better inter-particle adhesion. This might have been originated from melting of aluminium powders during spraying (which remain molten till reaching the substrate). Also addition of aluminium to red mud might have helped in joining of molten/semi molten particles during in-flight traverse as aluminium (metal) would remain in molten state for a longer time even after leaving the plasma jet. In this case, amount of cavitation is also less, as compared to the cases with feed materials.

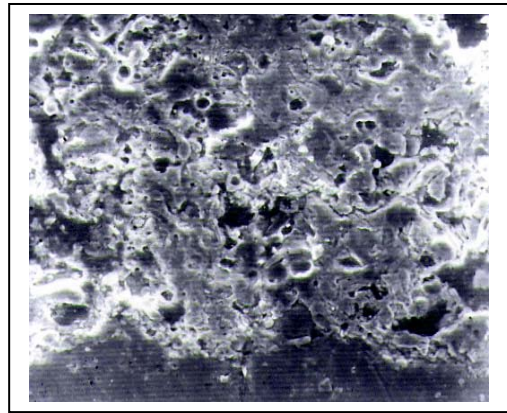
4.4.2 ANALYSIS OF COATING INTERFACE

The coating substrate interface plays the most important role on the adhesion of the coating. But the surface morphology of the coating cannot predict the interior (layer deposition) structures. The polished cross-sections of the samples are examined under SEM. The micro-structures of coatings on aluminium substrates (deposited at 6, 9, 12, 16 kW) are shown in figures 4.12 (a), (b), (c) and (d) respectively. Comparing these figures it can be seen that the morphology is more homogenous for the coating deposited at 12 kW. In case of coatings deposited at lower power level, some un-melted particles are seen along with large amount of cavitation. Cavities are also seen along the interface for the coatings deposited at 6 kW (fig. 4.12a) and at 16 kW (fig. 4.12d) which might have resulted poor adhesion of the coating , with a difference that , no un-melted particles are found at higher power level of coating deposition. At 16 KW power level cracks are developed along the coating layers which has deteriorated the coating homogeneity. Cracks are observed along the coating substrate interface; may be due to mismatch of thermal expansion coefficient of substrate and coating materials, resulted in lowering adhesion strength. Although some pores are observed (fig. 4.12c) those are spherical in shape and have helped in increasing the adhesion strength and longitudinal cracks observed at the inter particle layers (at 16 kW) reduces the adhesion strength.

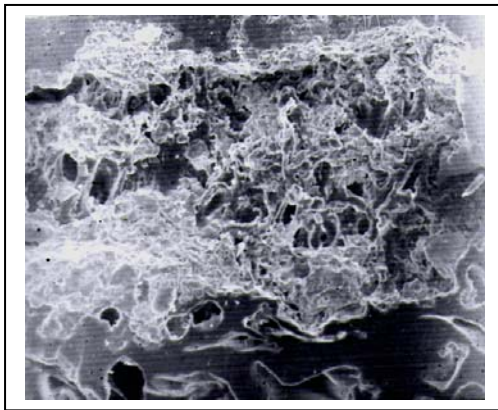
The coating interface morphology of red mud coatings deposited at 12 kW for different substrates as shown in figures 4.13 (a) (b) and (c). Comparing these figures, it is seen that there is no cavity formation along the coating-substrate interface for the coatings made on copper substrate. But some cracks are visible along the interface boundary in case of steel substrates. Cavity formation along the coating layers is observed in stainless steel substrate. However copper substrate shows better homogeneity in the coating. The crack/cavity formation



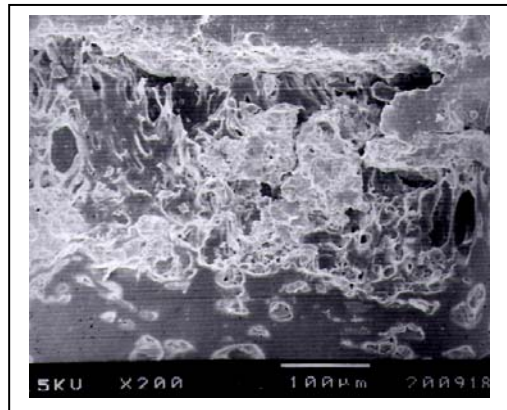
(a)



(b)

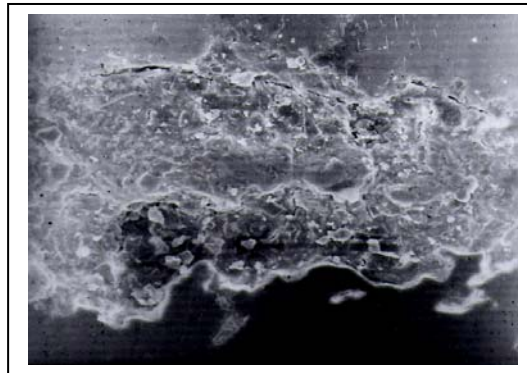


(c)

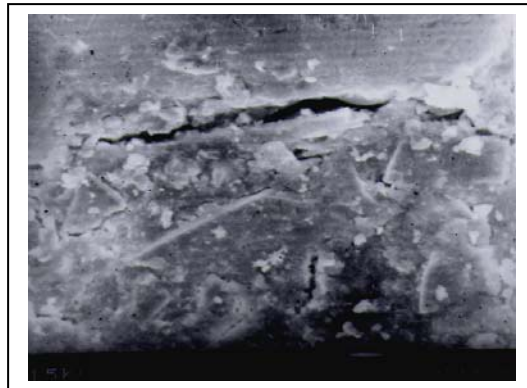


(d)

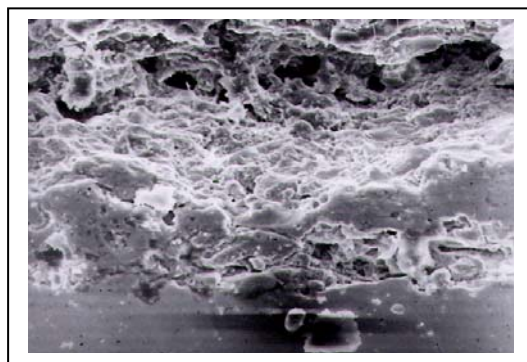
Fig. 4.12 Interface morphology of redmud coatings deposited on aluminium substrates at (a) 6 kW (b) 9 kW (c) 12 kW and (d) 16 kW operating power level



(a)



(b)



(c)

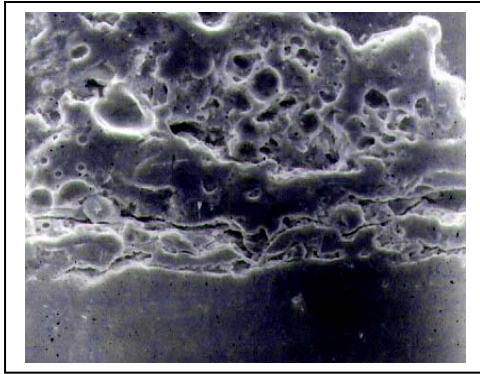
Fig. 4.13 Interface morphology of red mud coatings deposited at 12 kW power level on (a) copper (b) mild steel and (c) stainless steel substrates

at boundaries may also be the cause of difference in interface adhesion strengths of the coatings on different substrate.

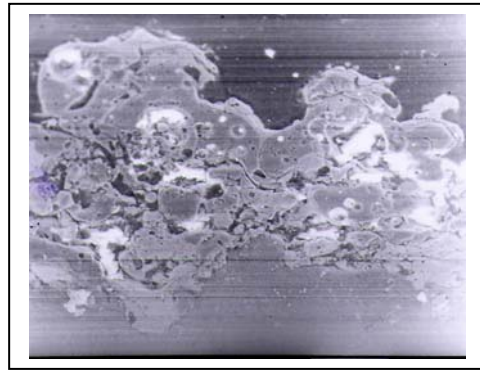
The morphology of the coatings made with addition of different materials (i.e. fly ash, carbon and aluminium etc.) with red mud are shown in figures 4.14 (a), (b), (c) and (d); for the specimens/ substrates in which maximum adhesion strength was recorded. Comparing these figures it can be seen that, with fly ash addition, (figures 4.14 a and b), particles are solidified from molten state forming flattened regions, improving inter-particle bonding. Cracks/cavities are noticed in between the deposited layers. Some micro weld regions at the coating-substrate interface are also visible (fig. 4.14 b). With addition of carbon powder, fig. 4.14 (c), the particles have taken up spheroidal shape and are finer than the previous figures. It appears that the inter particle fusion is not much favoured as in case of fig. 4.14 (a) and (b). The spheroidal shape might have been originated due to availability of carbon which had helped in reduction of oxides (partly) of the red mud. When aluminium is added to red mud, the structure is entirely different, fig. 4.14 (d). This shows almost equi-axed grains with homogenous distribution. Cavitation is the least than that of other cases. Some micro weld regions are also visible at the substrate interface. It appears that, by addition of aluminium metal powder, which remains in molten state during spraying, has helped in inter particle bonding. The molten/semi molten species (aluminium) have also helped in improving packing density of the powders during spray deposition. So high interface adhesion strength is obtained in such samples.

4.5 COATING POROSITY

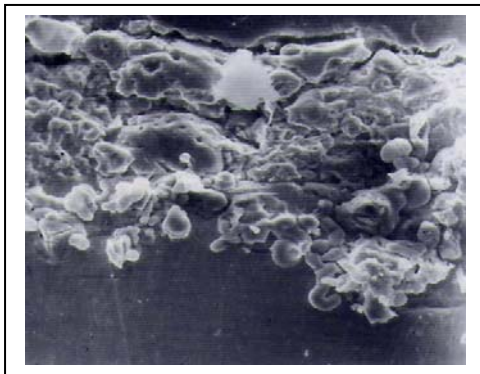
Measurement of porosity is done using the image analysis technique. The polished surfaces of various coatings under this study are kept under a microscope (Neomate) equipped with a CCD camera (JVC ,TK 870E).



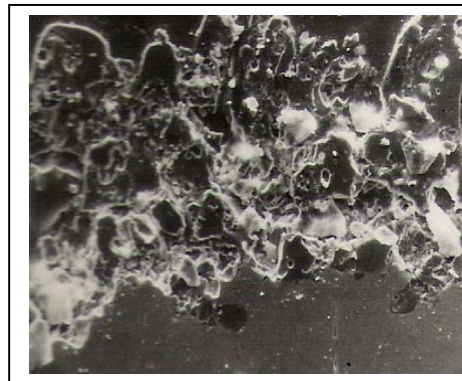
(a)



(b)



(c)



(d)

Fig. 4.14 Coating interface morphology for different materials deposited at 12 kW : (a) red mud + 30% fly ash (b) red mud + 50% fly ash (c) red mud + 20% carbon and (d) red mud + 5% aluminium

Coating material	Plasma torch input power (kW)	Porosity (%)
Red mud	6	10.24
	9	08.09
	12	08.20
	16	12.30
Red mud premixed with fly ash (70% Red mud + 30% Fly ash)	6	12.12
	9	11.50
	12	10.90
	16	12.98
Red mud premixed with fly ash (50% Red mud + 50% Fly ash)	6	11.89
	9	11.54
	12	10.17
	16	12.78
Red mud premixed with carbon (80% Red mud +20% Carbon)	6	11.42
	9	11.50
	12	10.28
	16	12.17
Red mud premixed with aluminium (95% Red mud + 5% Aluminium)	6	12.34
	9	11.67
	12	10.26
	16	12.18

Table 4.2 Porosity on coating surfaces for different specimens

From the digitized image obtained by this system, coating porosity was determined using VOIS image analysis software. The results are tabulated in table 4.2. It is observed that, porosity volume fraction of these coatings lie in the range from ~ 8% to ~13%. The amount of porosity is more in case of the coatings of all compositions, made at lower (i.e. at 6 kW) and at higher (i.e. at 16 kW) power levels. Porosity level is relatively low in case of coatings of pure red mud. Premixing of fly ash or other additives such as carbon or aluminium with red mud is not found to be beneficial in lowering the amount of porosity in the coatings. It may be mentioned that in conventional plasma sprayed ceramic coatings, porosity of about 3 -10 % is generally observed [187]. Thus the values obtained in the coatings under this study are acceptable.

4.6 COATING HARDNESS

Microscopic observation under optical microscope of the polished section of the coatings exhibits three distinctly different regions/ phases namely dull, white and spotted/mixed. Micro-hardness measurement was done on these optically distinguishable phases with Leitz Micro-Hardness Tester using 50Pa (0.493N) on all samples. The results are summarized in table 4.3 .The results show that these three structurally different phases bear three different ranges of hardness, varying from 488 to 588HV in red mud coatings. In case of coatings made with red mud + fly ash mixture, hardness has improved and this might be due to the increase in alumina and silica content in the composition of the feed material. Premixing of carbon to red mud is also found to enhance hardness values and a hardness of 760 HV is recorded in such coatings. But the maximum hardness 830 HV is recorded for coatings made with red mud + 5% aluminium. This may be due to the formation of alumina from aluminium particles and the formation of some inter-oxide compounds.

The obvious reason for improvement in coating hardness in case of red mud + fly ash and red mud + aluminium mixtures is the increase in Al_2O_3 and SiO_2 content in the feedstock and formation of alumino-silicate (mullite phase) during spray deposition.

4.7 XRD PHASE COMPOSITION ANALYSIS

Micro-hardness test shows different hardness values on different optically distinct regions on the coating cross-sections. Therefore, to ascertain the phases present and phase changes / transformation taking place during plasma spraying, the X-ray diffractograms are taken on the raw material and on some selected coatings using a Philips X Ray Diffractometer. The XRD results are shown in figures 4.15 to 4.22 .

From the diffractograms it is seen that the major constituents present in the red mud are hematite (Fe_2O_3), anatase / rutile / brookite (TiO_2) and silica. Presence of silica in amorphous form is well visualized in fig. 4.15. During plasma spraying some of the amorphous (silica) has transformed to crystalline forms. Transformation of hematite is also observed. As marked in fig.4.19, probably MgO and Fe_2O_3 have formed a compound $\text{Mg.Fe}_2\text{O}_4$. Some of the diffraction peaks found to be absent in coatings as compared to the raw material. This may be due to vaporization of oxides of alkali and alkaline earth metals (viz. CaO, MgO etc.) from the raw material as well as due to formation of complex oxides such as $\text{Mg.Fe}_2\text{O}_4$.

Coating Material	Plasma Torch Input Power (kW)	MICRO HARDNESS (HV)		
		Dull	White	Spotted
100% Red mud	6	540	488	496
	9	532	498	511
	12	586	513	508
	16	588	506	522
70% Red mud + 30% Fly ash	6	638	632	628
	9	648	642	636
	12	660	638	628
	16	680	612	632
50% Red mud + 50% Fly ash	6	696	679	658
	9	682	633	672
	12	726	712	660
	16	730	708	680
80% Red mud + 20% Carbon	6	393	490	558
	9	435	498	592
	12	478	522	652
	16	452	548	660
95% Red mud + 5% Aluminium	6	597	636	746
	9	596	662	739
	12	738	762	810
	16	705	723	770

Table 4.3 Coating micro-hardness for different feed materials deposited at different operating power level

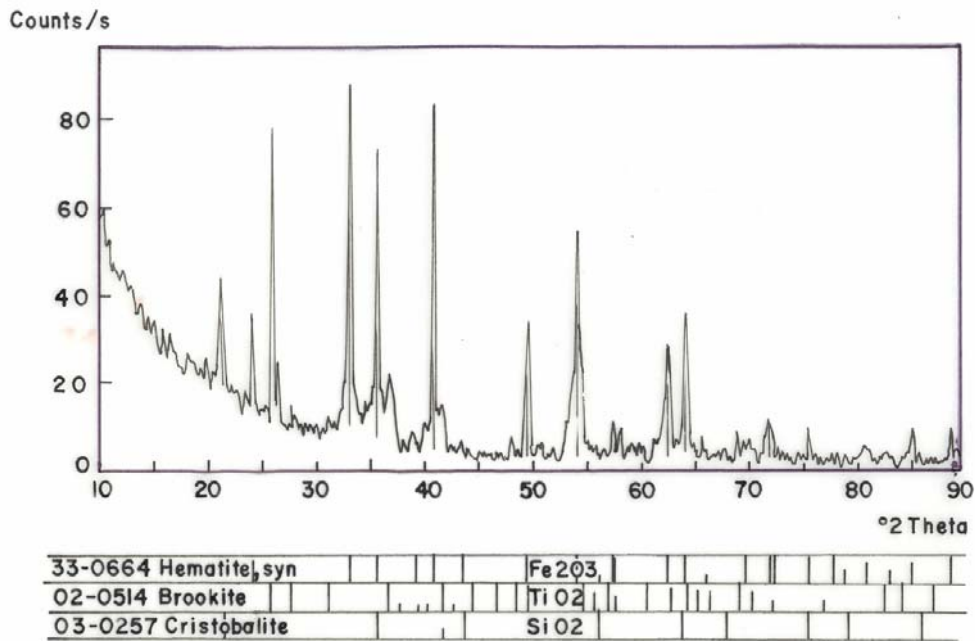


Fig. 4.15 X Ray Diffractogram of red mud collected from NALCO

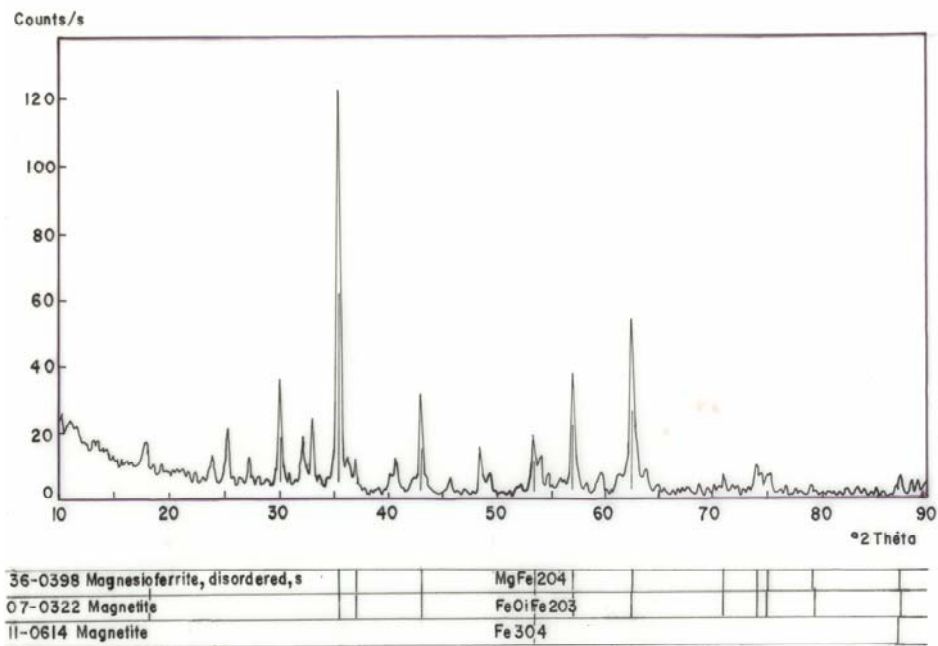


Fig. 4.16 X Ray Diffractogram of red mud coating deposited at 6 kW operating power level

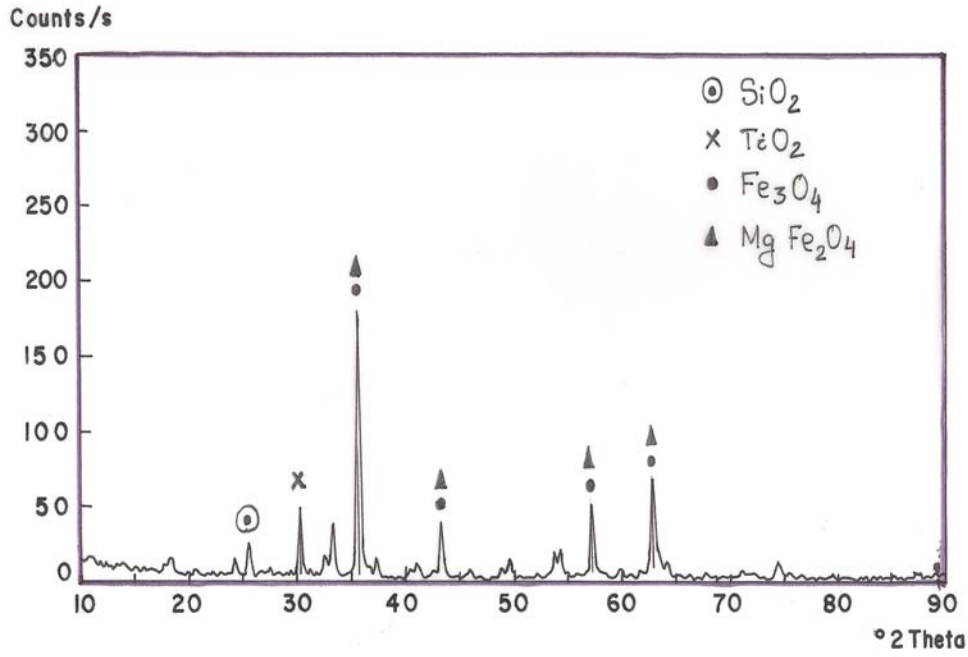


Fig. 4.17 X Ray Diffractogram of red mud coating deposited at 9 kW operating power level

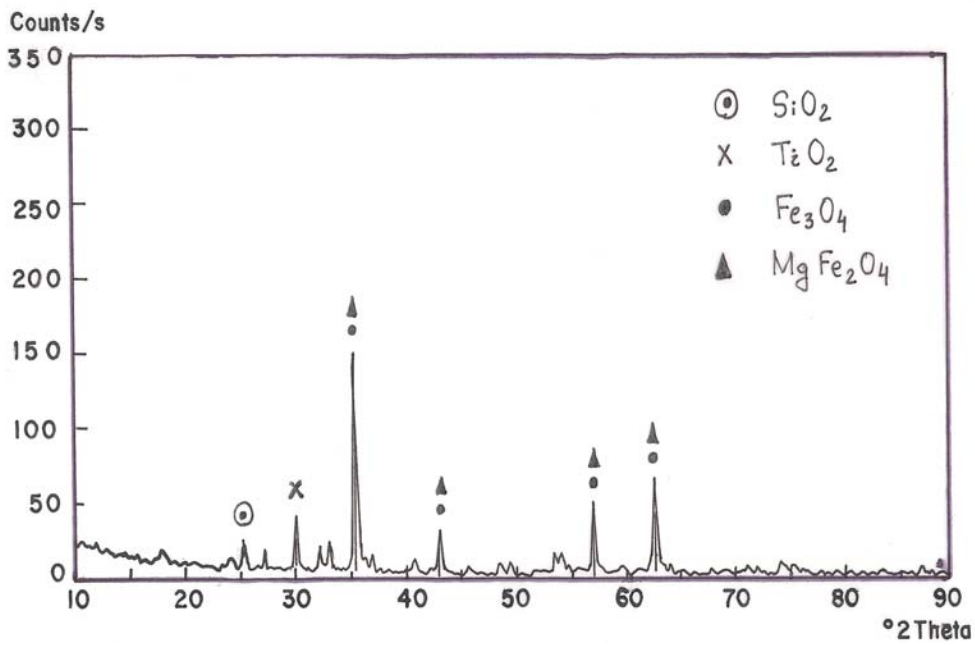


Fig. 4.18 X Ray Diffractogram of red mud coating deposited at 12 kW operating power level

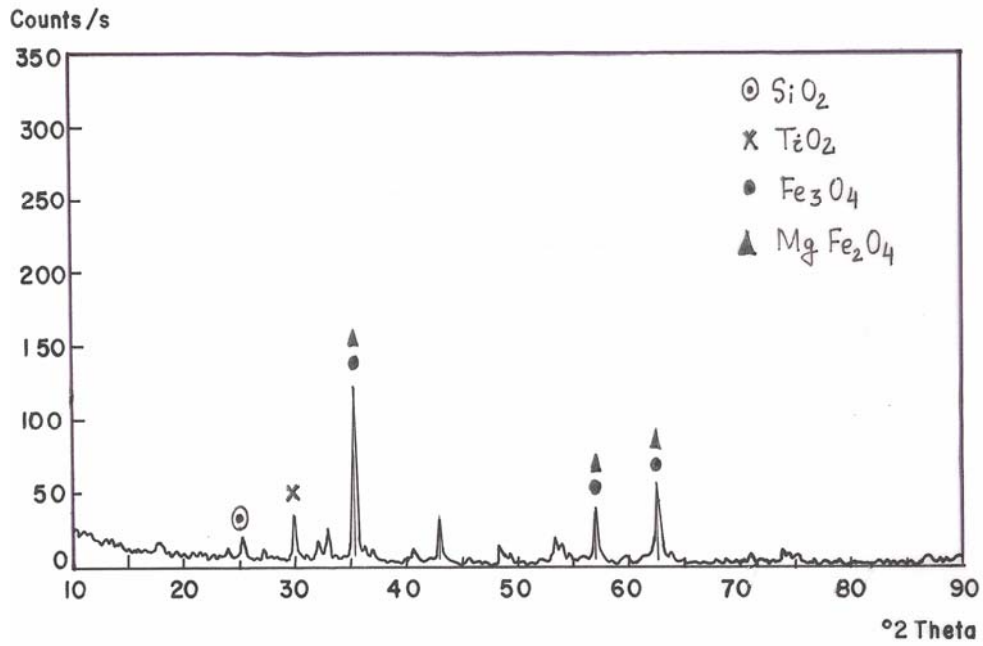


Fig. 4.19 X Ray Diffractogram of red mud coating deposited at 16 kW operating power level

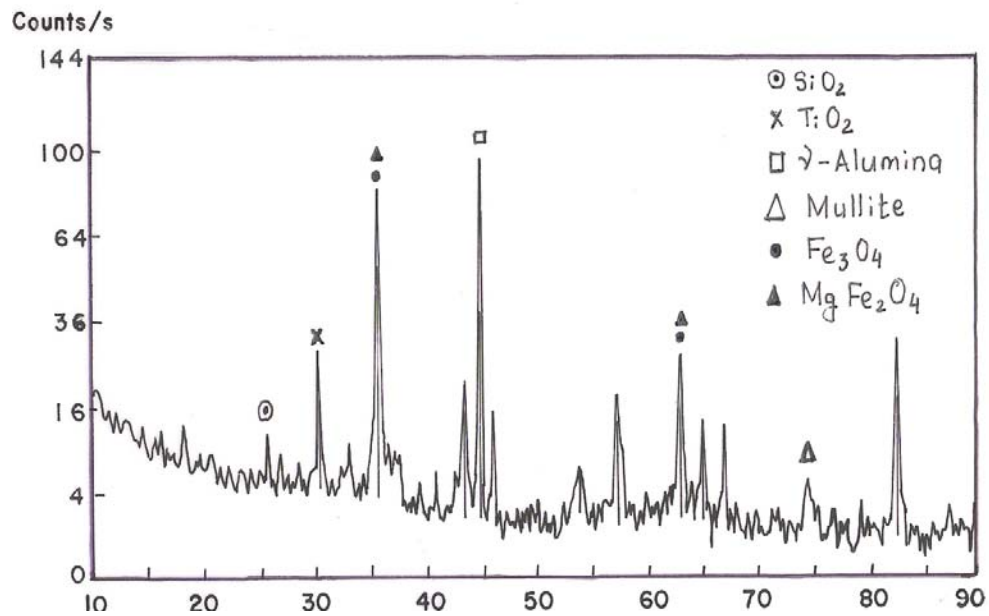


Fig. 4.20 X Ray Diffractogram of coating (red mud + 20% carbon) deposited at 12 kW operating power level

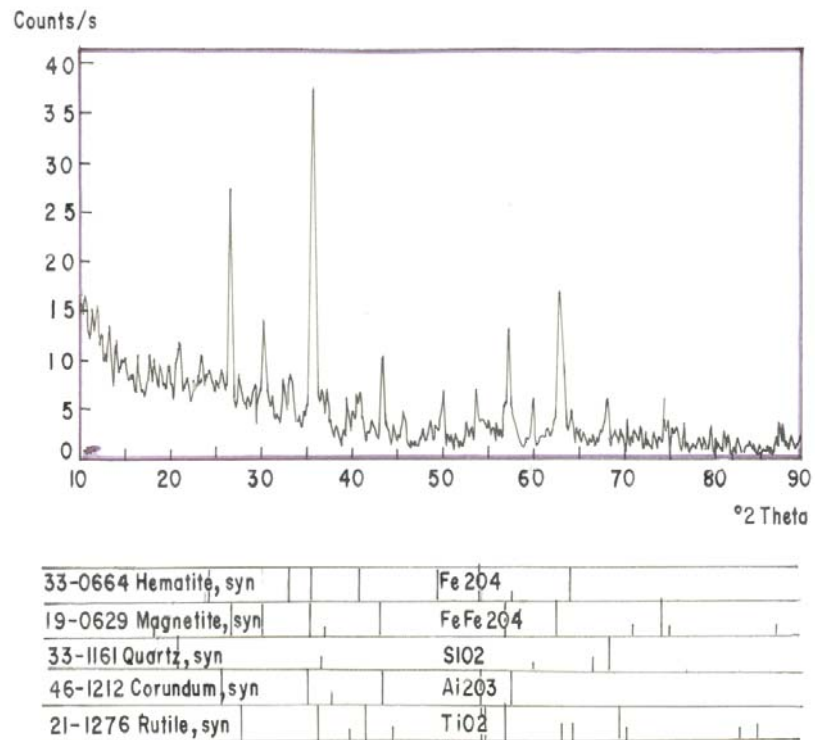


Fig. 4.21 X Ray Diffractogram of coating (red mud + 50% fly ash) deposited at 12 kW operating power level

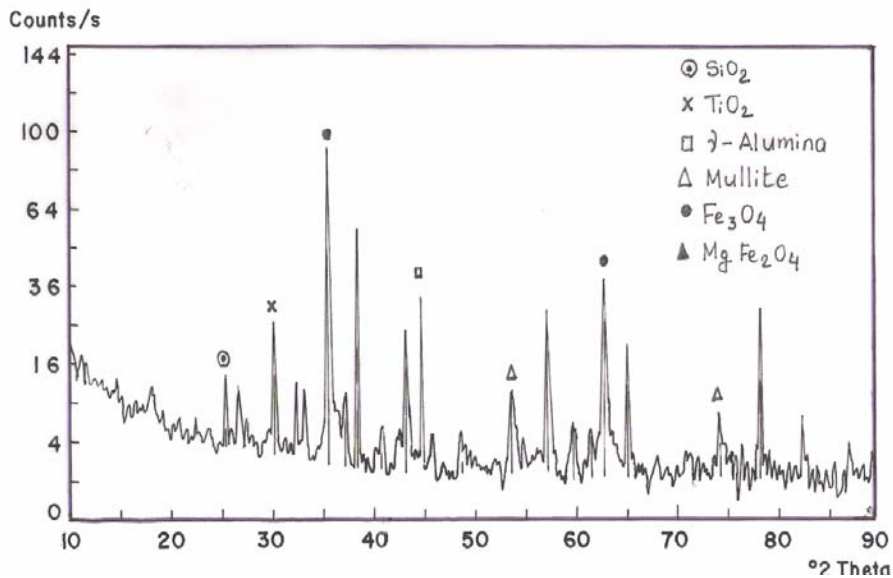


Fig. 4.22 X Ray Diffractogram of coating (red mud + aluminium) deposited at 12 kW operating power level

It can be visualized from fig. 4.15 to fig. 4.19 that, glassy (silica) phase, which is observed in the raw material (fig. 4.15) is not found in the coated samples. This may be due to the fact that, at high temperature amorphous silica has transformed to crystalline phases. X - ray diffractogram of the coating with red mud + 20% carbon, deposited at 12 kW is shown in fig.4.20. In this, γ - alumina and mullite phases are observed. This may probably be due to the enhancement of reaction kinetics for presence of carbon, which has helped in formation of mullite and γ - alumina phases. The diffractogram of the coating made with red mud + 50% fly ash at 12 kW power level is shown in fig. 4.21. Along with the other phases observed in the previous XRDs, the amount of α - alumina and mullite ($2\text{Al}_2\text{O}_3 \cdot 3\text{SiO}_2$) has increased (from comparison of peak intensities). This is for the obvious reason that, the percentage of alumina and silica has increased with addition of fly ash to red mud.

The diffractogram of the coating made with red mud + 5% aluminium at 12 kW power level is shown in fig. 4.22. There is not much difference in the phases as observed with red mud coating (at 12 kW) other than the peak intensity of the alumina phase. This is due to transformation of aluminium powder to alumina during plasma spraying. In general, it can be said that there is a transformation of Fe_2O_3 to Fe_3O_4 , which is favoured with increase in deposition power level. SiO_2 and Al_2O_3 phases are present in all the coatings. On addition of carbon and fly ash to red mud, γ - alumina and mullite phases are formed.

4.8 SOLID PARTICLE EROSION WEAR BEHAVIOUR

Solid particle erosion is a wear process where particles strike against a surface and promote material loss. During flight, a particle carries momentum and kinetic energy, which can be dissipated during impact due to its interaction with a target surface. In case of plasma spray coatings encountering such

situations, no specific model has been developed and thus the study of their erosion behavior has been mostly experimental data [139].

In this work, room temperature solid particle erosion trials on a few selected coated mild steel specimens are carried out using a compressed air blasting type rig under three different impact angles (30°, 60° and 90°). Coatings of red mud, red mud + 30 wt% fly ash and red mud + 5 wt% aluminium are taken for this investigation. Detailed description of the test is given in the previous chapter. The nozzle (2.2 mm ID) is kept at 200 mm stand-off distance from the target. 50 µm average size dry silica sand particles are used as erodent, with an average velocity of 30 m/s, as measured by double disc method [184]. 6.25 cm² area of each coating sample is exposed to the compressed air jet carrying dry sand particles. Weighing of samples at regular interval of time during impact is done with a precision electronic balance of ± 0.1 mg accuracy level to determine cumulative mass loss. Erosion rate, defined as the coating mass loss per unit erodent mass (mg/g) is calculated.

Figure 4.23 presents a typical erosion curve for different red mud coatings at 90° angle of impact. It is seen that initially the cumulative coating mass loss increases rapidly and later on becomes almost stagnant. This trend is observed in case of all the four coatings (made with the plasma torch operating at input power levels of 6,9,12 and 16 kW respectively). Fig. 4.24 to fig. 4.26 show the erosion wear rates of these coatings for 30°, 60° and 90° impact angles respectively. Similarly, erosion rates of coatings made with red mud premixed with 30% fly ash and with 5% aluminium are presented in fig. 4.27 and fig.4.28 respectively. It is evident from these figures that a transient regime in the erosion process exists, during which the incremental erosion rate decreases monotonically down to a constant steady state value. This constant value is referred to as the *steady state erosion rate*.

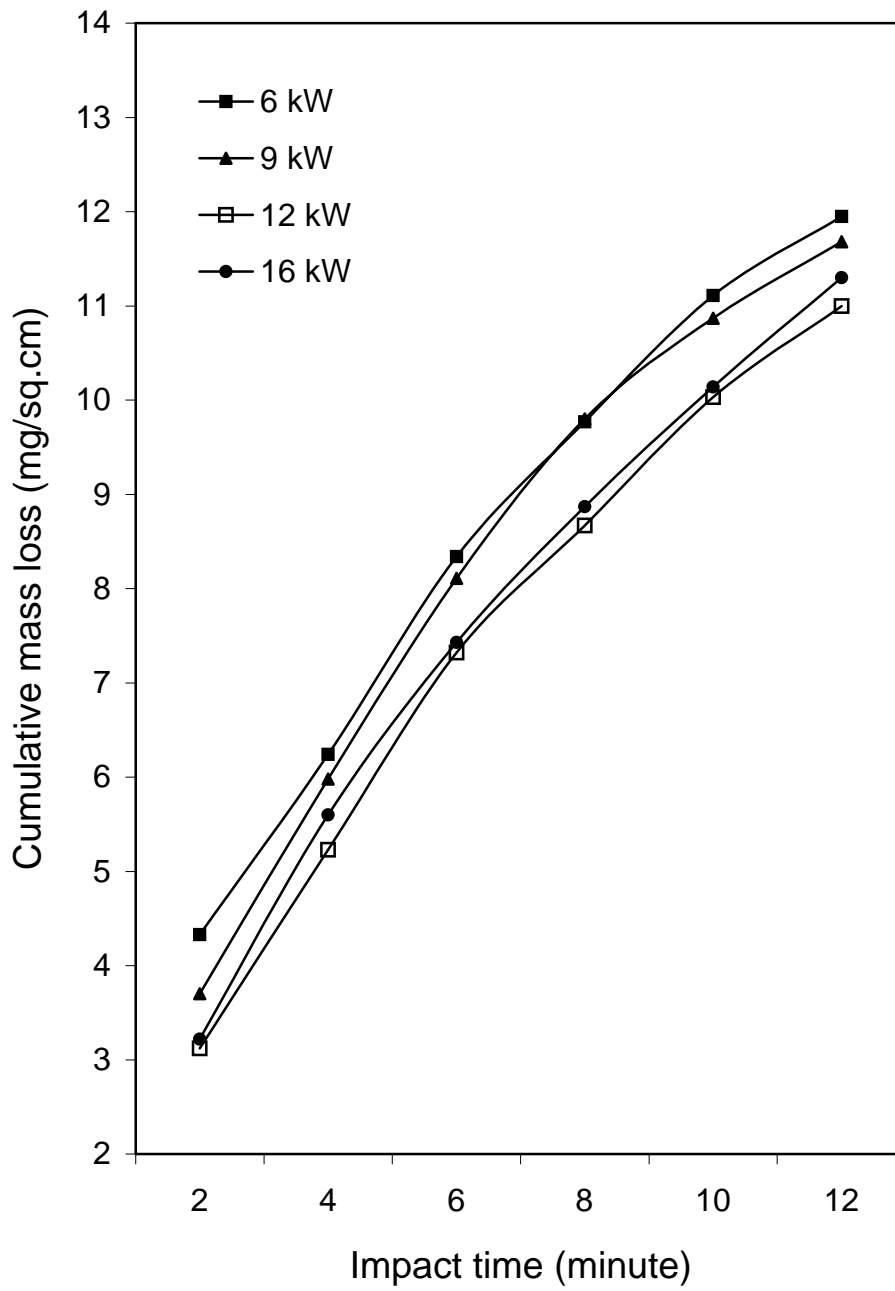


Fig 4.23 Cumulative mass loss of red mud coatings made at different operating power levels with 90° angle of impact

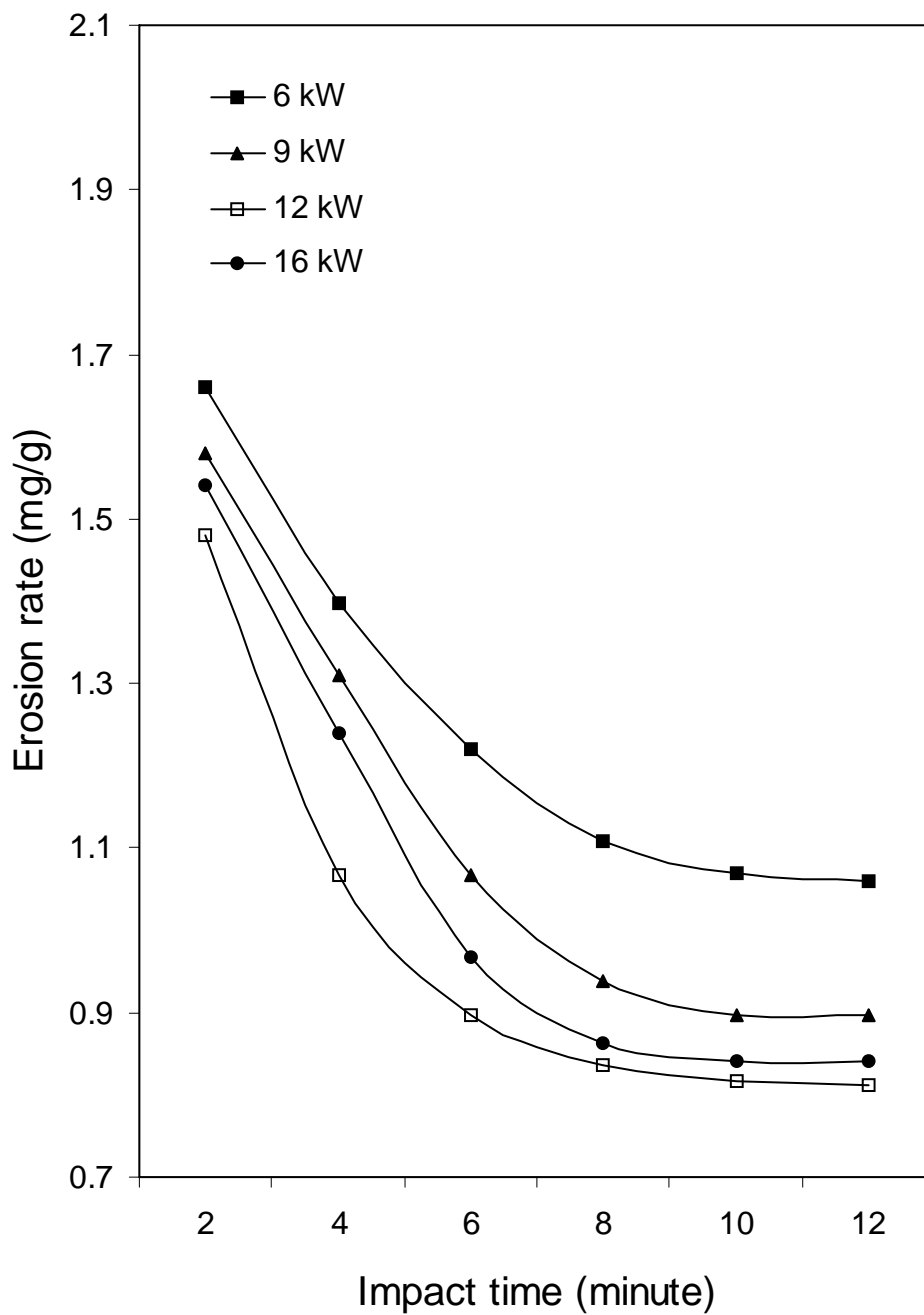


Fig 4.24 Variation of erosion wear rate of red mud coatings (deposited at 6,9,12,16 kW) with time of impact at 30° angle of impact

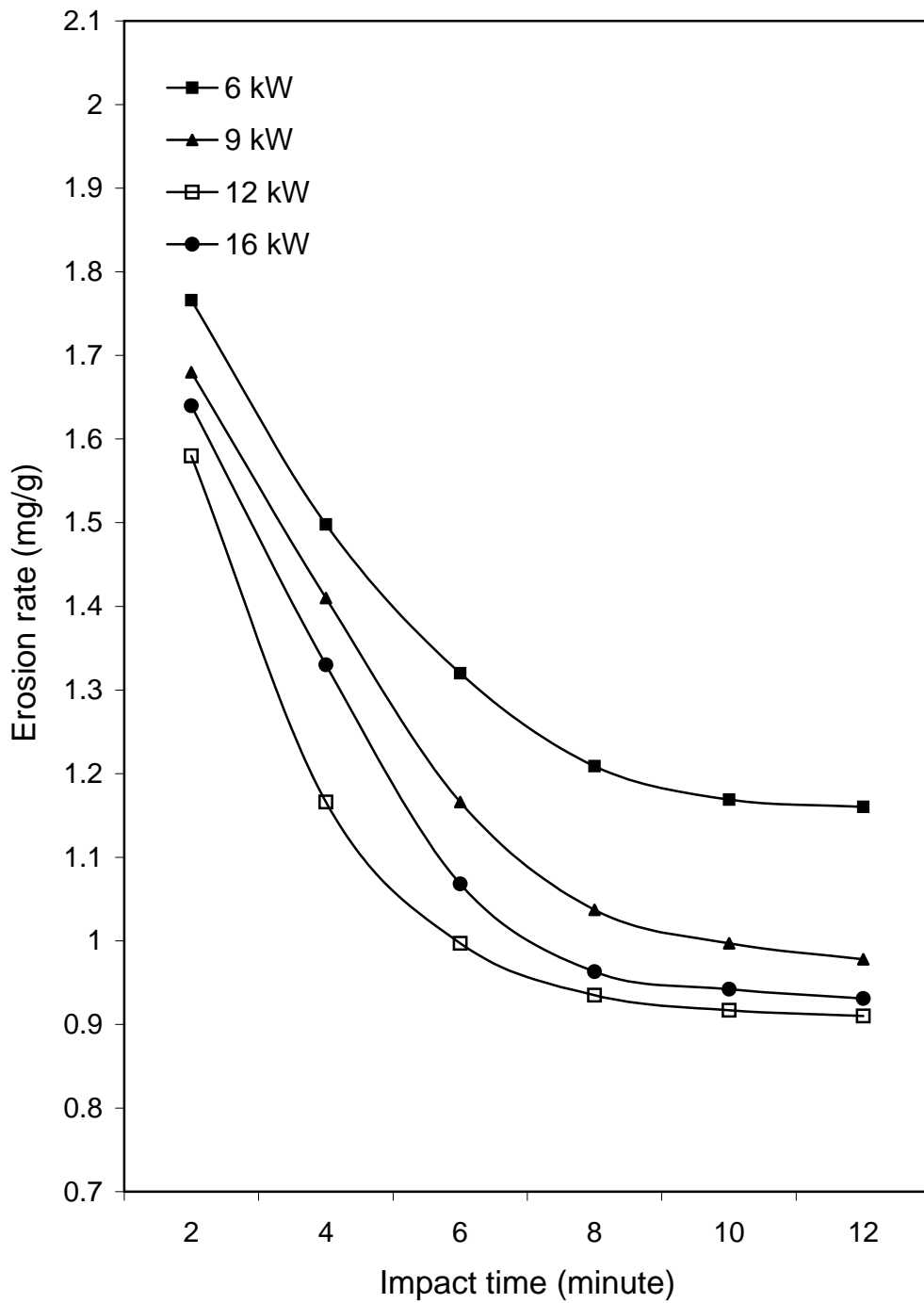


Fig 4.25 Variation of erosion wear rate of red mud coatings (deposited at 6, 9, 12, 16 kW) with time of impact at 60° angle of impact

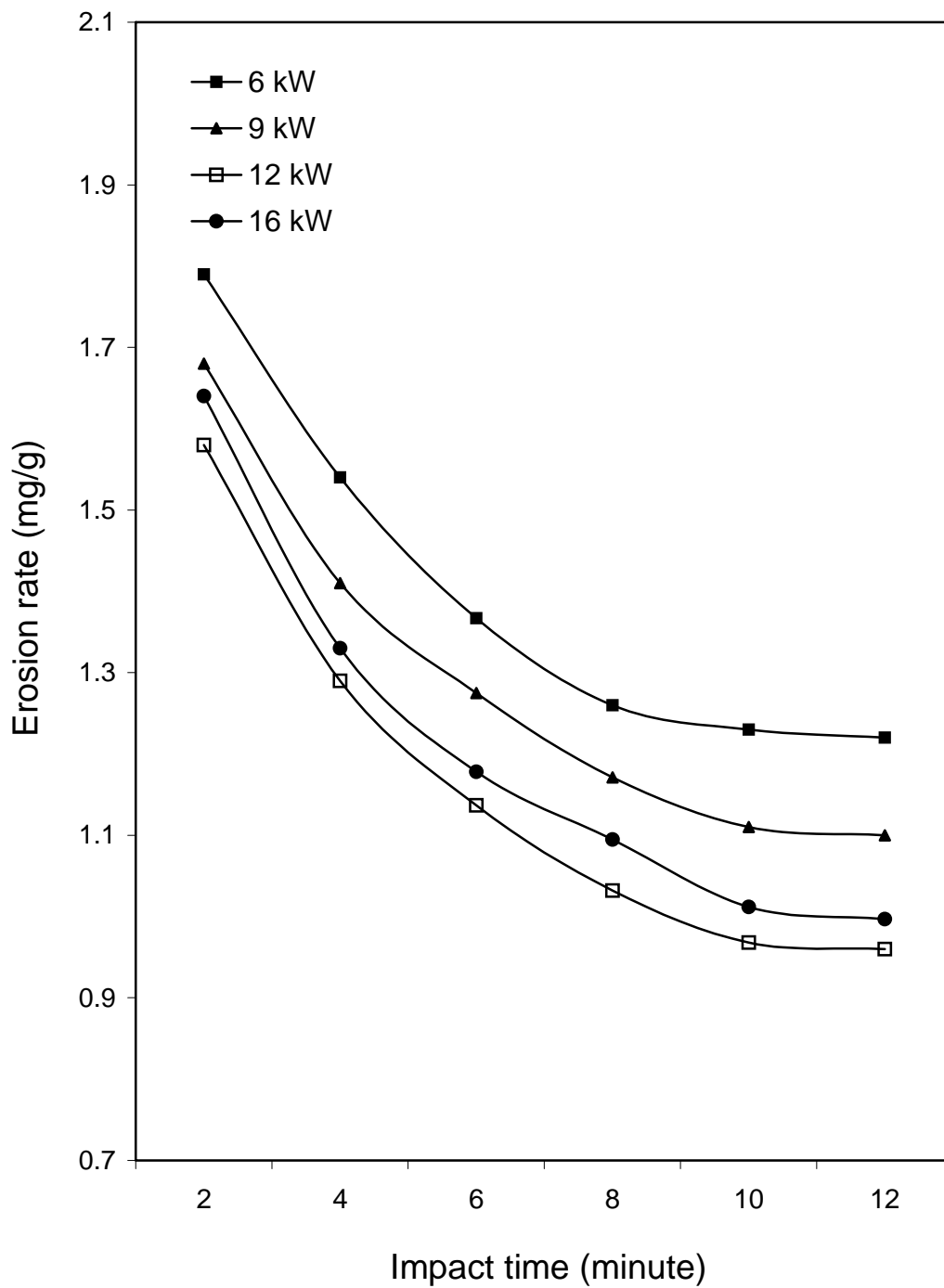


Fig 4.26 Variation of erosion wear rate of red mud coatings (deposited at 6,9,12,16 kW) with time of impact at 90° angle of impact

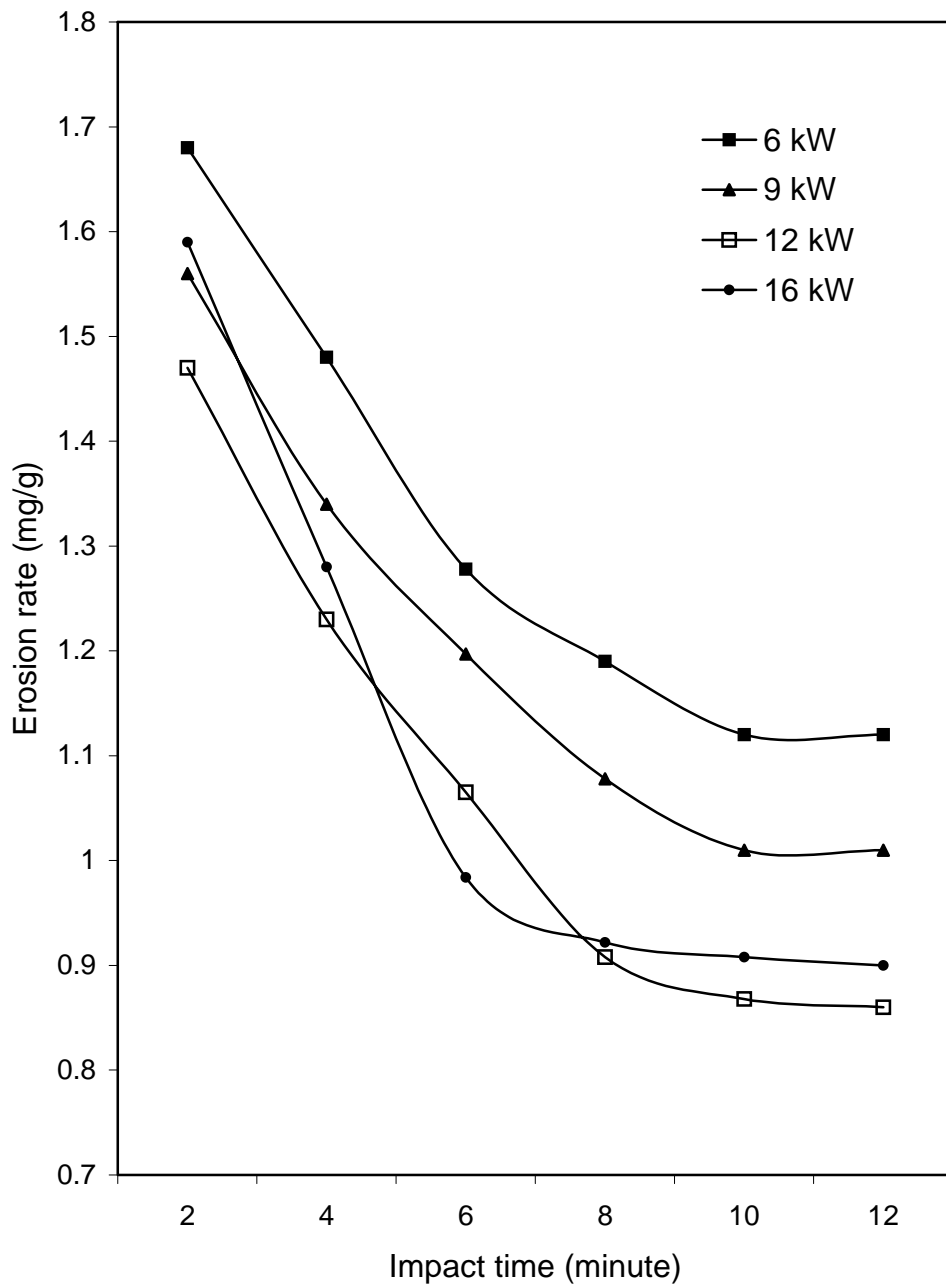


Fig 4.27 Variation of erosion wear rate of red mud + fly ash coatings (deposited at 6, 9, 12, 16 kW) with time of impact at 90^0 angle of impact

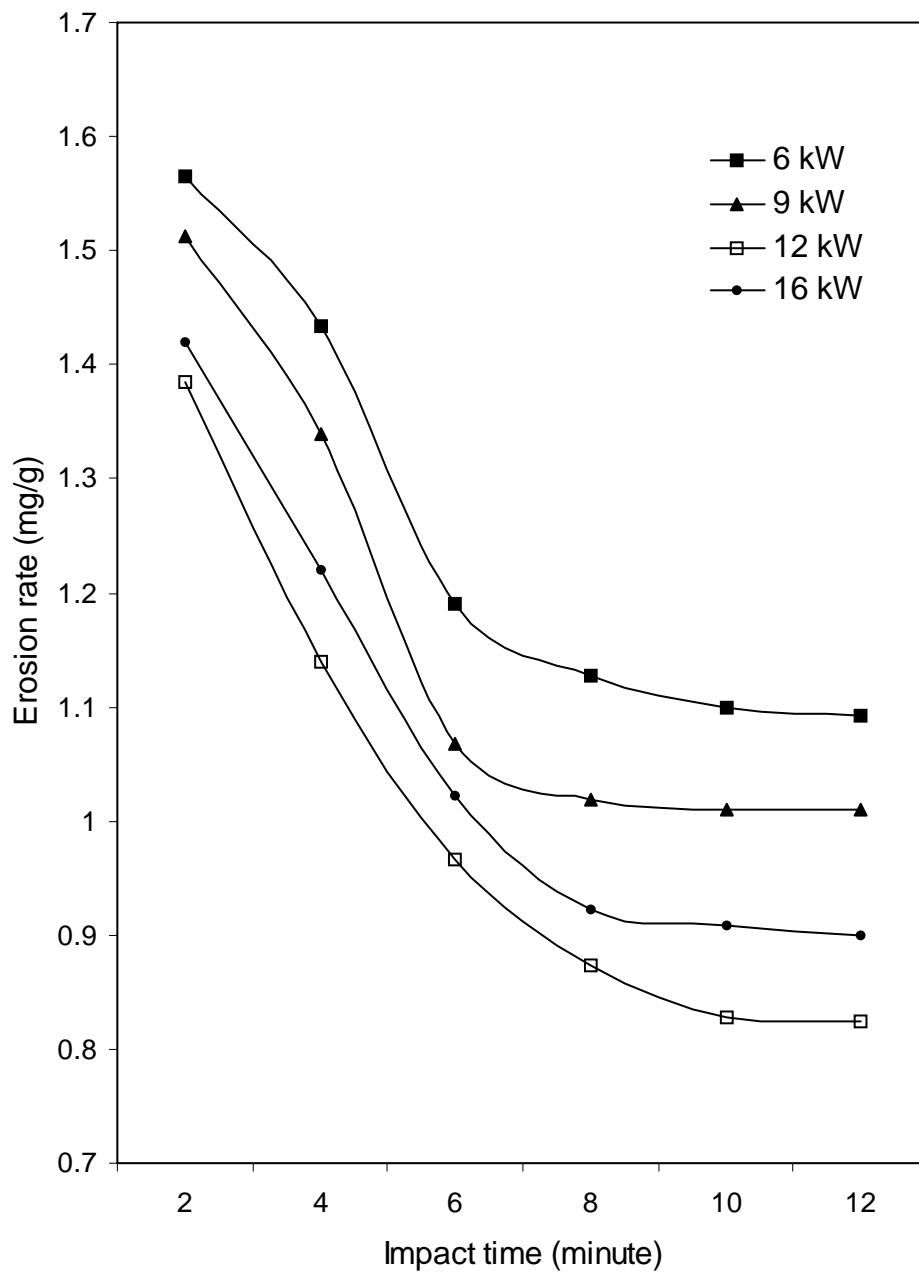


Fig 4.28 Variation of erosion wear rate of red mud + aluminium coatings (deposited at 6, 9, 12, 16 kW) with time at 90° angle of impact

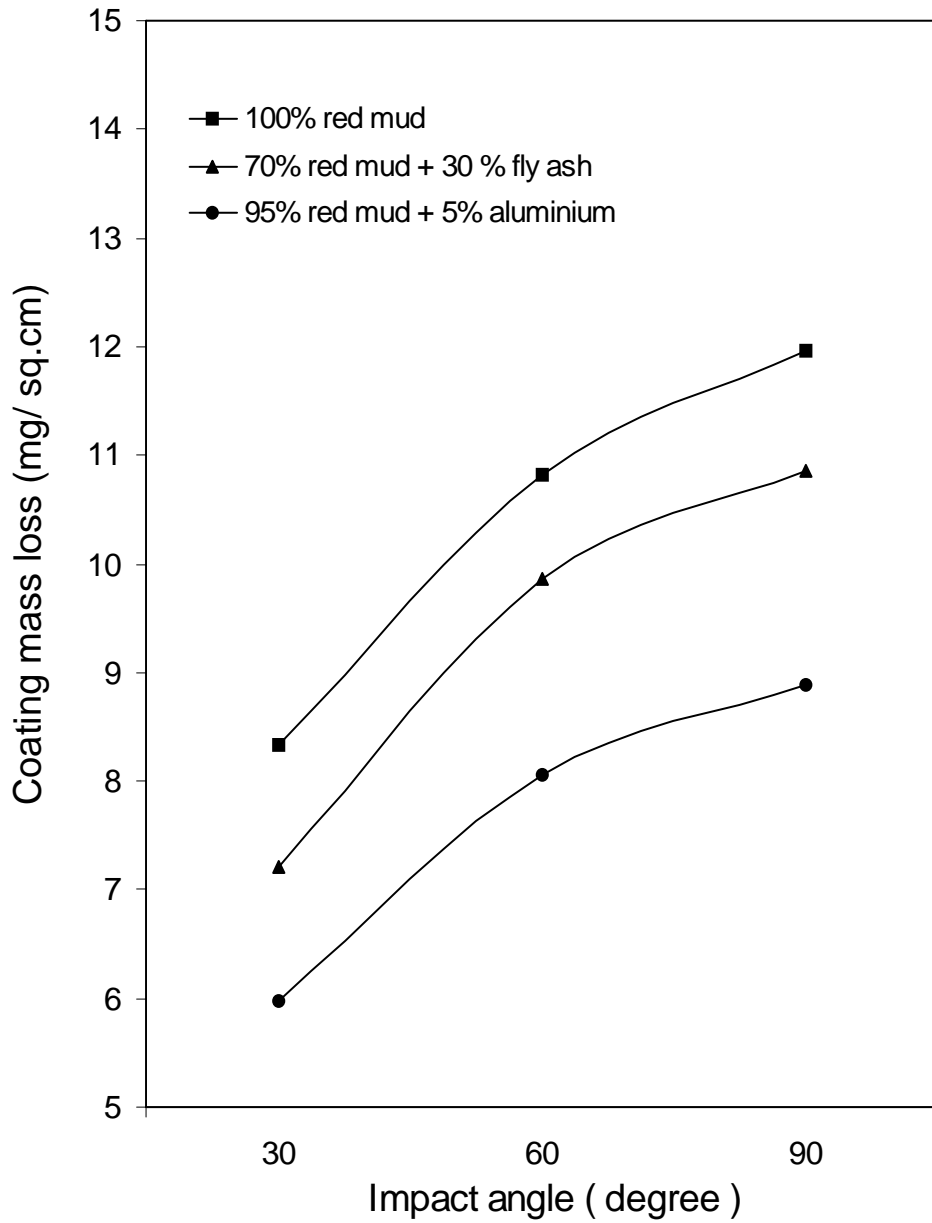


Fig 4.29 Variation of cumulative mass loss of different coatings made at 12 kW with angle of impact
 [Impact time = 12 minutes , SOD = 200 mm]

The decrease in the wear rate of various plasma sprayed coatings with erosion time (or erodent dose) has been reported earlier by Levy [188]. He has shown that, the incremental erosion rate curves of brittle materials start with a high rate at the first measurable amount of erosion and then decreases to a much lower steady state value [189] . In the present work also, this trend is found in case of all coatings subjected to erosion test at various impact angles. This can be attributed to the fact that the fine protrusions on the coating parts are relatively loose and can be removed with less energy than what would be necessary to remove a similar part from the bulk of the coating. Consequently, the initial wear rate is high. With increasing exposure time the rate of wear starts decreasing and in the transient erosion regime, a sharp drop in the wear rate is obtained. As the coating surface gradually gets smoothed, the rate of erosion becomes steady.

Figure 4.29 illustrates the effect of impact angle (α) on the mass loss of various coatings subjected to solid particle erosion. The erosion results for coatings of different materials deposited at 12 kW operating power of the plasma torch at impact angles of 30, 60 and 90 degrees are shown. Mass loss is measured after the samples are exposed to the erodent stream for 12 minutes. It is seen from the graph that irrespective of the feed material, the erosion mass loss is higher at larger angle of impact and the maximum erosion takes place at $\alpha = 90^0$. This is typical of all brittle coatings. The relationship between erosion rate E and impact angle (α) is suggested by Bayer [190] as

$$E = (K_d v^n \text{Cos}^n \alpha + K_b v^m \text{Sin}^m \alpha)M$$

For a particular test condition, velocity of impact v, erodent supply rate M are constant. The constants K_d , K_b m, n are determined by fitting the equation to experimental data. For typical brittle materials $K_d = 0$ and the erosion rate is maximum at 90^0 impact angle. For typical ductile material, $K_b=0$ and erosion rate is largest at $20^0 - 30^0$ impact angles.

The results obtained in the present work show that for 90° impact angle, red mud coating loses 11.96 mg per every cm^2 area in 12 minutes while the mass loss is only 8.34 mg/cm^2 in case of $\alpha = 30^{\circ}$. These values are 10.85 mg/cm^2 and 7.21 mg/cm^2 for red mud + fly ash coating, 8.89 mg/cm^2 and 5.98 mg/cm^2 for red mud + aluminum coating respectively. This variation of erosion wear loss confirms that the angle at which the stream of solid particles impinges the coating surface influences the rate at which the material is removed. It further suggests that, this dependency is also influenced by the nature of the coating material. The angle of impact determines the relative magnitude of the two components of the impact velocity namely, the component normal to the surface and parallel to the surface. The normal component will determine how long the impact will last (i.e. contact time) and the load. The product of this contact time and the tangential (parallel) velocity component determines the amount of sliding that takes place. The tangential velocity component also provides a shear loading to the surface, which is in addition to the normal load that the normal velocity component causes. Hence as this angle changes the amount of sliding that takes place also changes as does the nature and magnitude of the stress system. Both of these aspects influence the way a coating wears. These changes imply that different types of material would exhibit different angular dependency.

4.9 COATING DEPOSITION EFFICIENCY

Deposition efficiency of all coatings made within the scope of this investigation is evaluated. Coating deposition efficiency is defined as the ratio of the weight of coating deposited on the substrate to the weight of the expended feedstock. Weighing method is accepted widely to measure this. It can be described by the equation [183]

$$\eta = (G_c/G_p) \times 100 \%$$

Where η is the deposition efficiency

G_c is the weight of coating deposited on the substrate and

G_p is the weight expended feed stock

In this work, torch input power is selected as the parameter to investigate its influence on deposition of the entire series of powders taken on all the four substrates. Fig. 4.30 to fig. 4.34 present the variation of deposition efficiency with operating power level on the substrates for various coating materials. Similarly this variation is shown for all depositions on individual substrates in fig. 4.35 to fig. 4.38 (i.e. on aluminium, copper, mild steel and stainless steel substrates) respectively.

It is interesting to note that the deposition efficiency, in all cases, is increased in a sigmoidal fashion with the torch input power. For example: on aluminium substrates, the value increases from 7.2% to 23.59% (with input power to plasma torch increasing from 6 kW to 16 kW) for red mud deposition. Similarly, this value ranges from 9.3% to 31.23% when the coating material is a mixture of equal proportion of red mud and fly ash. Where as, when this material is deposited on copper substrates, the efficiency of deposition is seen to vary from 10.35% to 27.823%. The results obtained for all compositions (raw materials) i.e. red mud, red mud +fly ash, red mud +carbon and red mud + aluminium are presented in table 4.4. It reveals that efficiency of coating deposition is significantly influenced by the input power of the torch. The trend of variation is similar for all substrates and in case of all coating materials considered in this work.

Coating Material	Arc Current (amp)	Arc Voltage (Volt)	Torch Input Power (kW)	DEPOSITION EFFICIENCY (%)			
				Al	Cu	MS	SS
RM 100%	200	30	6	7.2	7	7.35	7
RM 100%	250	36	9	13.5	13.92	13.25	13.3
RM 100%	300	40	12	20.68	21.95	22.5	23
RM 100%	400	40	16	23.59	24	25.3	25.2
RM+30%FA	200	30	6	8.3	8.35	8.45	8.42
RM+30%FA	250	36	9	14.32	16	15.21	14.92
RM+30%FA	300	40	12	22.5	23.2	23.6	24
RM+30%FA	400	40	16	25.23	26.23	26.69	26.5
RM+50%FA	200	30	6	9.3	10.35	9.95	9.942
RM+50%FA	250	36	9	16.32	17.976	17.21	16.192
RM+50%FA	300	40	12	26.5	25.2	24.76	26.08
RM+50%FA	400	40	16	31.23	27.823	28.69	28.05
RM+20%C	200	30	6	8.39	8.359	8.675	8.92
RM+20%C	250	36	9	14.632	16.5	15.299	15.292
RM+20%C	300	40	12	22.599	23.298	23.987	24.998
RM+20%C	400	40	16	25.238	26.83	26.899	26.979
RM+5%Al	200	30	6	7.85	7.69	8.498	7.799
RM+5%Al	250	36	9	14.55	14.9	14.288	14.65
RM+5%Al	300	40	12	21.89	22.98	23.29	23.99
RM+5%Al	400	40	16	24.93	24.97	26.493	26.08

Table 4.4 Coating deposition efficiency at different spraying conditions

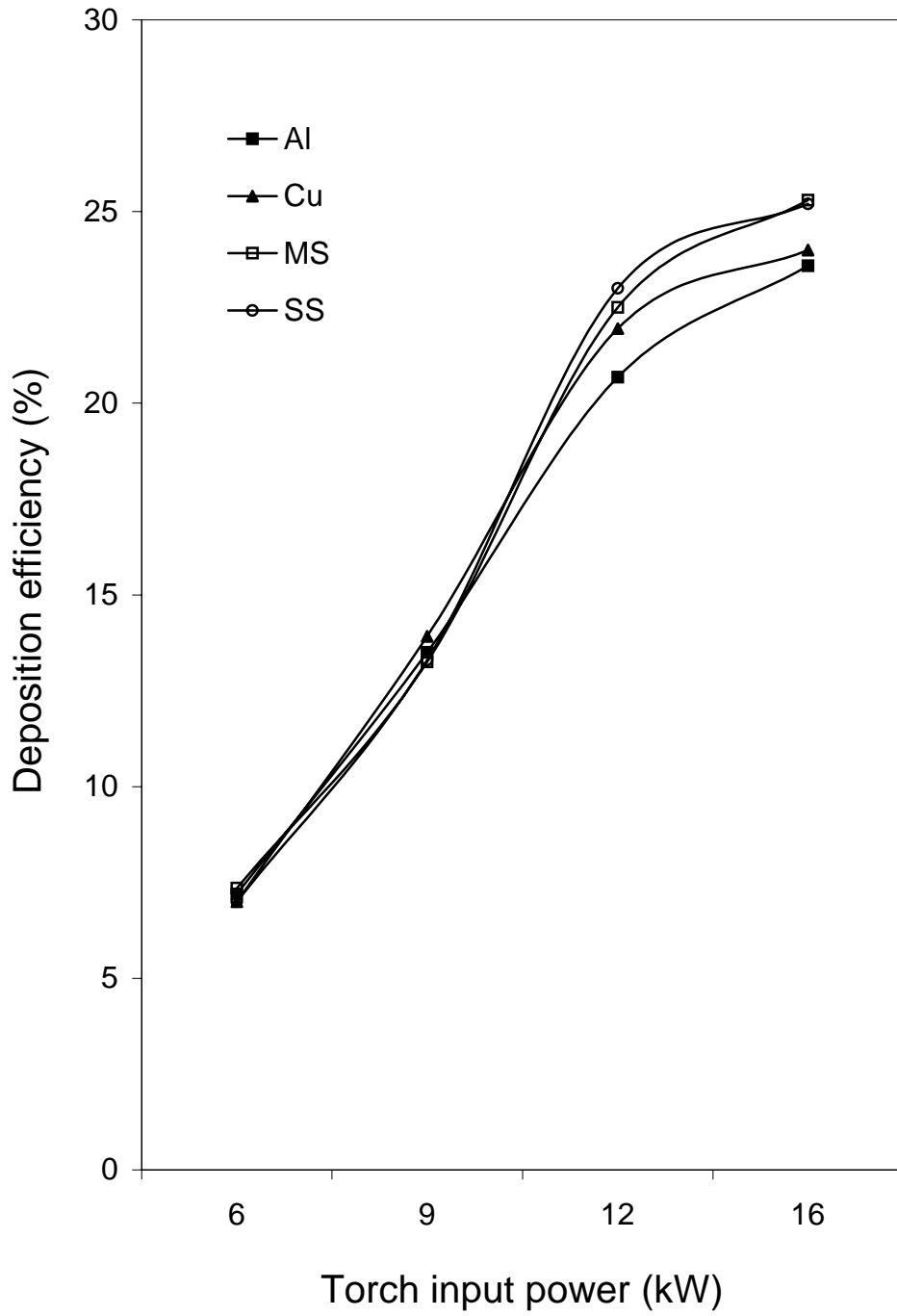


Fig 4.30 Deposition efficiency of red mud coatings made at different power level on different substrates

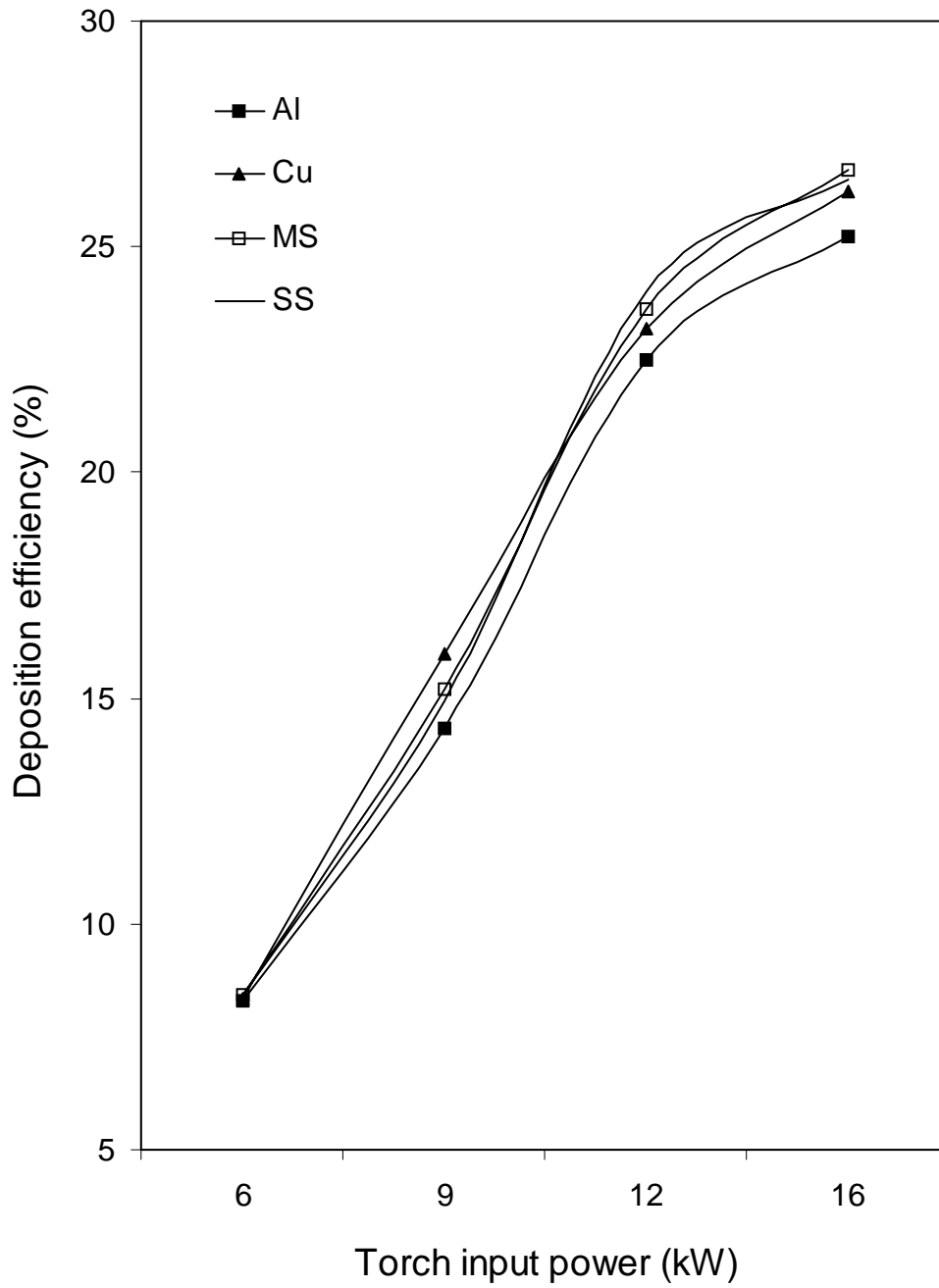


Fig 4.31 Deposition efficiency of red mud + 30% fly ash coatings made at different power level on different substrates

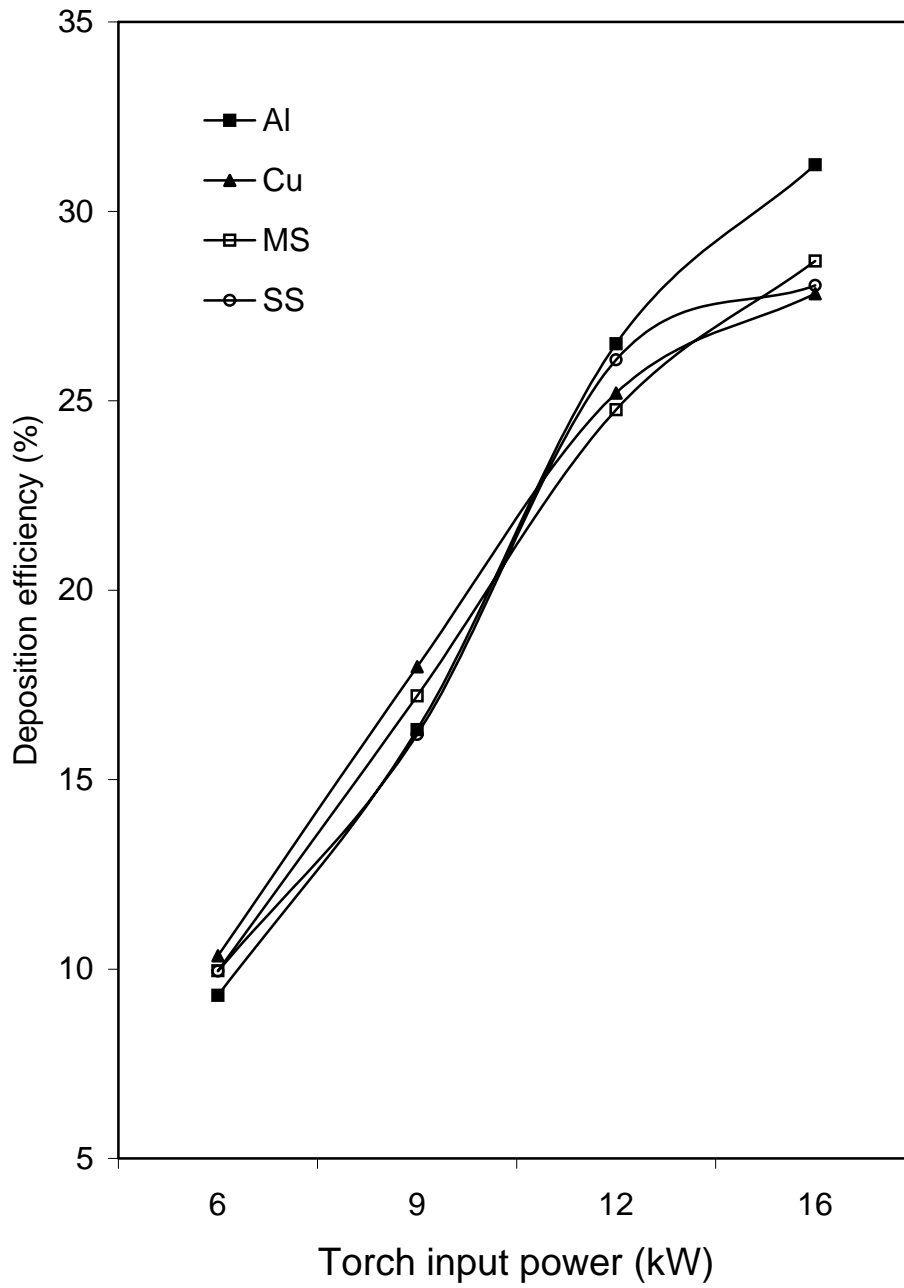


Fig 4.32 Deposition efficiency of red mud + 50% fly ash coatings made at different power level on different substrates

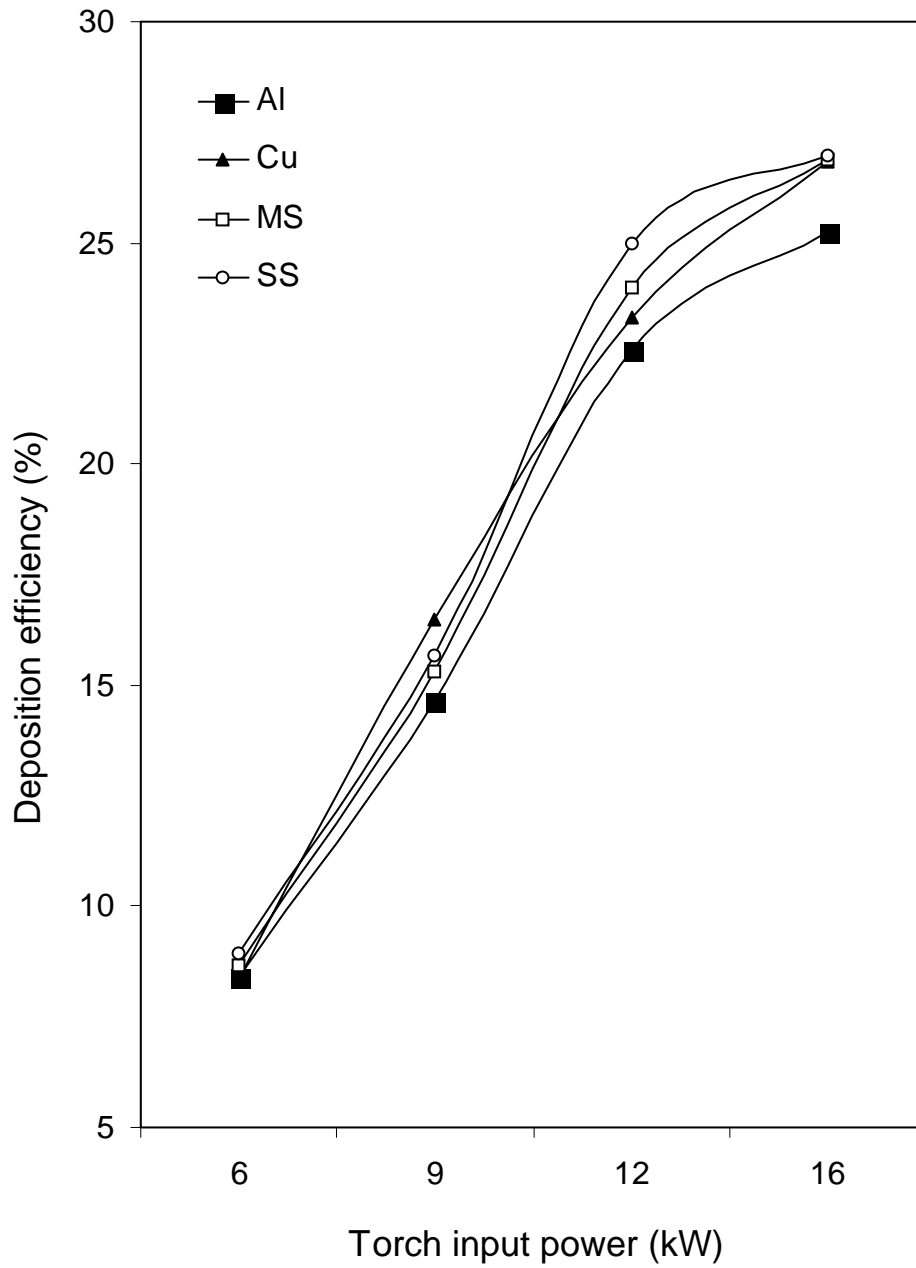


Fig. 4.33 Deposition efficiency of red mud + 20% carbon coatings made at different power level on different substrates

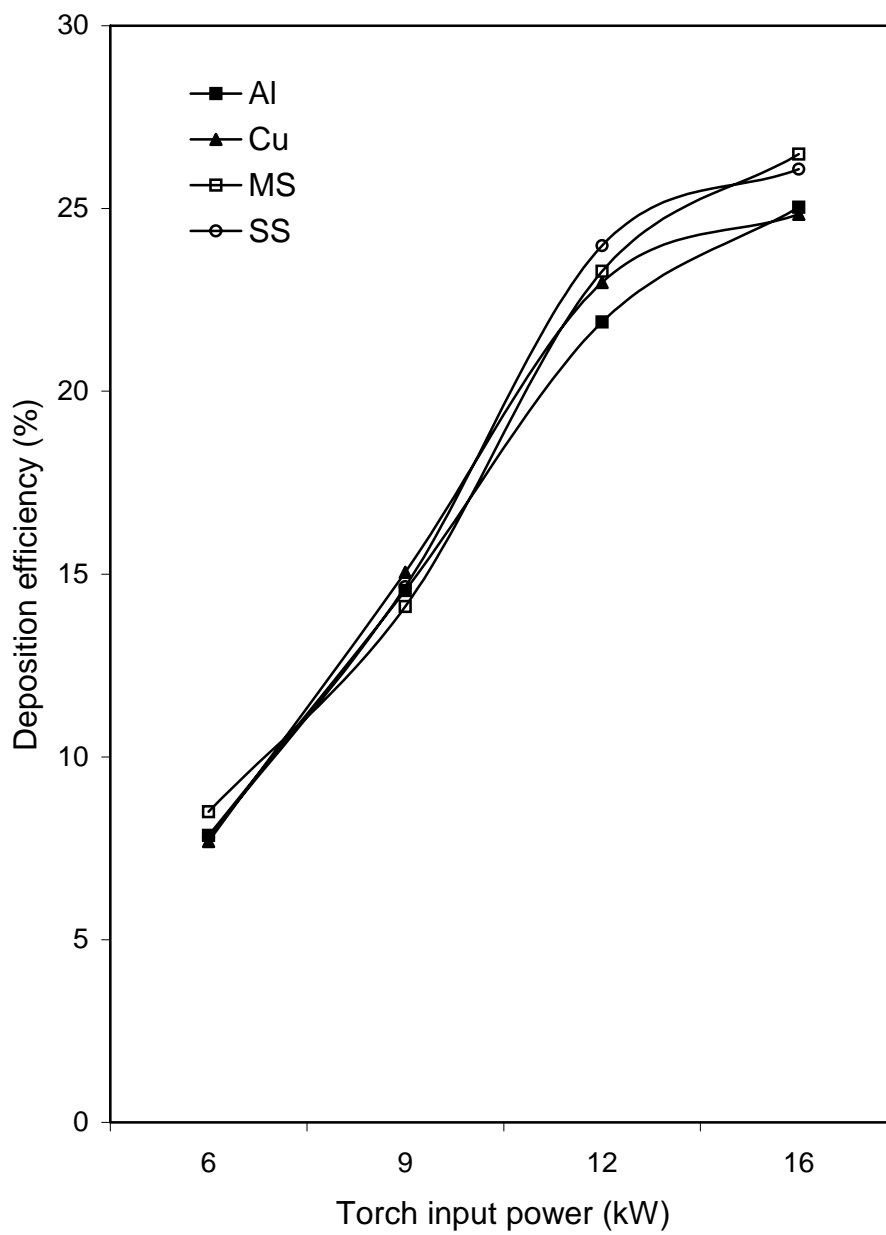


Fig. 4.34 Deposition efficiency of red mud + 5% aluminium coatings made at different power level on different substrates

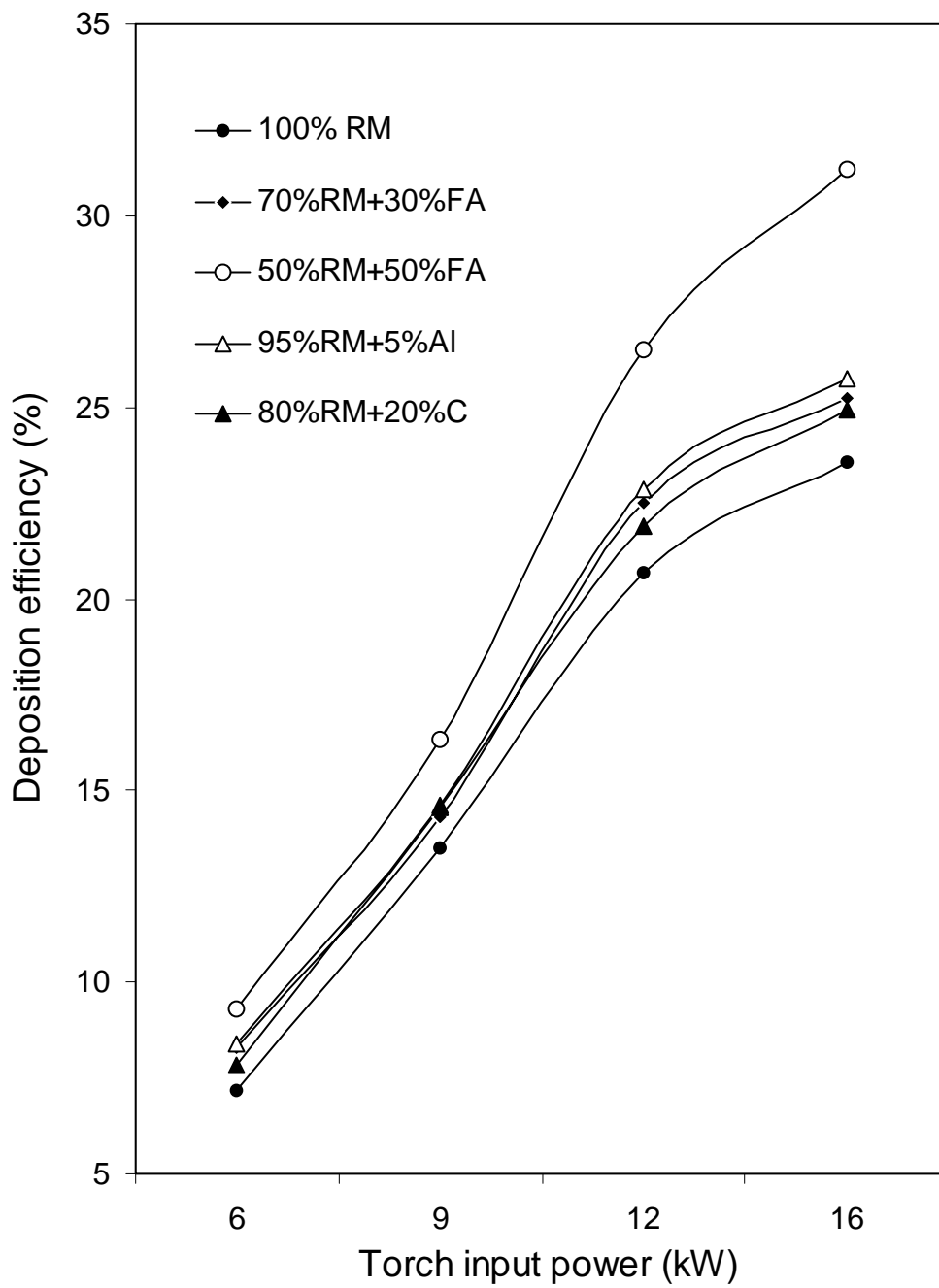


Fig 4.35 Deposition efficiency of coatings made of different feed materials on aluminium substrates

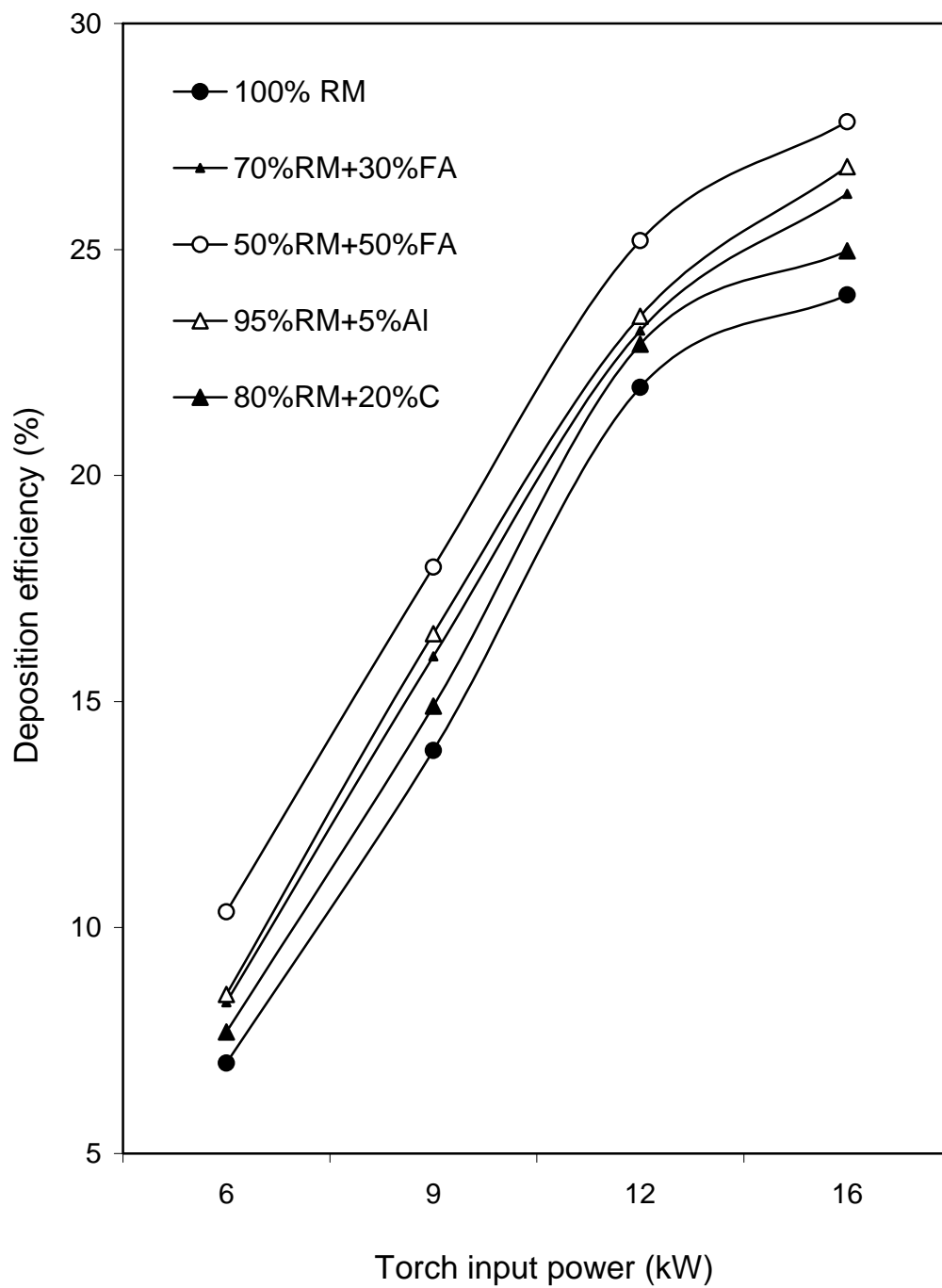


Fig 4.36 Deposition efficiency of coatings made of different feed materials on copper substrates

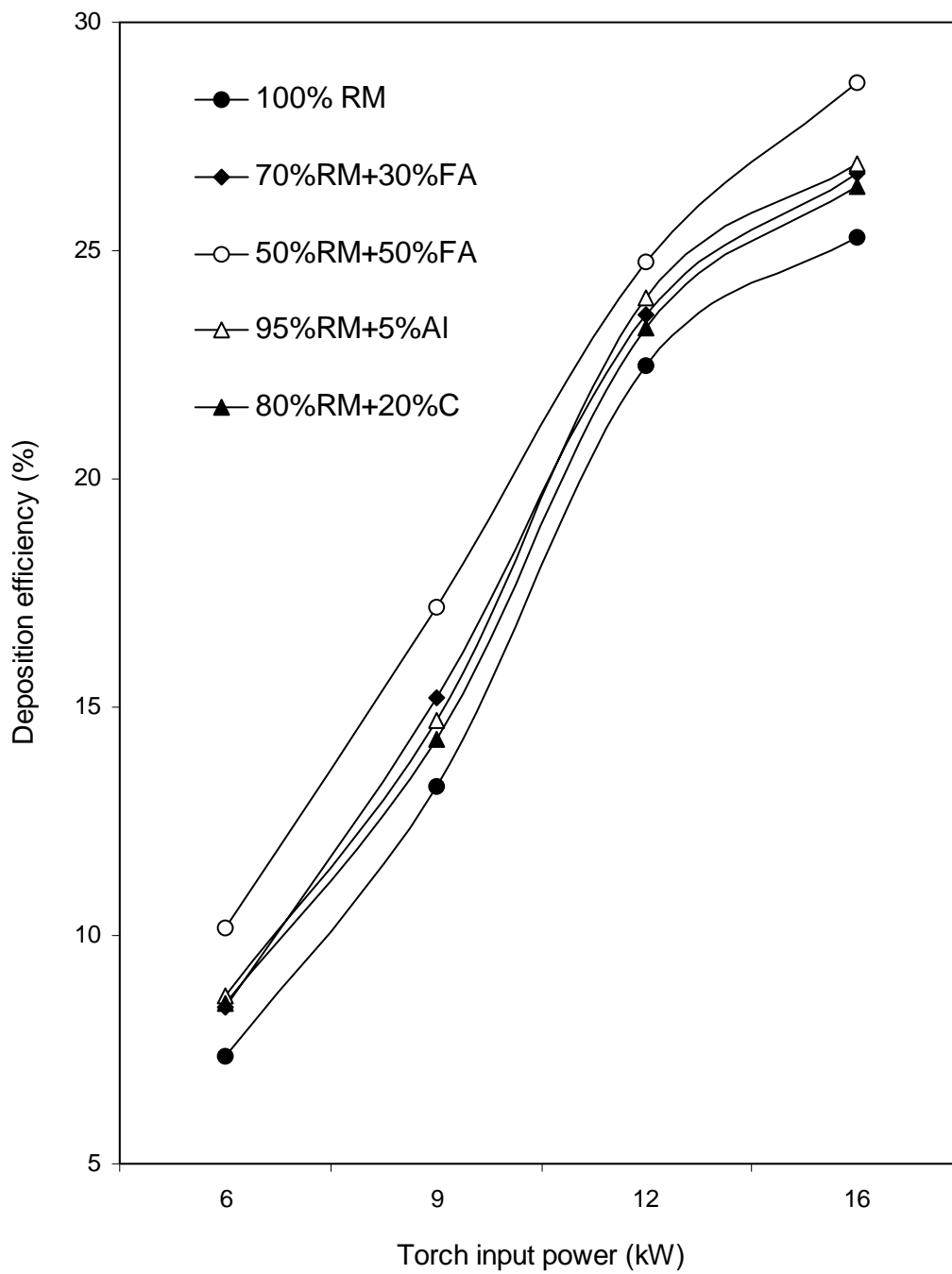


Fig 4.37 Deposition efficiency of coatings made of different feed materials on mild steel substrates

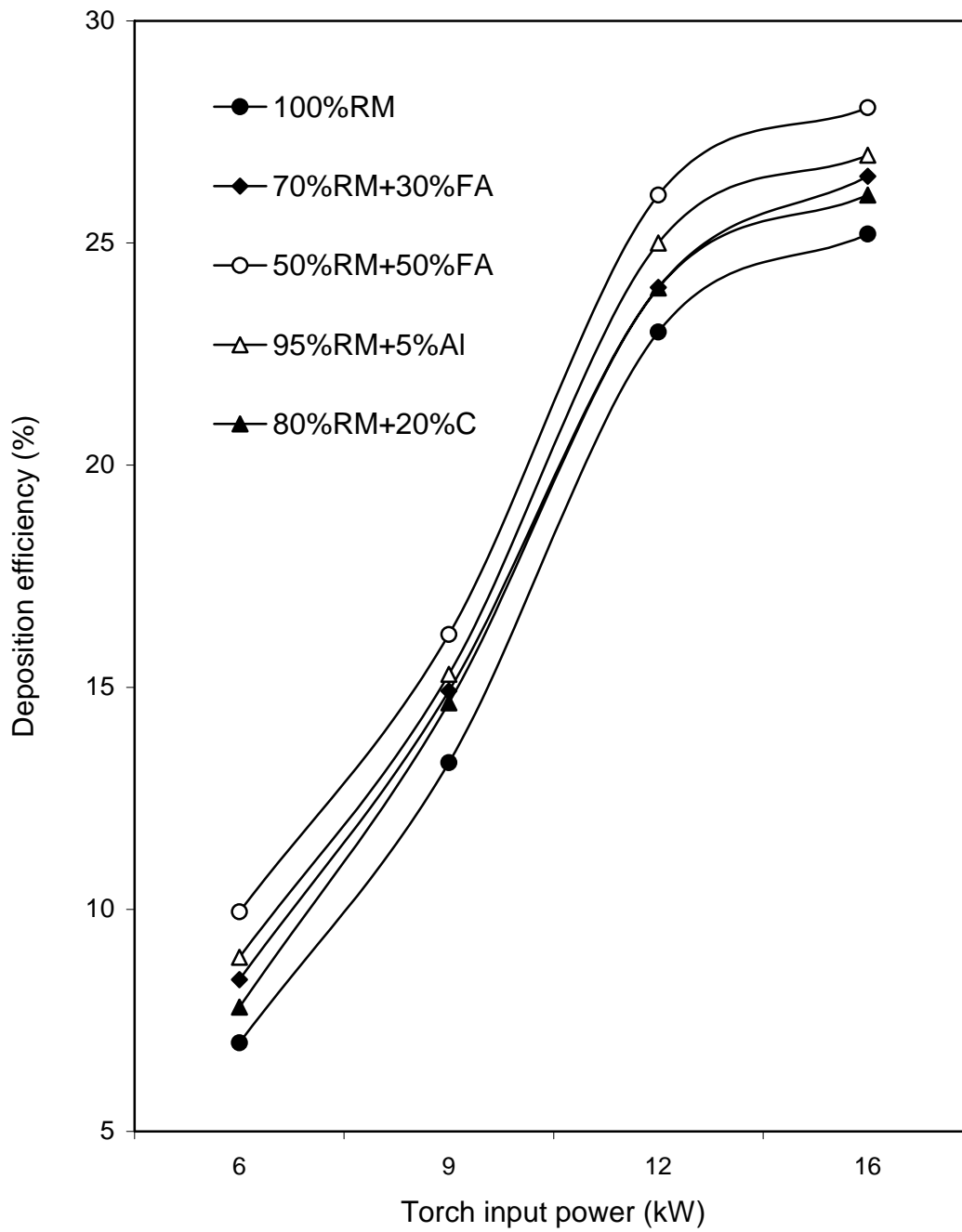


Fig 4.38 Deposition efficiency of coatings made of different feed materials on stainless steel substrates

Within the domain of experiments carried out in this work, the maximum deposition efficiency of 31.23% is obtained for coatings made with red mud + fly ash (50% by weight) mixture at 16 kW operating power level of the plasma torch (on aluminium substrate). The maximum deposition efficiency in case of copper, mild steel and stainless steel substrates are found out to be 27.823%, 28.69% and 28.05% respectively.

It is seen that with addition of fly ash to red mud, the deposition is improved substantially. It is also observed that pre-mixing of aluminium powder and carbon powder helps in improving the deposition efficiency of red mud coatings. It may be due to the improvement of inter particle bonding.

4.10 DISCUSSION

In thermal spray oxide coatings developed using atmospheric plasma spray (APS) technique, particle deposition i.e. the coating thickness is influenced mainly by the input power to the plasma torch. With increase in power level, the plasma density increases leading to a rise in enthalpy and thereby, the particle temperature. Hence more number of particles get melted during in-flight traverse through plasma jet. When these molten species hit the substrate, they get flattened and adhere to the surface. The deposition of layers is favoured with availability of more number of molten / semi molten particles which is enhanced by increasing the torch input power. This increases the coating thickness. But, beyond certain limit of operating power level; fragmentation and vaporization of sprayed particles do occur simultaneously and for these two mechanisms, some (powder) particles fly off during spraying restricting further increase in coating thickness.

In the present investigation, coatings are deposited on metal substrates of different thermal conductivity and thermal expansion coefficient. It is observed that the coating thickness varies with different substrate materials. This may be

mainly due to thermal conductivity of the substrate. When the sprayed particles impinge on the surface of the substrate, heat transfer takes place. The particles dissipate heat at a faster rate through the metal substrate. Subsequent particles accumulated / deposited on the top of the first layer restrict the heat transfer towards outside environment than through the metal surface. The dissipation of heat from the particles /coating layers is favoured with increased heat dissipation rate through the substrate. So in metals having higher thermal conductivity, the layer deposition is faster. In this work, the observation of higher coating thickness on copper substrate than that on aluminium, stainless steel and mild steel substrates may be attributed to this effect.

From the study of coating deposition efficiency, it is seen that, deposition efficiency has increased with increase in torch input power up to an optimum level (about 12 kW), beyond which there is no significant change. This is a measure of the amount of materials deposited per unit surface area. Berger *et al.* [191] have also reported similar observation that, the deposition of high quality coating is favoured at moderate temperature range.

Values of coating deposition efficiency for different feed stocks (i.e. red mud, red mud + fly ash , red mud + carbon , red mud + aluminium) as given in table 4.4, reveal that the deposition efficiency not only varies with operating power level, but also varies significantly with the type of sprayed material. In this investigation, addition of carbon to red mud has helped in phase transformation and formation of inter-oxides (as observed in X-ray diffractogram). By adding fly ash, the percentage of silica and alumina has increased favouring the formation of alumino-silicate inter-oxide compounds (mullite etc.). The improvement of coating deposition with addition of aluminium metal powder is obvious. Because during spray deposition, metal particles might have remained in molten/ semi-molten states and this has improved not only inter-particle bonding but also the bonding with the substrates.

The analysis of coating - substrate bond strength of all the sprayed materials on different substrates, presented in table 4.1 envisages that, (i) there is an increase in adhesion strength with increase in plasma torch operating power (up to 12 kW) for almost all the substrates and (ii) there is a variation in adhesion strength for feed materials of different compositions.

With increase in torch operating power, there is availability of more number of molten/ semi molten particles which on hitting the substrate, get fused and flattened at a relatively faster rate improving the mechanical inter-locking on the substrate and thereby increasing the bond strength . It has been shown in previous investigations [192] that , for a given material, the final coating properties depend on the velocity, temperature and type of particles just before impact on the substrate or on the coating layers already deposited. The plasma power effectively changes the temperature and particle velocity and therefore affects the coating properties. The composition of the coating materials also affects the coating adhesion strength due to transformation / formation of phases and inter-oxides that favour the inter particle bonding and adhesion to the substrate. In this investigation, higher adhesion strength in substrates of lower thermal conductivity (i.e. in mild steel) is observed. It is known that the oxides adhere weakly to a substrate of high thermal conductivity owing to a low contact temperature [193]. Hence the relatively lower adhesion strength on copper and aluminium substrates as compared to mild steel substrate is justified.

From the microscopic studies (fig. 4.9 to fig. 4.14) it is seen that, the particle size and their appearance have changed with the change in the operating conditions of the plasma torch and for different raw material compositions. Micro-cracks and cavities/pores are also seen in the deposited layers. This reflects in the type of reactions (indicative of whether the particles are molten, semi-molten, un- melted, fragmented and of possible phase transformation mechanisms) which might have taken place during in-flight traverse of the

powders through plasma. The molten or semi-molten species bear equi-axed type structure. The fragmented particles get melted completely exhibiting spheroidal shape and partially melted or unmelted powders get stacked in the coating layers during deposition. The formation of micro-cracks are possible in the coatings near to the substrate and open pores/cracks do originate along the direction of heat flow i.e. towards the substrate [194] due to shrinkage of particles parallel to the surface of the substrate. Hence such microstructures affect the coating homogeneity and adhesion with the substrate. Measured values of coating porosity, presented in table 4.2, show that the porosity varies with operating power as well with the feed material composition. However, a maximum porosity of about 12% is observed; which is very much within the limit as generally found with plasma sprayed ceramic coatings [187].

Micro-hardness measurement is made on optically distinguishable phases present in the coatings. The hardness values are different for different phases and appear to be not much dependent on torch operating power level. The existence of at least three different phases (which are optically distinguishable) might have been formed during plasma spraying. On referring to the X Ray diffractograms taken on raw material and coated samples, it becomes evident that during coating deposition, formation and transformation of phases have taken place. So during spraying, the phase transformation and/or formation of inter oxides (transformation of Fe_2O_3 to Fe_3O_4 , α -alumina to γ -alumina, silica to tridamite and/or crystabolite and formation of mullite phases) corroborate to different micro-hardness values obtained on various phases of the coatings.

To assess the suitability of these coatings for tribological applications, solid particle erosion wear behaviour is studied. From the observed results, it can be said that, the erosion wear rate is affected by (i) input power during the coating deposition and (ii) impact angle of the solid particles on the coating surface. With increase in angle of impact, the erosion wear increases and is maximum at

90⁰. Such type of observation of high rate of erosion wear is usual with plasma sprayed ceramic coatings [195].

The erosion wear for different coatings can be attributed to (i) the phase constituents of the coatings and (ii) the type, volume and distribution of pores/cavities/cracks present in the coatings. The XRD study and micro-hardness results obtained in this investigation show that the phase composition of the coatings for different feed stocks exhibit different hardness. It is known that, with increase in the material hardness, the erosion wear rate decreases [196]. So our findings on the wear behaviour of various coatings are at par with the concluding remarks of previous investigations.

Branco et al. (139) reported that, the coating porosity influences the erosion in three ways. Firstly, it reduces the material strength against plastic deformation or chipping since the material at the edge of a void lacks mechanical support. Secondly, the concave surface inside a void that is not under the shadow of some void edge will see an impinging particle at an angle higher than the average target surface to impact angle (which is detrimental for brittle materials). And finally, pores can impair strength by acting as stress concentrators and/or decreasing the load bearing surface. The coatings under this investigation are though brittle in nature, the effect of pore volume fraction on erosion wear needs a more detailed investigation.

ANALYSIS OF EXPERIMENTAL RESULTS USING STATISTICAL TECHNIQUES

5.1 INTRODUCTION

Coating deposition by plasma spraying involves a number of process variables, which contribute in a large way to the quality of the coating. During spraying, various operating parameters are determined mostly based on past experience. It therefore does not provide the optimal set of parameters for a particular objective. In order to obtain the best result with regard to any specific coating quality characteristic, accurate identification of significant control parameters is essential. Deposition efficiency of any coating is a characteristic which not only rates the effectiveness of the spraying method but also is a measure of the coatability of the material under study. This chapter is devoted to analyze the experimental results on the deposition efficiency of red mud coatings made at different operational conditions. For this purpose, two statistical techniques *fractional factorial testing* and *Taguchi experimental design* are used. Factors are identified according to their influence on the coating deposition. The most significant parameter is found. A prediction model using *artificial neural network* (ANN) is presented considering the significant factors.

5.2 FRACTIONAL FACTORIAL TESTING

In the plasma spray field there are at least three situations that frequently arises where optimum spray parameters must be experimentally determined: first,

when presented with new powders which have no published spraying parameters; secondly, when two or more standard powders are combined as a blend for spraying ; and third, when certain undesirable coating features develop and a relatively standard set of parameters needs to be evolved.

The first two situations are encountered in the present work during the deposition of red mud and of different mixtures of red mud and fly ash powders on metallic substrates. These materials are new in the field of plasma spray coating. The fractional factorial testing is chosen as the technique for analysis primarily for its ability to identify the most significant among the variables.

A full factorial test plan includes all possible combinations of the factors being tested, while a fractional factorial test plan is simply a desired fraction of the full factorial plan. In this method of testing, all the factors affecting the process are first selected. In plasma spraying, parameters viz. plasma arc current, arc voltage, electrical power level, surface roughness etc. are the main factors which affect the coating qualities. The values of any factor in an experiment are known as ‘ levels ’. Factorial testing is carried out in a manner, which will help in evaluation of all the factors independently. In a full factorial testing, each and every combination of parameters with different levels is considered. For a test involving seven parameters with each parameter being tested at two levels, the number of tests to be performed will be 2^7 , i.e. 128. In case of a fractional factorial test, only a small fraction of the full factorial testing is done. This test, though sacrifices the completeness, includes the effect of simultaneous parameter changes. The advantage of this test is that by performing just ‘ n ’ tests, ‘ n -1 ’ number of factors can be included [197].

5.2.1 Test Grids

The limit of fractionating a factorial plan is called fully saturated factorial test plan. A number of fully saturated test grids are available for testing, e.g. 3 factor 4 test grid, 7 factor 8 test grid etc. These grids are at two levels for each parameter. The two test levels are marked as ‘ + ’ and ‘ – ’ . For the present investigation, a 7 factor 8 test grid is selected to optimize the control parameters in just eight tests. The factors and levels chosen are based on experience and equipment capabilities. The evaluation of the coatings is done on the basis of deposition efficiency.

The parameters and the test levels selected for the test coatings are given in table 5.1. The complete test grid showing test layout with results is presented in table 5.2.

Parameter	Code	‘+’ Level	‘ – ’ Level
Arc current intensity(amp)	A	400	200
Arc voltage (volt)	B	40	30
Fly ash content (wt%)	C	50	0
Surface roughness(micron Ra)	D	6.8	4
Torch to base distance(mm)	E	125	100
Powder feed rate (gm/min)	F	15	10
Carrier gas flow rate (lpm)	G	10	7

Table 5.1 Control parameters and selected test levels

Test No.	A	B	C	D	E	F	G	Deposition efficiency (%)	
								Al	Cu
1	+	+	+	+	+	+	+	31.23	27.83
2	+	+	-	+	-	-	-	23.59	24.00
3	+	-	+	-	+	-	-	26.50	25.20
4	+	-	-	-	-	+	+	20.68	21.95
5	-	+	+	-	-	+	-	16.02	17.19
6	-	+	-	-	+	-	+	13.00	13.40
7	-	-	+	+	-	-	+	09.30	10.35
8	-	-	-	+	+	+	-	07.20	07.00

Table 5.2 Complete test grid with test outputs

5.2.2 Test Results

The outputs (experimental values of deposition efficiency on aluminium and copper substrates) are summed up for each level of a given factor to produce a comparison of levels for that factor. A favour ratio (FR) is calculated from the total of output values of the specimens with “+” levels and “-” levels of any factor. The level, which shows a better “total”, is considered as the favorable level over the other. The optimized set of parameters for a particular coating quality characteristic on any substrate will have the favoured levels of all the factors.

The favoured levels and their ratios are given in table 5.3. Factorial testing experience in plasma spraying suggests that a ratio above 1.20 is necessary to display significant benefit [198] . Therefore, factor G i.e. the carrier gas flow

rate and factor E i.e. the torch to base distance at favour ratios 1.019, 1.032 (for aluminium) and at 1.013, 1.020 (for copper) respectively do not greatly affect the coating at the levels chosen. The factorial test results then suggest the levels favoured as significantly better than their counterpart. It gives the optimized set of process within the test range so as to get the maximum deposition efficiency. It further suggests that factors A (plasma arc current intensity), B (arc voltage), C (fly ash content in the feed stock), F (powder feed rate) and D (substrate surface roughness), in that order, influence the deposition efficiency.

Code	Parameter	Favoured Level	Favour Ratio	
			Aluminium Substrate	Copper Substrate
A	Arc current intensity(amp)	400	2.24	2.232
B	Arc voltage(volt)	40	1.316	1.404
C	Fly ash content (wt %)	50	1.288	1.279
D	Surface roughness(micron Ra)	6.8	1.205	1.202
E	Torch to base distance(mm)	100	1.013	1.020
F	Powder feed rate(gm/min)	10	1.267	1.259
G	Carrier gas flow rate (lpm)	7	1.019	1.032

Table 5.3 Fractional factorial test results for deposition efficiency

Plasma arc current emerges as the most significant control parameter followed by arc voltage, fly ash content and powder feed rate. For further analysis only these factors will be considered

5.3 TAGUCHI EXPERIMENTAL DESIGN

Taguchi method of experimental design is a simple, efficient and systematic approach to optimize designs for performance and cost [199] . In the present

work, this method is applied to the process of plasma spraying for identifying the significant process variables/interactions influencing coating deposition efficiency. The levels of these factors are also found out so that the process variables can be optimized within the test range.

5.3.1 Experimental Design

Experiments are carried out to investigate the influence of the four selected control parameters (identified as significantly affecting coating deposition efficiency from the fractional factorial test) and that of the interactions among them. The code and levels of control parameters are shown in table 5.4. This table shows that the experimental plan has two levels. A standard Taguchi experimental plan with notation **L16 (2¹⁵)** is chosen as outlined in table-5.5. In this method, experimental results are transformed into a signal-to-noise (S/N) ratio. It uses the S/N ratio as a measure the quality characteristics deviating from or nearing to the desired values. There are three categories of quality characteristics in the analysis of the S/N ratio, i.e. the lower-the-better, the higher-the-better, and the nominal-the-better. To obtain optimal spraying parameters, the higher-the-better quality characteristic for deposition efficiency is taken.

Parameter	Code	Level 1	Level 2
Arc current intensity (amp)	A	400	200
Arc voltage (volt)	B	40	30
Fly ash content in feedstock (wt %)	C	50	0
Powder feed rate (gm/min)	D	15	10

Table -5.4 Control factors and selected test levels

Exp. No.	A	B	AxB	C	AxC	BxC		D	AxD	BxD		CxD				Coating Deposition Efficiency	S/N Ratio
	1	2	3	4	5	6	7	8	9	10	11	12	13	14	15		
1	1	1	1	1	1	1	1	1	1	1	1	1	1	1	1	30.73	29.7109
2	1	1	1	1	1	1	1	2	2	2	2	2	2	2	2	31.23	29.6914
3	1	1	1	2	2	2	2	1	1	1	1	2	2	2	2	23.19	26.9855
4	1	1	1	2	2	2	2	2	2	2	2	1	1	1	1	23.59	26.9403
5	1	2	2	1	1	2	2	1	1	2	2	1	1	2	2	25.90	29.2911
6	1	2	2	1	1	2	2	2	2	1	1	2	2	1	1	26.50	29.2649
7	1	2	2	2	2	1	1	1	1	2	2	2	2	1	1	20.19	27.5880
8	1	2	2	2	2	1	1	2	2	1	1	1	1	2	2	20.68	27.5635
9	2	1	2	1	2	1	2	1	1	1	2	2	2	1	2	15.22	24.5197
10	2	1	2	1	2	1	2	2	2	2	1	1	1	2	1	15.51	24.3910
11	2	1	2	2	1	2	1	1	2	1	2	2	1	2	1	12.27	23.1115
12	2	1	2	2	1	2	1	2	1	2	1	1	2	1	2	12.50	23.0785
13	2	2	1	1	2	2	1	1	2	2	1	1	2	2	1	08.98	18.5069
14	2	2	1	1	2	2	1	2	1	1	2	2	1	1	2	09.30	18.5697
15	2	2	1	2	1	1	2	1	2	2	1	2	1	1	2	07.07	17.0070
16	2	2	1	2	1	1	2	2	1	1	2	1	2	2	1	07.20	16.9860

Table 5.5 Experimental lay out and results with calculated S/N ratios for coating deposition efficiency

Level	A	B	AXB	C	AXC	BXC	D	CXD
1	28.379	26.054	26.101	25.49	24.767	24.682	24.59	24.55
2	20.770	23.096	23.048	23.65	24.383	24.468	24.55	24.589
Diff.	7.609	2.958	3.053	1.84	0.384	0.213	0.04	0.039
Rank	1	3	2	4	5	6	7	8

Table -5.6 The S/N response table for coating deposition efficiency

5.3.2 Analysis of control factor and interaction

Table 5.5 shows experimental lay out and results with calculated S/N ratios for deposition efficiency of the coatings. Analysis of the influence of each control factor on the coating efficiency is made with a signal-to-noise (S/N) response table, using MINITAB computer package. The response data of the testing process is presented in table 5.6. The influence of interactions between control factors is also analyzed in the response table. The control factor with the strongest influence is determined by differences values. The higher the difference, the more influential is the control factor or an interaction of two controls. The strongest influence on coating deposition efficiency is found out to be of plasma arc current intensity (A) followed by arc voltage (B) and weight fraction of fly ash in the feedstock (C) respectively. The analysis of interactions gives additional information about the deposition process. This table showed the analysis of all interactions obtained by calculating all four combinations of interaction of two control factors. For example, the interaction between the A and B (A x B) showed a much higher influence while the interactions of A x C, B x C and C x D showed very little or no significant influence on the coating deposition efficiency. The interaction between A and

B (A x B) physically represents the combined effect of factor A and factor B on the deposition efficiency of the coatings.

It is interesting to note that both the techniques; fractional factorial test and the Taguchi experimental design method identified plasma arc current as the most powerful factor influencing the deposition efficiency of the red mud coatings., The plasma arc voltage and the weight fraction of fly ash in the feedstock (red mud + fly ash mixture) emerge as the other significant factors affecting the coating deposition. The influence of interactions (among the control factors) is not included within the scope of the factorial test, but this task was taken up by Taguchi method. The S/N response values representing the significance of various interactions, suggest that the interaction of arc current and voltage has a very high degree of influence (next only to that of arc current) on coating deposition. This interaction physically represents the operating (input) power of the plasma torch during spraying. The torch input power, thus, is a significant process variable and in this work, is rightly taken as the basis for studying its effect on various coating quality characteristics.

5.4 NEURAL COMPUTATION

Plasma spraying is considered as a non-linear problem with respect to its variables: either materials or operating conditions. To obtain functional coatings exhibiting selected in-service properties, combinations of processing parameters have to be planned. These combinations differ by their influence on the coating properties and characteristics. In order to control the spraying process, one of the challenges nowadays is to recognize parameter interdependencies, correlations and individual effects on coating characteristics. Therefore a robust methodology is needed to study these interrelated effects. In this work, a statistical method, responding to the previous constraints, is implemented to correlate the processing parameters to

the coating properties. This methodology is based on artificial neural networks (ANN), which is a technique that involves database training to predict property-parameter evolutions. This section presents the database construction, implementation protocol and a set of predicted results related to the coating deposition efficiency. The details of this methodology are described by Rajasekaran and Pai [200].

5.4.1 ANN MODEL: DEVELOPMENT AND IMPLEMENTATION

The deposition efficiency describes the fraction of fed powder deposited on the substrate. For a given feed rate, it is mostly conditioned by the target material, coating material composition and the spraying parameters [201]. The plasma torch input power level has already been identified (from the outcome of Taguchi analysis) as the parameter significantly affecting the coating deposition. Hence, in the present analysis the operating power, the substrate material, the weight percentage of red mud and that of fly ash in the feedstock are taken as the four input parameters for training. Each of these parameters is characterized by one neuron and consequently the input layer in the ANN structure has four neurons.

The database is built considering experiments at the limit ranges of each parameter. Experimental result sets are used to train the ANN in order to understand the input-output correlations. The database is then divided into three categories, namely: (i) a validation category, which is required to define the ANN architecture and adjust the number of neurons for each layer. (ii) a training category, which is exclusively used to adjust the network weights and (iii) a test category , which corresponds to the set that validates the results of the training protocol. The input variables are normalized so as to lie in the same range group of 0-1. To train the neural network used for this work, about 64 data sets of different coatings applied on selected substrates are taken. It is ensured that these extensive data sets represent all possible input variations

within the experimental domain. So a network that is trained with this data is expected to be capable of simulating the plasma spray process. Different ANN structures (I-H-O) with varying number of neurons in the hidden layer are tested at constant cycles, learning rate, error tolerance, momentum parameter and noise factor and slope parameter. Based on least error criterion, one structure, shown in table 5.7, is selected for training of the input-output data. The learning rate is varied in the range of 0.001-0.100 during the training of the input-output data. The network optimization process (training and testing) is conducted for 1000,000 cycles for which stabilization of the error is obtained. Neuron numbers in the hidden layer is varied and in the optimized structure of the network, this number is 8. The number of cycles selected during training is high enough so that the ANN models could be rigorously trained.

Input Parameters for Training	Values
Error tolerance	0.01
Learning parameter(β)	0.01
Momentum parameter(α)	0.01
Noise factor (NF)	0.01
Maximum cycles for simulations	1000,000
Slope parameter (ϵ)	0.6
Number of hidden layer	1
Number of input layer neuron (I)	4
Number of output layer neuron (O)	1

Table 5.7 Input parameters selected for training

A software package NEURALNET for neural computing developed by Rao and Rao [202] using back propagation algorithm is used as the prediction tool for coating deposition efficiency at different operating power levels. The

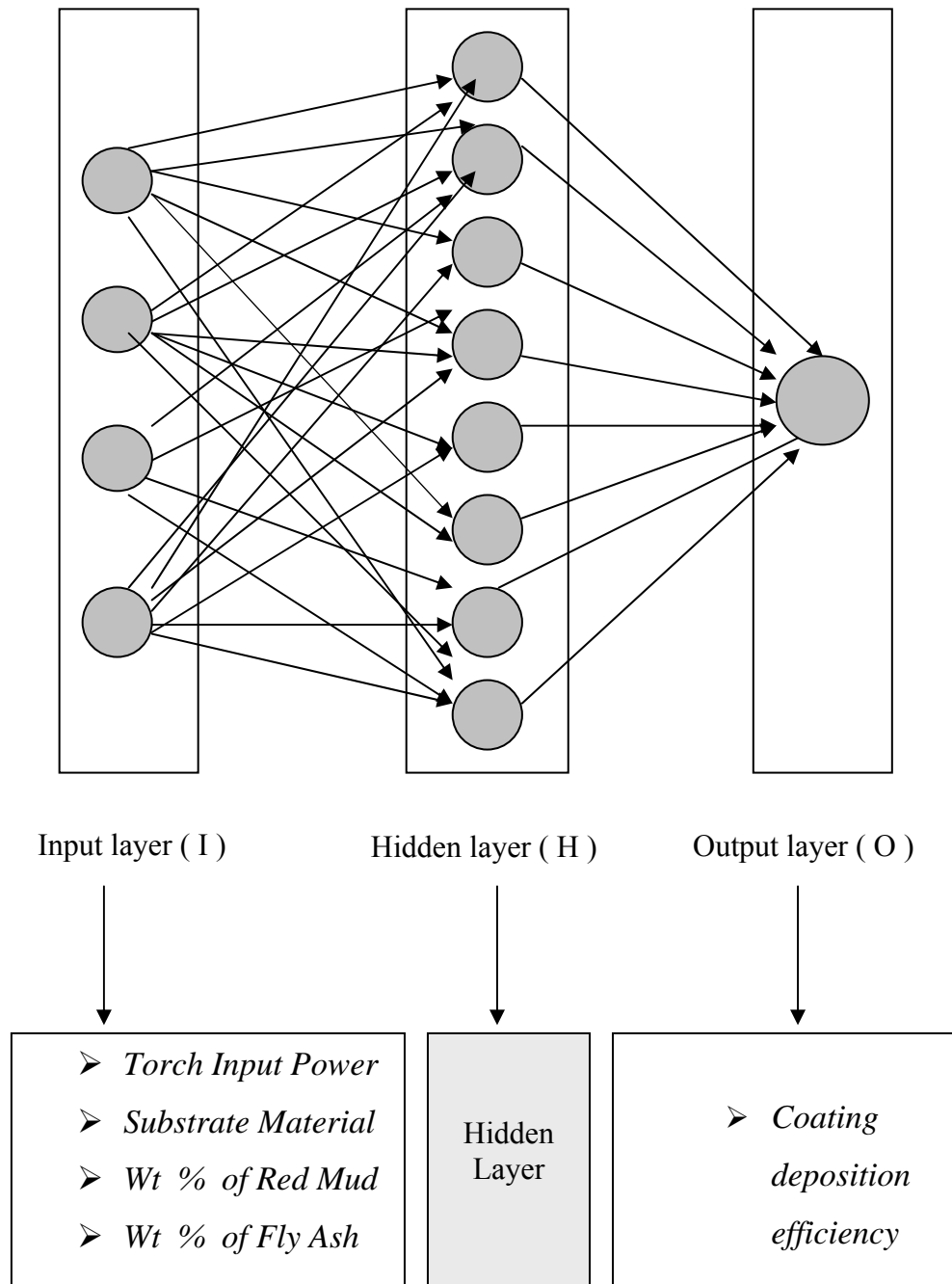


Fig. 5.1 The three layer neural network

three-layer neural network having an input layer (I) with four input nodes, a hidden layer(H) with eight neurons and an output layer (O) with one output node employed for this work is shown in fig. 5.1.

5.4.3 ANN PREDICTION OF DEPOSITION EFFICIENCY

The prediction neural network was tested with twelve data sets from the original process data. Each data set contained inputs such as torch input power, substrate material, powdered composition and an output value i.e. deposition efficiency was returned by the network. As further evidence of the effectiveness of the model, an arbitrary set of inputs is used in the prediction network. Results were compared to experimental sets that may or may not be considered in the training or in the test procedures. Fig. 5.2 presents the comparison of predicted output values for deposition efficiency with those obtained experimentally.

It is interesting to note that the predictive results show good agreement with experimental sets realized after having generalizing the ANN structures. The optimized ANN structure further permits to study quantitatively the effect of each of the considered input parameter. The range of any chosen parameter can be larger than the actual experimental limits, thus offering the possibility to use the generalization property of ANN in a large parameter space. In the present investigation, this possibility was explored by selecting the torch input power in a range from 2 kW to 20 kW, and sets of predictions for deposition efficiency on all the four substrates are evolved. Coatings of red mud pre-mixed with 0%, 10%, 30% and 50% fly ash (by weight) are considered. Fig. 5.3 to fig. 5.6 illustrate the predicted evolution of deposition efficiencies with respect to torch input power for aluminium, copper, mild steel and stainless steel substrates.

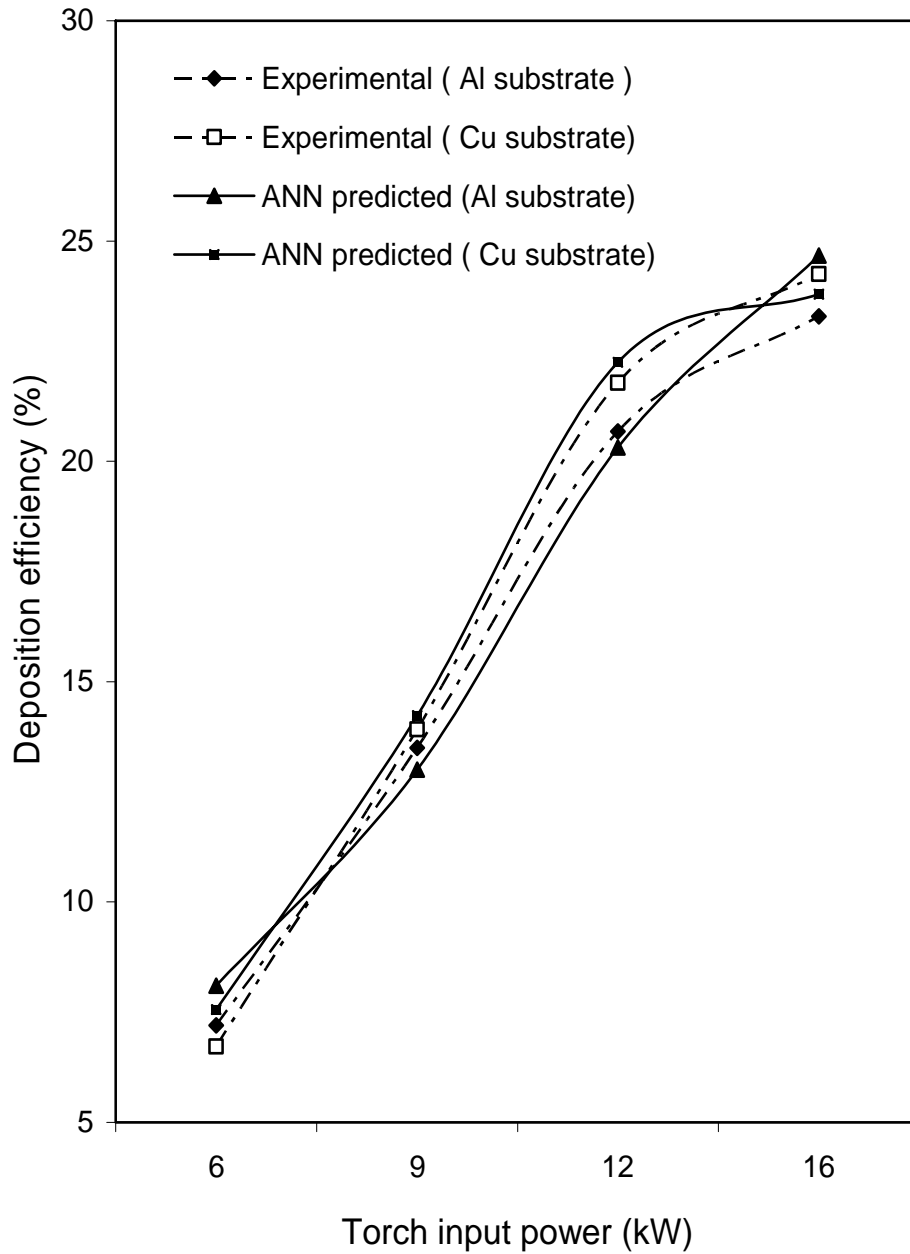


Fig. 5.2 Comparison plot for predicted and experimental values of deposition efficiency of red mud coatings on aluminium and copper substrates

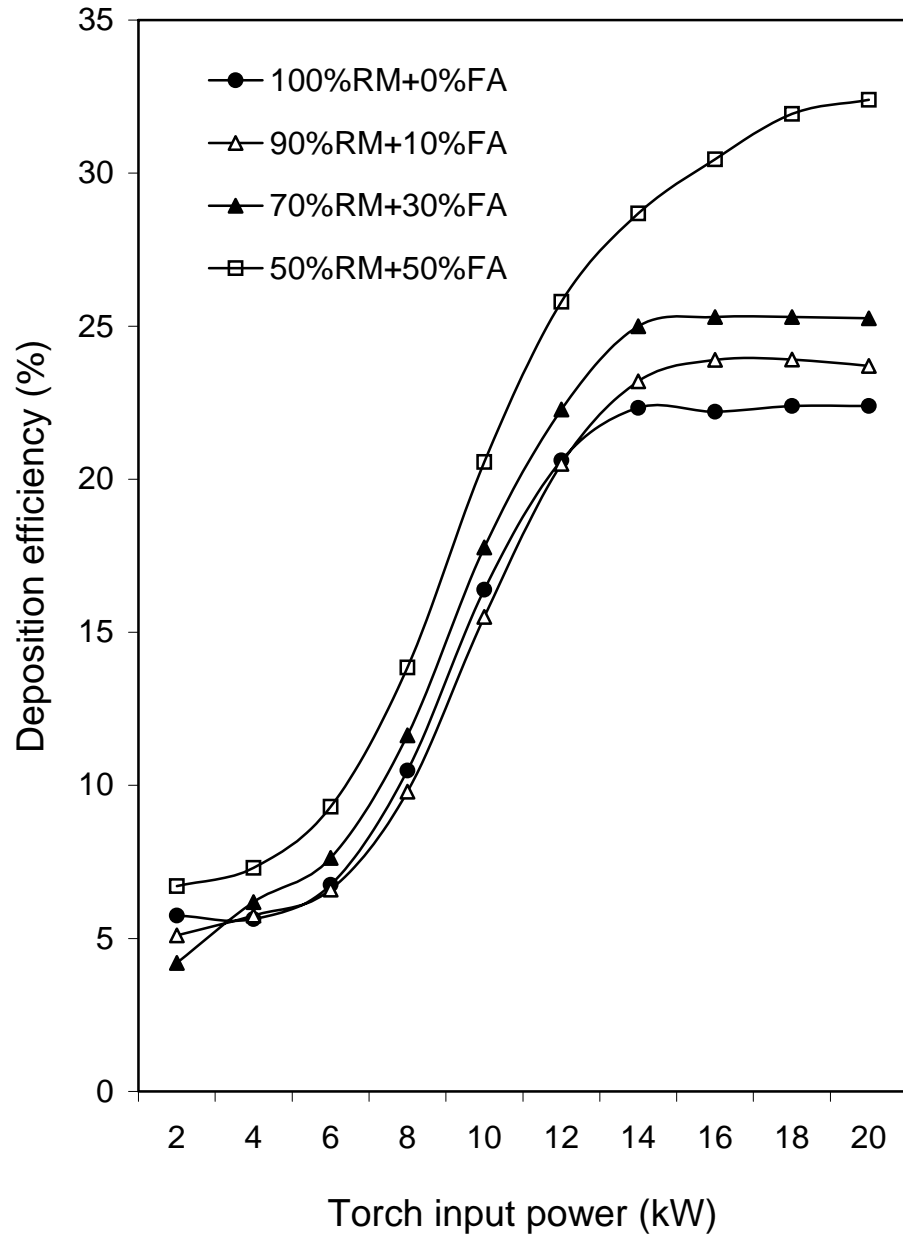


Fig. 5.3 Predicted coating deposition efficiency for different coating materials on aluminium substrate

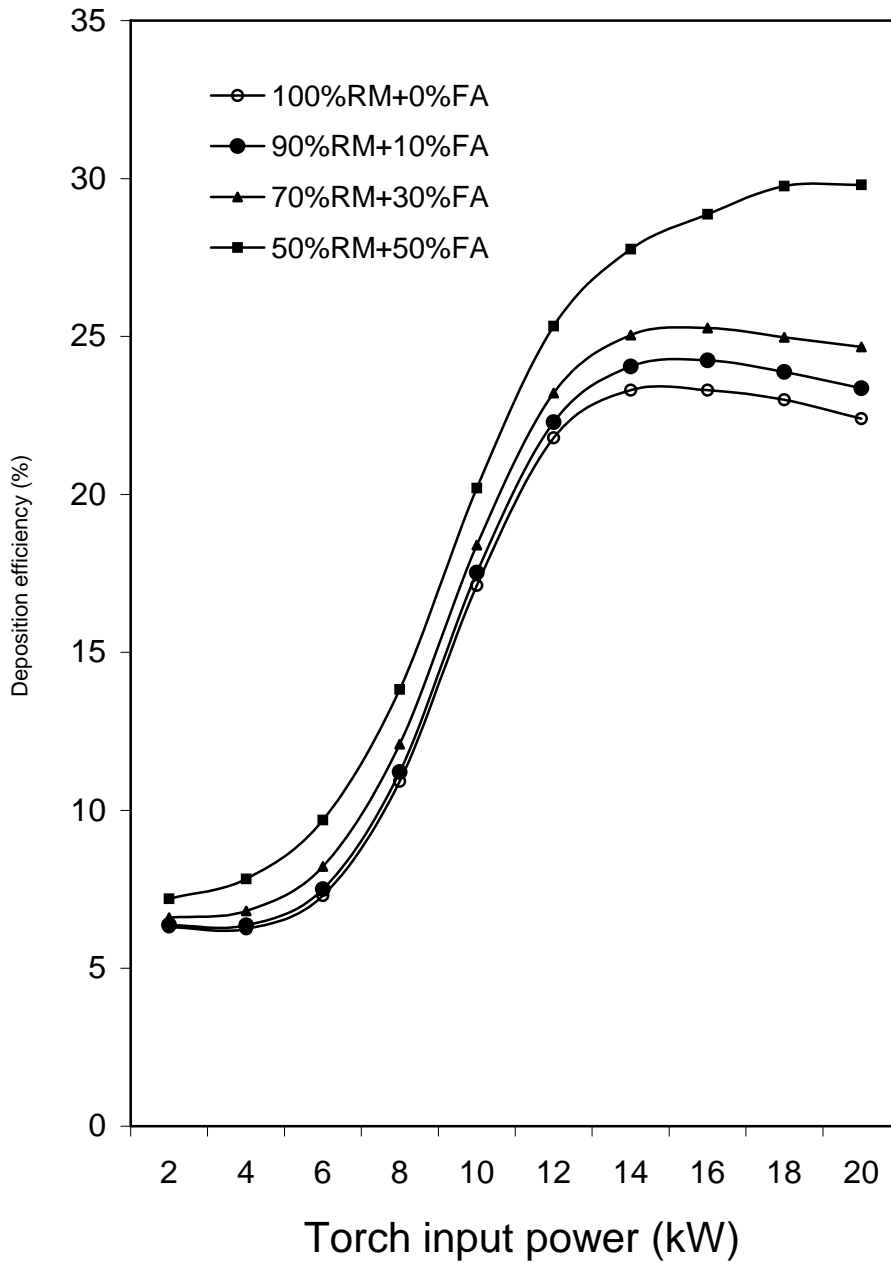


Fig. 5.4 Predicted coating deposition efficiency for different coating materials on copper substrate

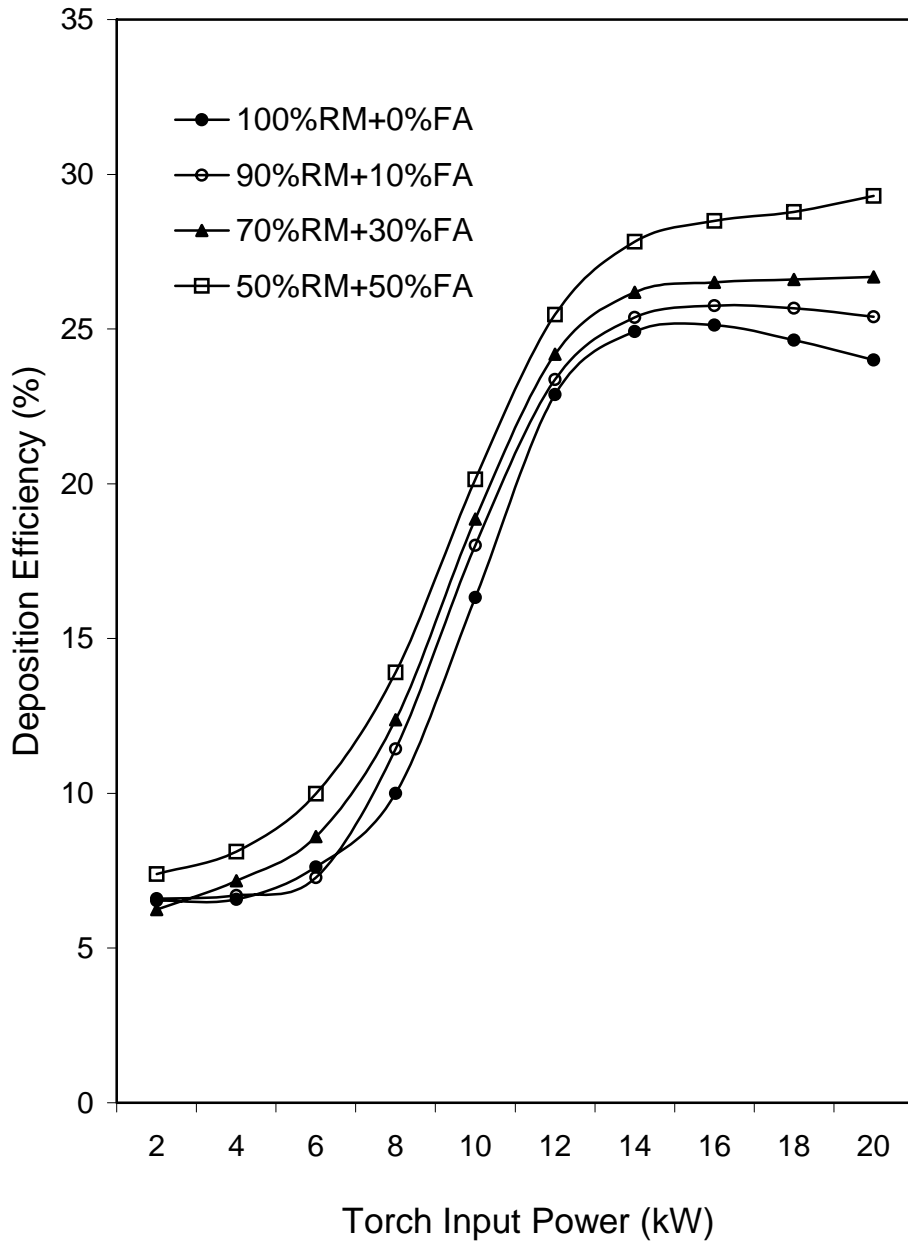


Fig. 5.5 Predicted coating deposition efficiency for different coating materials on mild steel substrate

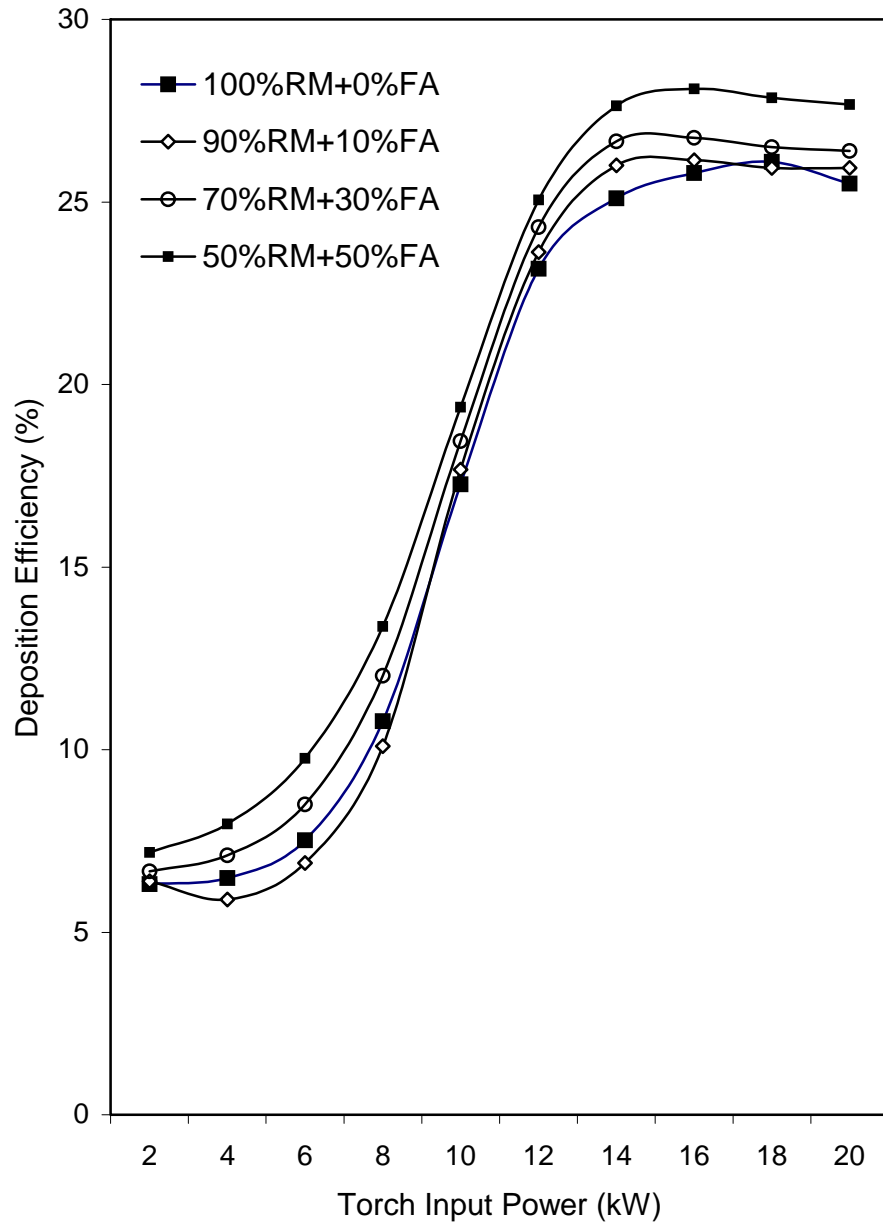


Fig. 5.6 Predicted coating deposition efficiency for different coating materials on stainless steel substrate

The deposition efficiency presents a sigmoid-type evolution with the torch input power (fig. 5.3 to fig. 5.6). As the power level increases, the total and the net available energies increase (the arc current intensity increases from 200A to 400A for operating power increasing from 6 kW to 16 kW). This leads to a better in-flight particle molten state and hence to higher probability for particles to flatten. The deposition efficiency reaches a plateau for the highest current levels due to the plasma jet temperature increasing which in turn increases both the particle vaporization ratio and the plasma jet viscosity.

5.5 REMARKS

Functional coatings have to fulfill various requirements. The deposition efficiency is one the main requirements of the coatings developed by plasma spraying. It represents the effectiveness of the deposition process as well as the coatability of the powders under study. In order to achieve certain values of deposition efficiency accurately and repeatedly, the influence parameters of the process have to be controlled accordingly. Since the number of such parameters in plasma spraying is too large and the parameter-property correlations are not always known, statistical methods can be employed for precise identification of significant control parameters for optimization. Neural computation can be used as a tool to process very large data related to a spraying process and to predict any desired coating characteristic the simulation can be extended to a parameter space larger than the domain of experimentation.

CONCLUSIONS

The conclusions drawn from the present work are as follows:

- Red mud, the waste generated from alumina plants is eminently coatable on metal substrates employing thermal plasma spraying technique. Coatings made with red mud possess desirable coating characteristics such as good adhesion strength, hardness etc. comparable to those of other conventional plasma sprayed ceramic coatings.
- Maximum adhesion strength of ~ 8 MPa is recorded for red mud coatings on mild steel. Addition of fly ash to red mud improves the interface bond strength and a maximum value of ~ 14 MPa is obtained for coatings made of red mud pre mixed with equal amount of fly ash on mild steel substrate. The coating adhesion strength is also enhanced by the addition of aluminium metal powder to red mud prior to plasma spraying.
- Deposition efficiency of $\sim 25\%$ is obtained for red mud coatings and this improves with addition of fly ash to red mud. With increase in percentage of fly ash (up to 50%) in the feedstock, this improvement becomes more pronounced. A maximum deposition efficiency of $\sim 31\%$ is recorded for coatings with red mud mixed with equal amount of fly ash, on aluminum substrate. Pre-mixing of carbon and aluminium powder to red mud also improves the efficiency of coating deposition.

- Operating power level of the plasma torch influences the coating adhesion strength, deposition efficiency and coating hardness to a great extent. The coating morphology is also largely affected by the torch input power.
- Due to phase transformations and inter-oxide formation during plasma spraying, changes in the coating characteristics such as hardness etc. are observed.
- The entire series of coatings developed in this work (of red mud and red mud pre-mixed with fly ash, carbon and aluminium etc.) are much harder than the parent metals on which they are deposited. Hence, these coatings may be recommended for tribological applications. The solid particle erosion wear resistance of the red mud coatings is fairly good and is comparable to that of conventional ceramic coatings. This further improved by addition of fly ash and aluminium to red mud.
- Spraying parameters such as plasma arc current, torch input power, arc voltage, surface roughness of the substrate significantly affect the efficiency of coating deposition. Identification of these factors and their significance on any coating characteristic is possible by statistical techniques like fractional factorial test and Taguchi experimental design. Artificial neural networks can be gainfully employed to simulate property-parameter correlations in a space larger than the experimental domain. It is evident that with an appropriate choice of processing conditions a sound and adherent ceramic coating is achievable using industrial wastes like red mud and fly ash.

Scope for Future Work

The present work leaves a wide scope for future investigators to explore many other aspects of red mud coatings. Evaluation of thermal stability of these coatings may be done to find high temperature applications. Sliding wear behaviour under different operating conditions may be investigated to identify suitable application areas. Post heat treatment of these coatings may also be made to study further improvement in coating quality and properties.

References

- 1 P. R. Taylor -- *Thermal Plasma Processing of Materials— Power Beams and Materials Processing PBAMP 2002*, Ed. A.K. Das et al., Allied Publishers Pvt. Ltd., Mumbai, India, pp. 13-20 (**2002**)
- 2 P.P.Bandopadhyaya- *Processing and Characterization of Plasma Sprayed Ceramic Coatings on Steel Substrate—Ph.D. Thesis* , IIT, Kharagpur, India (**2000**)
- 3 R.B. Heiman, '*Plasma Spray Coating, Principle and Application*', VCH, Weinheim, Germany, **1996**.
- 4 R. Edwards, *Cutting Tools*, The Institute of Materials, UK, **1993**.
- 5 K. G. Budinski, *Surface Engg. For Wear Resistance*, N.J., USA, **1988**.
- 6 K. N. Stratford, **1984**, *Coatings and Surface Treatments for Corrosion and Wear Resistance*, Inst. Of Corrosion Sc. And Tech., Birmingham, UK.
- 7 L. J. Durney, **1984**, *Electroplating Engineering Handbook*, Van Norstand, NY, USA.
- 8 T. Biestek and J. Weber, **1976**, *Electrolytic and Chemical Conversion Coating*, Portcullis Press Ltd, Warsaw, Poland.
- 9 N. A. Tape, E. A. Baker and B. C. Jackson, **1976**, *Plating and Surface Finishing*, October, p 30.
- 10 N. Fieldstein, **1981**, *Materials Engg.*, July, P 38.
- 11 C. F. Spencer, **1975**, *Metal Finishing*, January, p 38.
- 12 J. Mcdermott, **1972**, *Electroless Plating and Coating of Metals*, Noyes Data Corp, NJ., USA.
- 13 M. F. Ashby and D. R. H. Jones, **1980**, *Engineering Materials*, Pergamon press, NY, USA.
- 14 C. R. Brooks, **1979**, *Heat Treatment of Ferrous Metals*, Hemisphere Publishing Co., Washington, USA.
- 15 C. Dawes and D. F. Tranter, **1983**, *Metal Progress*, December, p 17.

- 16 A. V. Linial and H. E. Hunterman, **1979**, *Wear of Materials*, ASME, NY, USA.
- 17 S. Bhattacharya and F. D. Seaman, **1985**, *Laser Heat Treatment for Gear Application in "Laser Processing of Materials"*, The Metallurgical. Soc. Of AIME, p 211.
- 18 F. A. Smidt, **1983**, *Ion Implantation for Material Processing*, Noyes Data Corp, NJ, USA.
- 19 R. F. Bunshah, **1982**, *Deposition Technologies for Films and Coatings*, Noyes Publications, NJ, USA.
- 20 J. Vossen and W.Kern, **1978**, *Thin Film Processes*, Academic Press, NY, USA.
- 21 H. S. Legg and K. O. Legg, **1989**, *Ion Beam Based Techniques for Surface Modification in "Surface Modification Technologies"*, by T.S. Sudarsan (ed), Marcell Dekker Inc, USA, p 219.
- 22 J. M. Blocher, **1966**, *Vapour Deposited Materials in "Vapour Deposition"*, by C. F. Powell, J. H. Oxley and J. M. Blocher (eds), Willwy, NY, USA.
- 23 D. G. Bhatt, **1989**, *Chemical Vapour Deposition, in "Surface Modification Technologies"*, by T. S. Sudarsan (ed), Marcell Dekker Inc, USA, p 141.
- 24 R. L. Little, **1979**, *Welding and Welding Technology*, TMH Publications, New Delhi, India.
- 25 The Welding Handbook, **1980**, American Welding Soc., USA.
- 26 P. T. Houldcroft, **1967**, *Welding Process Tech.*, Welding Process Tech., Cambridge Univ Press, UK.
- 27 L. F. Longo, **1985**, *Thermal Spray Coatings*, ASM, USA.
- 28 V. Meringolo, **1983**, *Thermal Spray Coating*, Tappi Press, Atlanta, USA.
- 29 J. L. Morris, **1951**, *Welding Principle for Engineers*, Prentice Hall, USA.
- 30 L. Powloski, **1995**, *The Sc. And Engg. Of Thermal Spraying*, Willey, USA.
- 31 E. Lugscheider, **1992**, *Technica*, v 19, p 19.
- 32 D. G. McCartney, **1998**, *Surf. Engg.*, v 14(2), p 204.

- 33 V. V.Sobolev, J.M. Guilemany, J. Nutting and J.R. Miquel, **1997**, Int. Mat. Rev, v 42(3), p117.
- 34 B. Xu, M. Shinning and J. Wang, **1995**, Surf. Engg., v11(1), p 38.
- 35 *Metco Plasma Spraying Manual*, **1993**, Metco, USA.
- 36 J. Wrigren, **1991**, Surf. Coat. Tech., v 45, p 263.
- 37 M. G. Nicholas and K. T. Scott, **1981**, Surfacing Journal, v 12, p 5.
- 38 W. Funk and F. Goebe, **1985**, *Thin Solid Film*, v 128, p 45.
- 39 B. Wielage, V. Hofmann, A. Steinhauser and G. Zimmerman, **1998**, *Wear*, v 14(2), P 136.
- 40 N. Y. Lee, D. P. Stinton, C.C. Brandt, F. Erdogan, Y. D. Lee and Z. Mutasim **1996**, J. Am. Cer. Soc., v 79(12), P, 3003.
- 41 A.Pajares, L. Wei, B.R. Lawn and C.C. Berndt., **1996**, J. Am. Cer. Soc., 79(7), p 1907.
- 42 R. C. Novak, **1988**, J. Gas Turbines and Power, v-110, p 110.
- 43 A.R. Nash, N. E. Weare and D. L. Walker, July, **1961**, J. Metals, July, p 473.
- 44 H. Gruner, **1984**, *Thin Solid Film*, v 118, p 409.
- 45 H. Eaton and R. C. Novak, **1986**, Surf. and Coating Technology ., v 27, p 257.
- 46 H. Eaton and R. C. Novak, Proc. Int. Conf on metallurgical Coatings, San Diego, USA.
- 47 K. Ramchandran and P. A. Selvarajan, **1998**, Thin Solid Film, v 315, p 149.
- 48 H. S. Ingham and A. J. Fabel, February, **1975**, Welding Journal, p 101.
- 49 S. Oki, S. Gonda and M. Yanokawa, **1998**, Proc. 15th International Thermal Spray Conference, 25 – 29th May, France, p 593.
- 50 A.F. Puzryakov, S. A. Levitin and V. A. Garanov, **1985**, Poroshkovaya Metallurgya, v 8 (272), p 55.
- 51 J. Hennaut, J. Othzemouri and J. Charlier, **1995**, Mat. Sc and Tech., 1995, v 11, p 174.

- 52 S. Sampath, R. A. Neiser, H. Herman, J. P. Kirkland and W. T. Elan., **1993**, *J. Mat. Res.*, v 8(1), p 78.
- 53 J. Hennaut, J. Othmezouri and J. Charlier, **1995**, *Mat. Sc and Tech.*, 1995, v11, p 174.
- 54 B.Elvers, S. Hawkins and G. Schultz (eds), **1990**, *Uhlmann's Encyclopedia of Industrial Chemistry*, v 1/16, VCH, p 433.
- 55 C.J. Kubel, *Adv. Mat. Proc.*, **1990**, v12, p 24.
- 56 M. Codenas, R. Vijande, H. J. Montes and J. M. Sierra, **1997**, *Wear*, v 212, p 244.
- 57 Nolan, P. Mercer, and M. Samadi, **1998**, *Surf. Engg*, v11(2), p 124.
- 58 Y.Naerheim, C. Coddet and P. Droit, **1995**, *Surf. Engg*, v11(1), p 66.
- 59 K. Hojmrle and M. Dorfman, **1985**, *Mod. Dev. Powder. Met.*, v 15(15), p 609.
- 60 O. Knotek, E. Lugscheder and H. Reiman, **1975**, *J. Vac. Sc. Tech A*, v 12(4), p 75.
- 61 M. Roy, C.V.S. Rao, D. S. Rao and G. Sundarrajan, **1999**, *Surface Engineering*, v 15(2), p 129.
- 62 Chuanxian, H. Bingtang , L. Hailing, **1984**, *Thin Solid Film*, v 118, p 485
- 63 J.M.Guilemay, J.M.De Paco,**1998**, *Surface Engineering.*, v.11 (2), p 129.
- 64 Y. Wang, **1993**, *Wear*, v 161, p 69.
- 65 Y. Wang, J. Yuansheng and W. Shizhu, **1988**, *Wear*, v 128, p 265.
- 66 A.Tronche and P. Fauchais, **1988**, *Wear* , v 102, p 1.
- 67 A.A. Stuart, P. H. Shipway and D. G. McCartney, **1999**, *Wear*, v 225-229, p 789.
- 68 S. Economou, M. De Bonte, J.P. Celis, J. R. Roos, R. W. Smith, E. Lugscheider and A. Valencic, **1995**, *Wear*, v185, p 93.
- 69 U. Menne, A. Molar, M. Bonner, C. Varpoort, K. Ebert and R. Bauman, **1993**, *Proc. Thermal Spraying – 93*, 1993, p 280.
- 70 M. Mohanty, R. W. Smith, M. De Bonte, J. P. Celis and E. Lugscheder, **1996**, *Wear*, v 198, p 251.

- 71 J. F. Li, C. X. Ding, J. Q. Huang and P. Y. Zhang, **1997**, v, p 177.
- 72 J. M. Cuertos, E. Fernandez, R. Vijandez, A. Rucon and M. C. Perez, **1993**, *Wear*, v 169, p 173.
- 73 W. Jainjun and X. Qunji, **1993**, *Wear*, v 162 – 164, p 229.
- 74 J. F. Lin and T. R. Li, **1990**, *Wear*, v 160, p 201.
- 75 A.S. Ahn and O. K. Kwon, **1999**, *Wear*, v 225 – 229, p 814.
- 76 W. Jainjun, X. Qunji and W. Huiling, **1992**, *Wear*, v 152, p 161.
- 77 S. Lathabai, M.Ottmuller , I. Fernandez, **1998**, *Wear*, v 221,p 93.
- 78 L.Zhou, Y. M.Gao, J.E. Zhou, Q.D.Zhou, **1994**, *Wear* , v 176,p 39.
- 79 A.S. Ahn and O. K. Kwon, **1993**, *Wear*, v 162 – 164, p 636.
- 80 T. F. J. Quinn and W. O. Winer, **1985**, *Wear*, v 102, p 67.
- 81 A.Y. Kim, D. S. Lim and H. S. Ahn, **1993**, *J. Kor. Cer. Soc.*, v 30, p 1059.
- 82 H. S. Ahn, J. Y. Kim and D. S. Lim, **1997**, *Wear*, v 203 – 204, p 77.
- 83 Y. Fu, A. W. Batchelor, H. Xing and Y. Gu, **1997**, *Wear*, v 210, p 157.
- 84 Y. Sun, B. Li, D. Yang, T.Wang,Y. Sasaki and K. Ishii, **1998**, *Wear*, v 215, p 232.
- 85 Y. S. Song, J. C. Han, M.H. Park, B.H.Ro, K. H. Lee, E. S. Byun, S. Sasaki, **1998**, Proc. 15th International Thermal Spray Conference, 25th – 29th May, France, p 225.
- 86 M. I. Mendelson, **1978**, *Wear*, v 50, p 71.
- 87 *Metco Technical Bulletin on TiO₂*, **1971**, Metco Inc., NY, USA.
- 88 W. W. Dai, C. X. Ding, J. F. Li, Y.F. Zhang and P. Y. Zhang, **1996**, *Wear*,196, p 238.
- 89 N. P. Suh, **1973**, *Wear*, v 25, p 111.
- 90 H. So, **1995**, *Wear*, v 184, p 161.
- 91 T. S. Eyre, **1975**, *Wear*, v 34, p 383.
- 92 Halling, Principles of Tribology, The Mcmillan Press Ltd, NY, USA, **1975**.

- 93 Y. Guilmad, J. Denape and J. A. Patil, **1993**, Trib. Int. v 26, P 29.
- 94 M. G. Gee, **1992**, *Wear*, v 153, p 201.
- 95 R. Mcpherson, **1973**, J. Mat. Sc., v 8, P 859.
- 96 R. Mcpherson, **1980**, J. Mat. Sc., v 15, P 3141.
- 97 A.R.D.A. Lopez , K. T.Faber, **1999**, J. Am. Cer. Soc., v 82(8), p 2204.
- 98 H. Ono, T. Teramoto and T. Shinoda, **1993**, Mat and Mfg. Processes, v 8(4&5), p 451.
- 99 S. Musikant, **1991**, *What Every Engineer Should Know About Ceramics*, Marcell Dekker Inc, NY, USA.
- 100 R. P. Wahi, and B. Lischner, **1980**, J. Mat. Sc, v 15, p 875.
- 101 T. Yamamota, M. Olsson , S. Hogmark, **1994**, *Wear*, v – 174, p 21.
- 102 A.Lamy and T. N. Sopkow, **1990**, Proc. 3rd National Thermal Spray Conference, Long Beach, CA, USA, 20 – 25th May, p 491.
- 103 D. Matejka and B. Bonko, *Plasma Spraying of Metallic and Ceramic Materials*, Willey, Chichester, UK, **1989**.
- 104 M. A. Moore and F. A. King, **1980**, *Wear*, v 60, p 123.
- 105 Cheo, W. D. Kulhmann and D. M. David, **1994**, *Wear*, v 173, p 1
- 106 A. L. Fernandez, R. Rodriguez, Y. Wang, R. Vijande and A. Rincan, **1995**, *Wear*, v 181 – 183, p 417.
- 107 Y. S. Wang, S. M. Hsu and R. G. Munro, **1991**, *J. Soc. Of Tribologists and Lubri. Engg.*, v 47(1), p 63.
- 108 Metals Handbook, ASM, Metals Park, Ohio, USA.
- 109 S. Atamert and J. Stekly, Microstructure, **1993**, Surf. Engg., v 9(3), p 231.
- 110 M. O. Price, T. A. Wolfla and R. C. Tucker, **1977**, *Thin Solid Films*, v 45, p 309.
- 111 M. A. Moore, **1994**, *Wear*, v 28, p 59.
- 112 P. L. Hurricks, **1972**, *Wear*, v 22, p 291.
- 113 M. G. Habsur and R. V. Miner, **1986**, Mat. Sc. Engg, v 83, p 239.

- 114 A. E. Spear, **1989**, J. Am. Cer. Soc., v 72, p171.
- 115 A. Marakawa, **1997**, Mat. Sc. Forum, v 247, p 1.
- 116 K. Oyoda, S. Komatsu, S. Matsumoto, Y. Moriyoshi, **1991**, J. Mat. Sc., V 26, p 3081.
- 117 W. Zhu, B. H. Tan and H. S. Tan, **1993**, *Thin Solid Films*, v 236, p 106.
- 118 P. Hollman, A. Alhelisteten, T. Bjorke and S. Hogmark, **1994**, *Wear*, v 179, p 11.
- 119 A. Alhelisten, *Abrasion of Hot Flame Deposited Diamond Coatings*, *Wear*, **1995**, v 185, p 213.
- 120 Angle, P. A. *Impact Wear of Materials*, (Elsevier; New York, **1976**).
- 121 Tilly, G.P. "*Erosion Caused by Impact of Solid Particles*", in H. Herman (ed), *Treatise on Materials Science and Technology*, vol. 13:D. Scott(ed), *Wear*. (Academic Press: New York, **1979**) p. 287 – 320.
- 122 *Erosion by Liquid and Solid Impact*. (Cavendish Laboratory, University of Cambridge: Cambridge, England, **1979**).
- 123 *Erosion by Liquid and Solid Impact*. (Cavendish Laboratory, University of Cambridge: Cambridge, England, **1987**).
- 124 Evans, A. G. "*Impact Damage Mechanism – Solid Projectile*", in H. Herman (ed.), *Treatise on Materials Science and Technology*, Vol. 16: C. M. Preece (ed.), *Materials Erosion*, (Academic Press: New York, **1979**), p. 1 – 67.
- 125 *The erosion and abrasion characteristics of alumina coatings plasma sprayed under different spraying conditions* R. Westergard, L. C. Erickson, N. Axen, H. M. Hawthorne and S. Hogmark, *Tribology International*, Volume #1, Issue %, May **1998**, Pages 271 – 279.
- 126 Tucker, R. C. Jr., *On the relationship between the microstructure and the wear characteristics of selected thermal spray coatings*. Proceeding of ITSC, Kobe, Japan, **1995**, pp. 477 – 482.
- 127 H. M. Hawthorne, L. C. Erickson, D. Ross, H. Tai and T. Troczynski, *The microstructural dependence of wear and indentation behaviour of some plasma sprayed alumina coatings*. *Wear* 203 – 204 (1997), pp. 709 – 714.
- 128 Erickson, L. C., Troczynski, T., Ross, D., Tai, H. and Hawthorne, H. M., *Processing – dependent microstructure and wear – related surface properties of plasma sprayed alumina coatings*, presented to World Tribology Congress, London, U. K., September **1997**.

- 129 Erickson, L. C., Troczynski, T., Hawthorne, H. M., Tai, H. and Ross, D., *Alumina coatings by plasma spraying of monosize sapphire powders*, published in the proceedings of ITSC'98, Nice, France.
- 130 A. Ohmori, C. – J. Li and Y. Arata, *Influence of Plasma spray conditions on the structure of Al₂O₃ coatings*. Trans. Of JWRI 19 2 (1990), pp. 99 – 110.
- 131 F. Alonso, I. Fagoaga and P. Oregui.- " *Erosion Protection of carbon – epoxy composites by plasma sprayed coatings*", Surface & Coatings Technology, Volume 49, Issues 1 – 3, 10 Dec, 1991, pp. 482 – 488,
- 132 W. Tabakoff, V. Shanov. -- " *Erosion rate testing at high temp. for turbo machinery use*", - Surface & Coatings Technologies, Vol. 76 – 77, Part I, Nov 1995, pp. 75 – 80,
- 133 C. He, Y. S. Wang, J. S. Wallace and S. M. Hsu, 1993, *Wear*, V 162 – 164, p 314.
- 134 O. O. Ajayi and K. C. Ludema, 1991, *Wear*, v 124, p 307.
- 135 R. Mcpherson, 1989, Surf. Coat. Tech., v 39/40, p 173.
- 136 B. Wang, 1996, *Wear*, v 199, p 24.
- 137 F.M. Hawthorne, L. C. Erickson, D. Ross, H. Tan and T. Troczynski, 1997, *Wear*, v 203 – 204, p 709.
- 138 X. S. Zhang, T. W. Clyne and I. M. Hutchings, 1997, Surf. Engg., v 13(5), p 393.
- 139 Jose Roberto Tavares Branco, Robert Gansert, Sanjay Sampath, Christopher C. Berndt, Herbert Herman-- *Solid Particle Erosion of Plasma Sprayed Ceramic Coatings*—Materials Research. Vol.7. No.1.147-153 , 2004
- 140 Chinloy, D. R. and Holzwarth, R. K., 1984, " *Steady state simulation of the bayer Process*", LIGHT METALS pp. 13 – 26.
- 141 Hall, C. M., 1889, US Patent 400766.
- 142 Mahapatra, B. K., Rao, M. B. S., Bhima Rao, R. and Paul, A. K., " *Characteristics of red mud generated at NALCO refinery, Damanjodi, India*", LIGHT METALS, 2000, pp. 161 -165.
- 143 Solimar, K, Sajo, I, Steiner, J, and Zoldi, J. 1992, " *Characteristics and separability of red mud*," LIGHT METALS, pp.209 - 223.
- 144 Sahin S, 1998, *Correlation between silicon-dioxide and iron-oxide contents of red mud samples*, Hydrometallurgy, 47, pp.371 – 376.

- 145 Wang, Q, Gu, S, Han, Z, and Li, D., *Irreversible thixotropic behaviour of red mud slurry and exploitation in dry disposal process Nonferrous Metals (China)*, 50(2), **1998**, pp. 85 – 91.
- 146 Thakur, R. S. and Das. S. N., *Red Mud – Analysis and Utilization -- Publication & Information Directorate*, New Delhi and Wiley Eastern Limited, New Delhi, India. (1994).
- 147 Banvolgyi, G, and Siklosi, P., **1998**, *The improved low temperature digestion (ILTD) process: An economic and environmentally sustainable way of processing gibbsitic bauxites*, LIGHT METALS, pp. 45 – 53.
- 148 Galarraga, R. A., Carneiro, R. R., Keane, R. E and Nguyen, G., **2002**, *"CVG – Bauxilum red mud neutralization"*, LIGHT METALS, pp. 133 – 137.
- 149 Brown, S. O, and Kirkpatrick, D. B., **1999**, *"Red mud product development"*, LIGHT METALS, pp. 25 – 30.
- 150 Kirkpatrick, D. B., 1996, *Red mud Product Development*, LIGHT METALS, pp. 75 – 80. Cited from ref. 16.
- 151 Goldstein, G. L. and Reimers, R. S. 1999, *"Trace element partitioning and bioavailability in red mud synthetic free water sediment"*, LIGHT METALS, PP. 19 – 24.
- 152 Kovalenko, E. P., 1998, *"Improvement of the process of alumina production at Nilolaev alumina plant"*, LIGHT METALS, pp.55 – 58.
- 153 D.Patel, B. K. Padhi, P. Vidyasagar, A. K. Pattnaik., Res. Ind. 37 (**1992**) 154.
- 154 J. Pera, R.Boumaza, J.Ambroise, Cem.Conc. Res. 34 (**1997**) 1513.
- 155 R. N. Summers. N. R. Guise, D. D. Smirk, Fert. Res. 34 (**1993**) 85.
- 156 Smirnov, D. I, Molchanova, T. V. and Vodolazov, L. I., **1999**, *"Associated components of bauxites and ways for their utilization"*, Tsvetnaya Metallurgia, 4, pp. 31 – 34.
- 157 Martinent – Catalot, V, Lamerant, J-M, Tilmant, G, Bacou, M-S. Ambrosi,J.P., **2002**, *Bauxaline: a new product for applications of Bayer process red mud*, LIGHTMETALS, pp.125– 131.
- 158 Liu, S; **1998**, *"Removal of Toxic Metals from Landfill Leachate and Wastewater by Spent Bauxite"*, Ph. D. Thesis, Tulane University. Cited from: Ref – 16.

- 159 Pradhan, J, Das,S.N., Thakur, R.S., **2000**, *Removal of Ni from aqueous solution using activated red mud* , LIGHT METALS, pp.157 – 160.
- 160 Zouboulis, A.I, Matis, K.A, Solozhenkin, P.M. , Nebera,V.P., **1999** *Removal of ions of toxic metals from solutions using industrial solid waste products,--Tsvetnye Metally*, 12, pp.45-48.
- 161 Yalcin, N. and Sevinc, V., **2000** , " *Utilization of bauxite waste in ceramic glass,*" *Ceramics International*, 26(5), pp.485-493.
- 162 Balasubramanian, G, Nimje, M. T. and Kutumbarao, V. V., **2000**, " *Conversion of aluminium industry wastes into glass-ceramic products*", Fourth Int. Symposium on Recycling of Metals & Engineered Materials, Warrendale, USA, pp.1223 – 1228.
- 163 Mahata, T, Sharma, B. P, Nair, S. R. and Prakash, D., **2000**, " *Formation of aluminium titanatemullite composite from bauxite red mud*" , *Met. Mat. Trans. B*, 318, pp. 551 – 553.
- 164 Laszlo T and Jozsef K., **1957**, " *Chlorination of red mud (from the manufacture of alumina)*" , *Kohaszati Lapok*, 90, 460 – 465.; cited from Chem. Abstr. 195852, 19035.
- 165 Heck, C., **1953**, " *Iron powder from Bayer-process waste*" , *Ger. Pat.* 894 843, 29 Oct.: cited from Chem. Abstr. 1958, 52, 11722 h.
- 166 Marvin, J. U., **1958**, " *Recovery of iron, titanium oxide, and alumina from ores and wastes*" , *U. S. Pat.*2, 830, 892, 15 Apr. 1958; cited from Chem. Abstr. 1959, 53, 13847 f.
- 167 Ni, L P., **1960**, " *The extaction of aluminium, iron and sodium oxide from red mud*" , *Izvest. Akad. Nauk. Kazakh, S.S.R. Ser. Met. Obogashchen. I Ogneuporov.*, 1, pp. 21 – 26., cited from Chem. Abstr. 1961, 55, 16316 a.
- 168 Watanabe, T. and Yuki, E., 1960, *Jap. Pat.* 13202, **1960**; *cited from Chem. Abstr.*1962, 56, 4477 g.
- 169 Braithwait, M., *Benefication of iron oxide waste.*, *GB Patent No.* 2078211 – A., Jan. **1982**.
- 170 Agency of Ind. Sci. Tech., J, **1977**, *Patent No.* 52152896 – A., Dec. **1977**.
- 171 Mozhareenko, N M; Noskov, V A., **2001**, " *Possible directions in the use of red mud in metallurgical production*" , *Metallurgicheskaya I Gornorudnaya Promyshlennost*, 2, pp. 127 – 128.
- 172 Xiang,Q, Liang,X, Schlesinger, M.E., Watson, J.L. ,**2001**, *Low temperature reduction of ferric iron in redmud*, *LIGHT METALS* pp 157-162.

- 173 Mishra, B, Staley, A. and Kirtepatrick, D., **2001**, "*Recovery and utilization of iron from red mud*", LIGHT METALS, pp.149 – 156.
- 174 Liu, P., Huo, Z., Gu, S, Ding, J., Zhu, J. and Liu, G., **1995**, "*Magnetic dressing iron mineral concentrate from Bayer red mud*", LIGHT METALS, pp. 149 – 153.
- 175 Dobos, D., Jambo, J. and Vishn' ovskii, L., **1964**, *Utilization of Bayer Process red mud for the production of Fe and Al.*, Tsvent. Metall., 37(2), pp. 36 – 40.
- 176 Tathavadkar, V., Antony, M P and Jha, A., **2002**, "*Improved extraction of aluminium oxide from bauxite and red mud,*" LIGHT METALS, pp.199-203.
- 177 Kasliwal, P. and Sai, P S T., "*Enrichment of titanium dioxide in red mud: a kinetic study*", Hydrometallurgy, 53, (1), pp. 73 – 87.
- 178 Sayan, E. and Bayramoglu, M., **2000**, "*statistical modeling of sulfuric acid leaching of TiO₂ from red mud*", Hydrometallurgy, 57, pp. 181 – 186.
- 179 Rayzman, V. L. and Filipovich, I. K., **1999**, "*Intigrating coal combustion and red mud sintering at an alumina refinery*", JOM, 51(8), pp. 16 – 18.
- 180 Misra, B., Kirtepatrick. D and Slavik, M., **2000**, "*Pyrometallurgical extraction of alumina and iron from red mud*", (Eds): Taylor, P. R., EPD Congress 2000 (TMS – AIME, Warrandale, PA), pp. 369 – 381.
- 181 S. C. Mishra. K. C. Rout, P. V. Ananthapadmanabhan and B. Mills *Plasma Spray Coating of Fly Ash Pre-Mixed with Aluminium Powder Deposited on Metal Substrates.* J. Material Processing Technology **2000**. 102, 1 – 3 , pp. 9 – 13.
- 182 L. Rama Krishna, D. Sen, D. Srinivasa Rao, and G. Sundararajan: *Cotability and Characterization of Fly Ash Deposited on Mild Steel by Detonation Spraying.* J. of Thermal Spray Technology Volume 12 (1) March **2003**, pp. 77 – 79.
- 183 H. Chen, S.W. Lee, Hao Du, Chuan X Ding and Chul Ho Cho; "*Influence of feed stock and spraying parameters on the deposition efficiency. and microhardness of plasma sprayed zirconia coatings*" -- Materials Letter Vol 58, Issues 7 – 8, March **2004** pp. 1241 – 1245

- 184 B. Venkataraman – *Evaluation of Tribological Coatings* – Proc. of DAE-BRNS Workshop on Plasma Surface Engineering, BARC, Mumbai, September **2004**, pp. 217 – 235.
- 185 G .Lalleman – Tallaron, *Study of Microstructure and adhesion of spinelles coatings formed by plasma spraying*, Ph. D. Thesis No. 96 – 58 (**1996**) E. C. Lyon, France.
- 186 C.R.C. Lima, R.E.Trevisan. J.Themal Spray Tech. 62, **1997** , p. 199.
- 187 Lech Pawlowski – *The Science and Engineering of Thermal Spray Coatings*, John Wiley & Sons, New York (**1995**) pp. 218.
- 188 Levy, A. V. The erosion corrosion behavior of protective coatings, Surf. and Coat. Techn., v. 36. p. 387 – 406, **1988**.
- 189 Weight, I. G.; Shetty, D. K. *A Phenomenological Approach to Modelling the Erosion of WC – Co Alloy*, 7th ELSI. Paper 43.
- 190 R. G. Bayer – *Mechanical Wear Prediction and Prevention* – Marcel Dekkar, Inc., New York (**1994**) pp. 396.
- 191 L. M. Berger, W. Hermal, P. Vuoristo, T. Mantyla, W. Lengaure, P. Ettmayer – *Structure, Properties and Potentials of WC – CO, Cr₃C₂ – NiCr and TiC – Ni – Based Hard metal like Coatings* – Proceedings of the 9th National Thermal Spray Conference, CC. Berndt (Ed.), Published by ASM International USA, (**1996**)
- 192 A.Vardelle, M. Vardellet, R. Mc.Pherson, P. Fanchais – Proc. of 9th National Thermal Spray Conference (**1980**) pp.155
- 193 Lech Pawlowski – *The Science and Engineering of Thermal Spray Coatings*, John Wiley & Sons, New York (**1995**) pp. 235.
- 194 H.Johner, V. Wilms, K. K. Schweltzer, P. Adam – *Experimental and Theoretical Aspects of Thick Thermal Barrier Coatings for Turbine Applications* – Thermal Spray: Advances in Coatings Technology, David L.Houck (Ed.) Published by ASM Int. USA (**1987**) pp.155– 166.
- 195 R. G. Bayer – *Mechanical Wear Prediction and Prevention* – Marcel Dekkar, Inc., New York (**1994**) pp. 395
- 196 Y. Arata, A. Ohmori, Chang Jiu Li – *Fundamental Properties of the ACT – 5P (Arata Coating Test with Jet Particles)* – Thermal Spray : Advances in Coatings Technology, David L. Houck (Ed.), Published by ASM International, USA (**1987**) pp. 79 – 83.
- 197 Plakkett R.L. and Burman J.P. ,Biometrica 33,305 (**1946**)

- 198 Stephen L , Van Doren - *A Statistical Method of Plasma Spray Parameter Testing* , Koppers Co.Inc., Baltimore, USA (**1984**)
- 199 Y.Sahin - *The Prediction of Wear Resistance Model for The Metal Matrix Composites*, Wear 258 (**2005**) pp. 1717-1722
- 200 S.Rajasekaran , G. A. Vijayalakshmi Pai --*Neural Networks, Fuzzy Logic And Genetic Algorithms—Synthesis and Applications* -Prentice Hall of India Pvt. Ltd. , New Delhi (**2003**)
- 201 R.Kingswell , K. T. Scott , L. L. Wassell , *Optimizing the Vacuum Plasma Spray Deposition of Metal, Ceramic and Cermet Coatings using Designed Experiments*, J. Thermal Spray Technology 2 (**1993**) 179
- 202 V. Rao and H. Rao 'C++ *Neural Networks and Fuzzy Systems*' BPB Publications, **2000**.

LIST OF PUBLICATIONS

- 1 **Plasma Spray Coating of Red Mud on Metals** – S. C. Mishra, Alok Satapathy, P.V.Ananthapadmanabhan, K.P.Sreekumar – *Power Beams and Materials Processing* , published by Allied Publishers Ltd. , Mumbai, 2002 , pp. 709 – 712.
- 2 **Characterization of Red Mud Coatings Prepared by Plasma Spraying-** Alok Satapathy, S.C. Mishra, K.P.Sreekumar, P.V.Ananthpadmanabhan, – Proceedings of the International Conference on Advances in Surface Treatment: Research and Applications, Nov, 2003, Hyderabad, India. pp. 545 – 550.
- 3 **Deposition of Red Mud–Carbon Coating on Metals by Plasma Spraying–** Alok Satapathy, S.C.Mishra, K.P.Sreekumar, P.V.Ananthapadmanabhan – Proceedings of the International Conference on Advances in Surface Treatment : Research and Applications Nov, 2003, Hyderabad, India. pp. 537 – 540.
- 4 **Use of Red Mud and Fly Ash for High Valued Applications--**S.C. Mishra, Alok Satapathy, P.V.Ananthapadmanabhan, K. P. Sreekumar – *Mineral Processing Technology*, published by Allied Publishers Pvt. Ltd. , 2004, pp. 757 – 762.
- 5 **Resistance of Plasma Sprayed Red Mud Coatings to Solid Particle Impingement-** Alok Satapathy S.C.Mishra, P.V.Ananthapadmanabhan, K.P.Sreekumar-- Proceedings of DAE–BRNS National Workshop on Plasma Surface Engineering, Bhabha Atomic Research Center, Mumbai, India , published by Allied Publishers Ltd., Mumbai, 2004 , pp. 361 – 363.
- 6 **Coatability of Red Mud on Metal Substractes** - Alok Satapathy, S.C.Mishra, P.V.Ananthapadmanabhan, K.P.Sreekumar– Proceedings of DAE – BRNS National Workshop on Plasma Surface Engg, Bhabha Atomic Research Center, Mumbai ; published by Allied Publishers Ltd., Mumbai, 2004 , pp. 350 – 352.
- 7 **Prediction of Interface Bond strength of Plasma Spray Coatings using Artificial Neural Network** - Alok Satapathy , S.C. Mishra, P.V.Ananthapadmanabhan, K.P. Sreekumar – Proceedings of 19th National Symposium of Plasma Science Society of India, PLASMA-2004 , p 109.

- 8 **Numerical Prediction of Deposition Efficiency in Atmospheric Plasma Spray Coatings-** Alok Satapathy , S.C. Mishra, K.P. Sreekumar, P.V.Ananthapadmanabhan,- Proceedings of 19th National Symposium of Plasma Science Society of India, PLASMA-2004 , p 110

- 9 **Tribological Behaviour of Plasma Sprayed Red Mud-Fly Ash Coatings –** Alok Satapathy, S.C.Mishra, P.V.Ananthapadmanabhan, K.P.Sreekumar – Proceedings of 4th International Conference on Industrial Tribology, Tribological Society of India, Mumbai, 2004 pp.454-459.

- 10 **Erosion Wear Behaviour of Red Mud Coatings -** Alok Satapathy, S. C. Mishra, P.V.Ananthapadmanabhan, K. P. Sreekumar – Proceedings of the 1st international conference on Advanced Tribology, Singapore, Dec, 2004 .pp.c3-4.

- 11 **Sliding Wear Characteristics of Red Mud Coatings -** Alok Satapathy, S.C.Mishra, P. V. Ananthapadmanabhan, K. P. Sreekumar – Proceedings of the 1st international conference on Advanced Tribology, Singapore, Dec, 2004 pp.c19-20.

- 12 **Use of Red Mud; A Solid Waste from Alumina Plants –** Alok Satapathy, S. C. Mishra, P.V. Ananthapadmanabhan, K. P. Sreekumar -- Communicated to the *Journal. of Solid Waste Technology and Management*, Widener, USA.

- 13 **Wear Characteristics of Red Mud Coatings -** Alok Satapathy, S. C. Mishra, P.V. Ananthapadmanabhan, K. P. Sreekumar – Communicated to *Tribology International*, Elsevier.

- 14 **Development of Wear Resistant Overlay Coatings Using Industrial Wastes ---** Alok Satapathy, S.C. Mishra, P. V. Ananthapadmanabhan, K. P. Sreekumar, K.C.Sabat-- P - 9, Souvenir and Abstracts-- Presented at the International Conference on Design and Characterisation of Advanced Materials DCAM 2004 , Varanasi, Dec, 2004.

- 15 **Erosion Wear Behaviour of Red Mud-Fly Ash Composite Coatings --** Alok Satapathy, S. C. Mishra, P. V. Ananthapadmanabhan and K. P. Sreekumar --- Presented at the International Conference on Recent Advances in Composite Materials ICRAACM 2004 , Varanasi, Dec, 2004.

- 16 **Parameter Optimization in Plasma Spraying using Fractional Factorial Technique –** Alok Satapathy, S. C. Mishra, K. P. Sreekumar and P. V. Ananthapadmanabhan -- Accepted for presentation at the 20th National Symposium of Plasma Sci. Society of India, PLASMA 2005, Cochin, India

Brief bio data of the author

The author, **Sri Alok Satapathy**, born on 20-12-1968 graduated in Mechanical Engineering from the University College of Engineering, Burla in 1990. He obtained his Masters Degree (M.E) in Heat Power Engineering from Birla Institute of Technology, Mesra (Deemed University) in 1993. The same year, he joined National Institute of Technology (formerly known as Regional Engg. College), Rourkela as a faculty in the Department of Mechanical Engineering.

The author is engaged in research in the area of thermal plasma processing of materials since 2000. He has been associated with the Laser & Plasma Technology Division of Bhabha Atomic Research Center, Mumbai for collaborative research on plasma sprayed coatings. He had been sanctioned (as the principal investigator) a thrust area project in technical education entitled **Use of Plasma Technology to Develop Ceramic Coatings Using Industrial Wastes** by the Ministry of HRD, Govt. of India in 2002. He has presented about 20 research papers related to the field of plasma spraying at various national and international conferences held in India and abroad.

At present, he is working as a Senior Lecturer in the Department of Mechanical Engineering at National Institute of Technology, Rourkela.
